SUPPLEMENTARY INFORMATION

A Versatile Stereocontrolled Synthesis of 2-Deoxyiminosugar *C*-Glycosides and their Evaluation as Glycosidases Inhibitors

Alexandre Lumbroso,[a] Clément Berthonneau,[a] Isabelle Beaudet,[a] Jean-Paul Quintard,[a] Aurélien Planchat,[a] M. Isabel García-Moreno,[b] Carmen Ortiz-Mellet,[b] Erwan Le Grognec[a]*

[a] Université de Nantes, CNRS, CEISAM, UMR 6230, 44000 Nantes, France.
e-mail: erwan.legrognec@univ-nantes.fr

[b] Department of Organic Chemistry, Faculty of Chemistry, University of Seville, c/ Professor García Gonzalez 1, 41012, Seville, Spain

Table of Contents

I-NMR spectra and NOESY analysis

^{1}H NMR of compound **3** (400 MHz, $CDCl_3$, 300K)

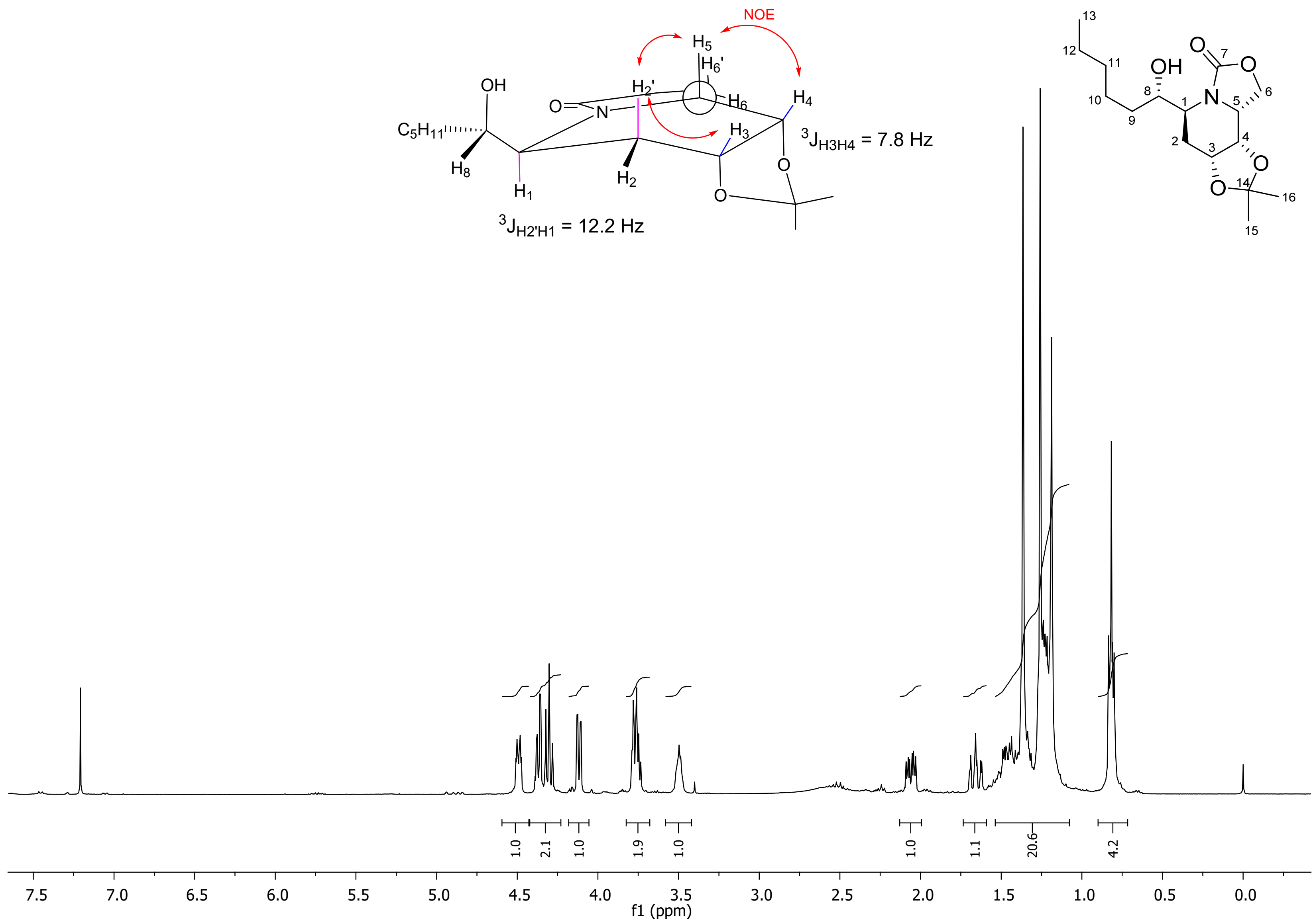

^{13}C NMR of compound **3** (100 MHz, $CDCl_3$, 300K)

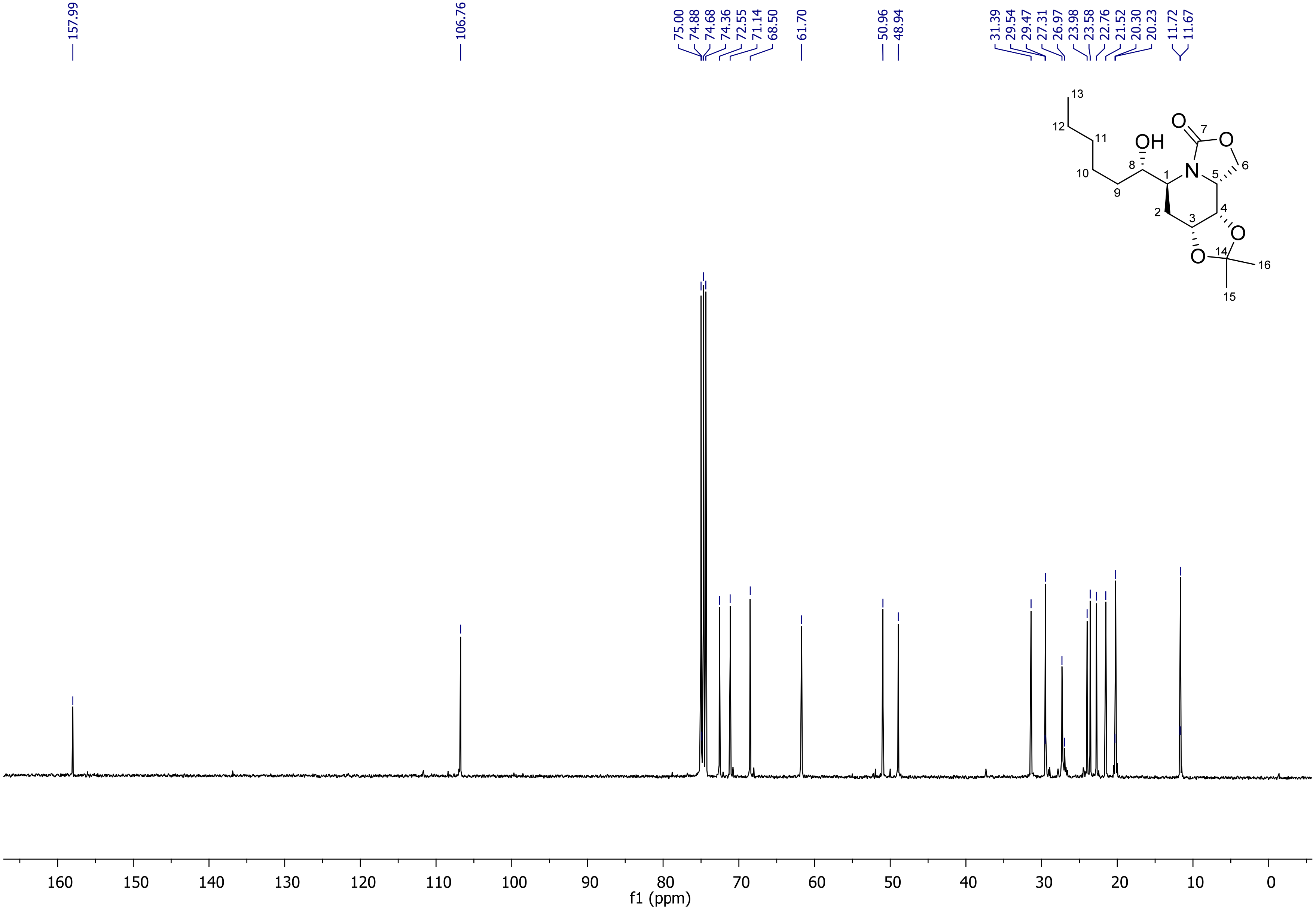

^{1}H NMR of compound **4** (400 MHz, $CDCl_3$, 300K)

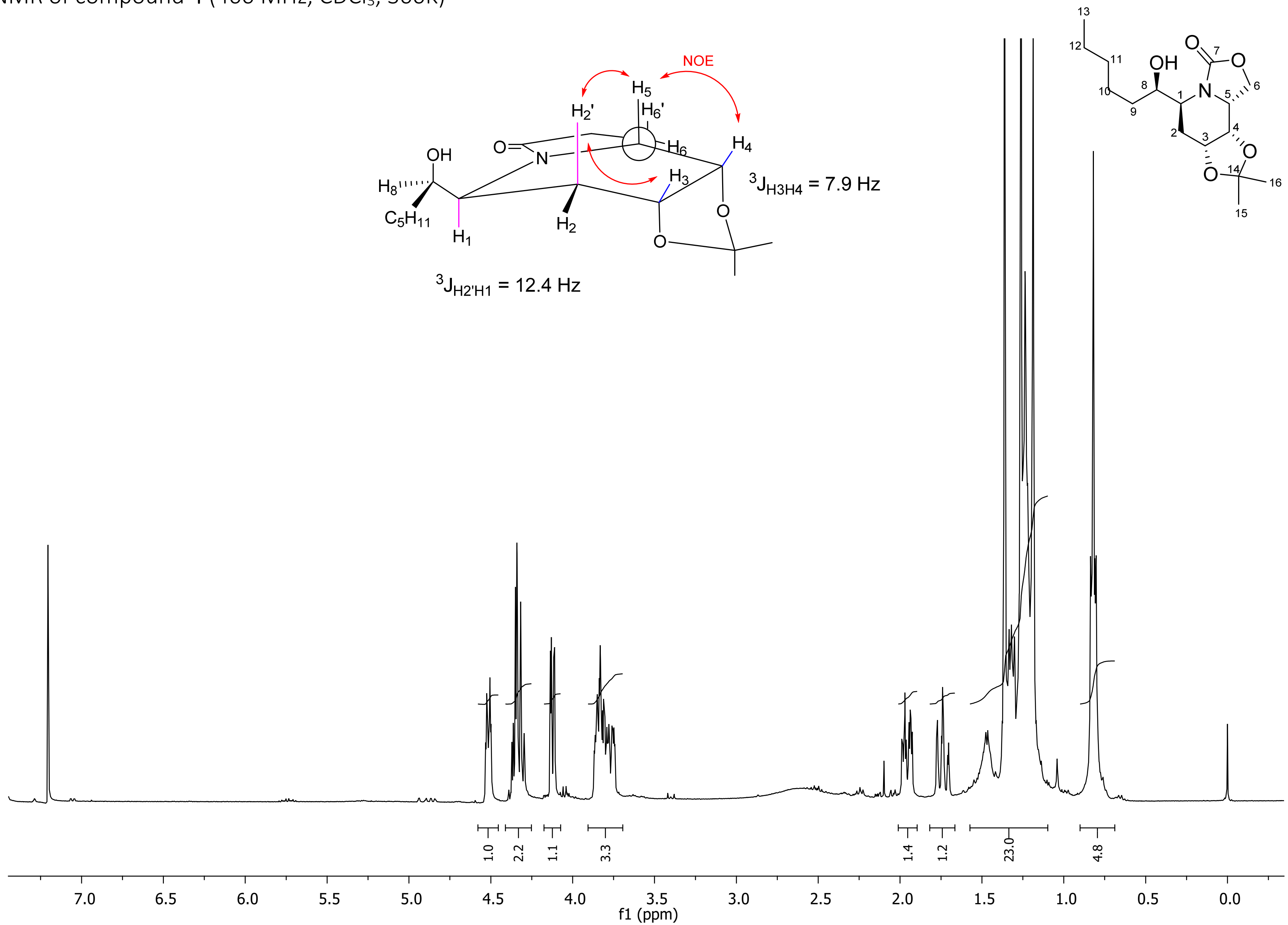

^{13}C NMR of compound **4** (100 MHz, $CDCl_3$, 300K)

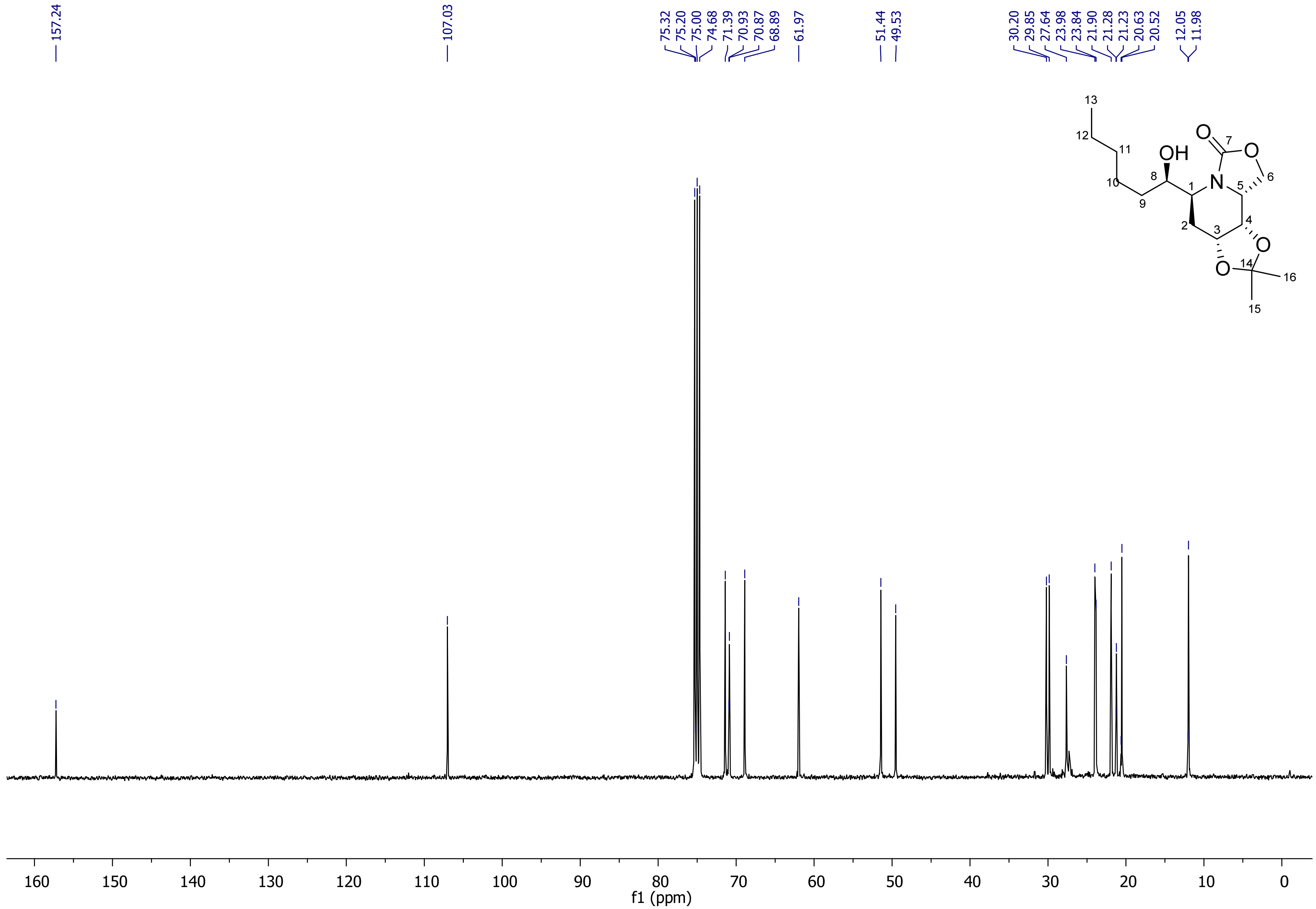

^{1}H NMR of compound **5-*exo*** (400 MHz, $CDCl_3$, 300K)

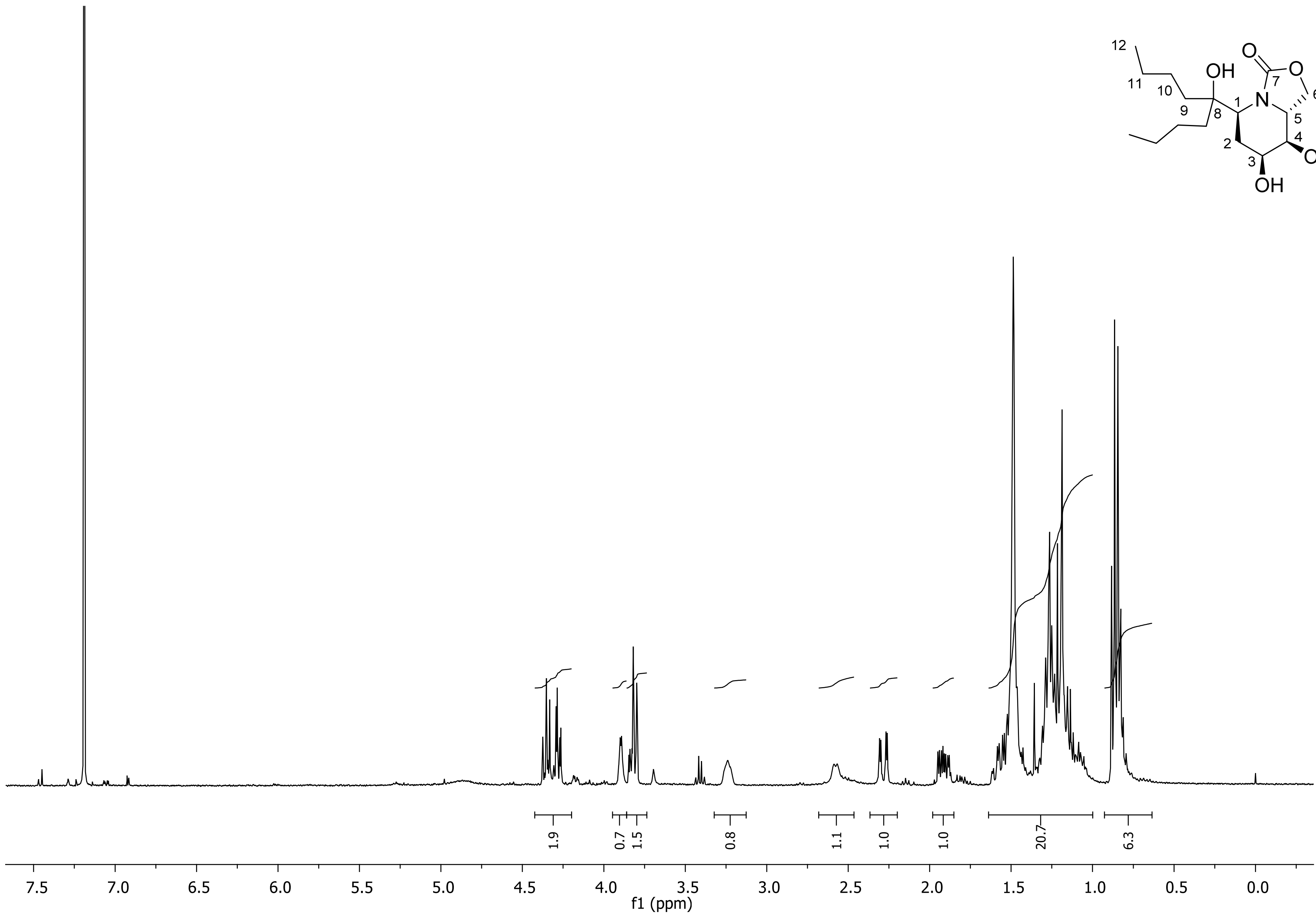

^{13}C NMR of compound **5-*exo*** (100 MHz, $CDCl_3$, 300K)

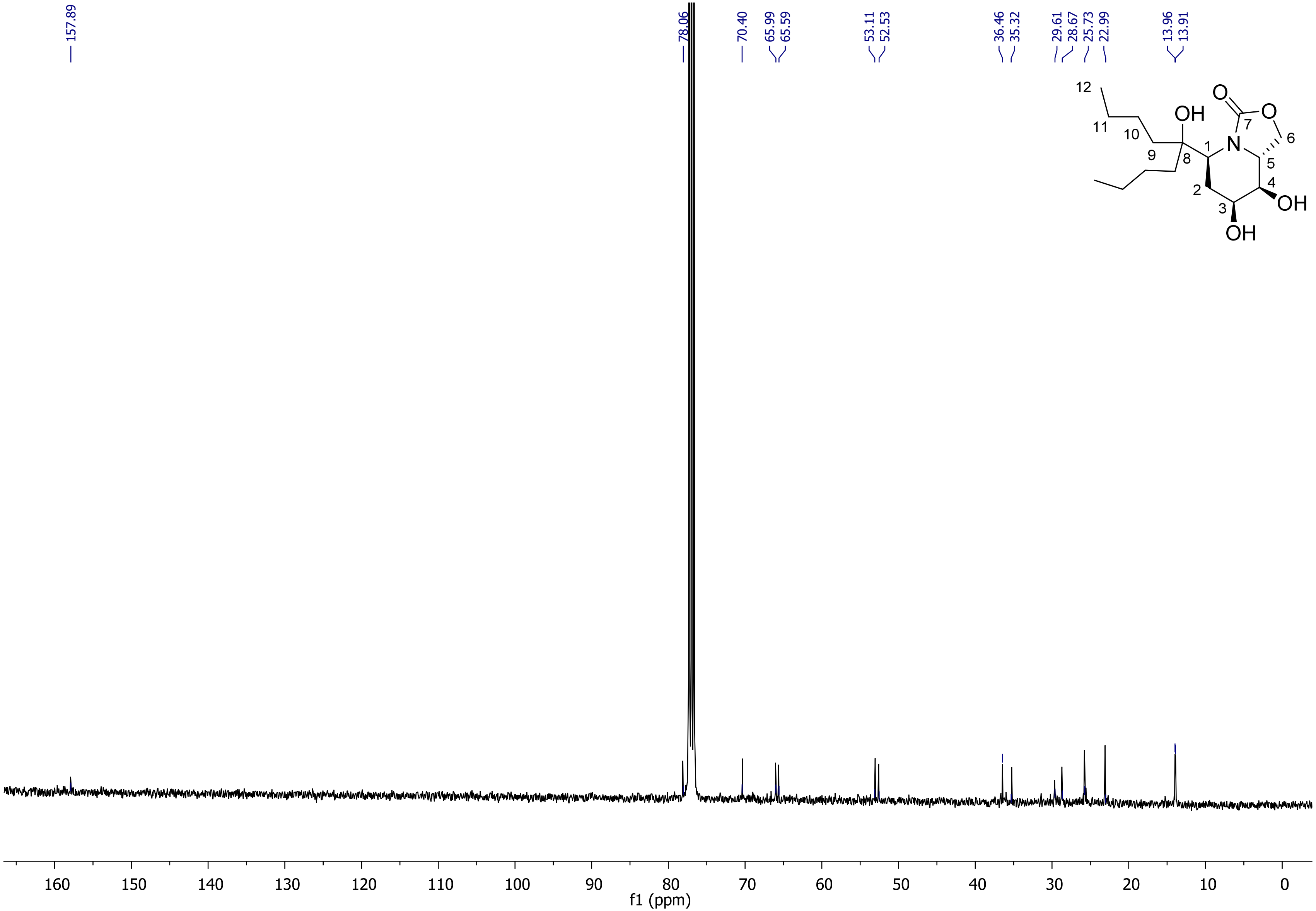

^{1}H NMR of compound **5-*endo*** (400 MHz, $CDCl_3$, 300K)

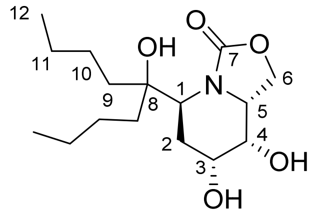

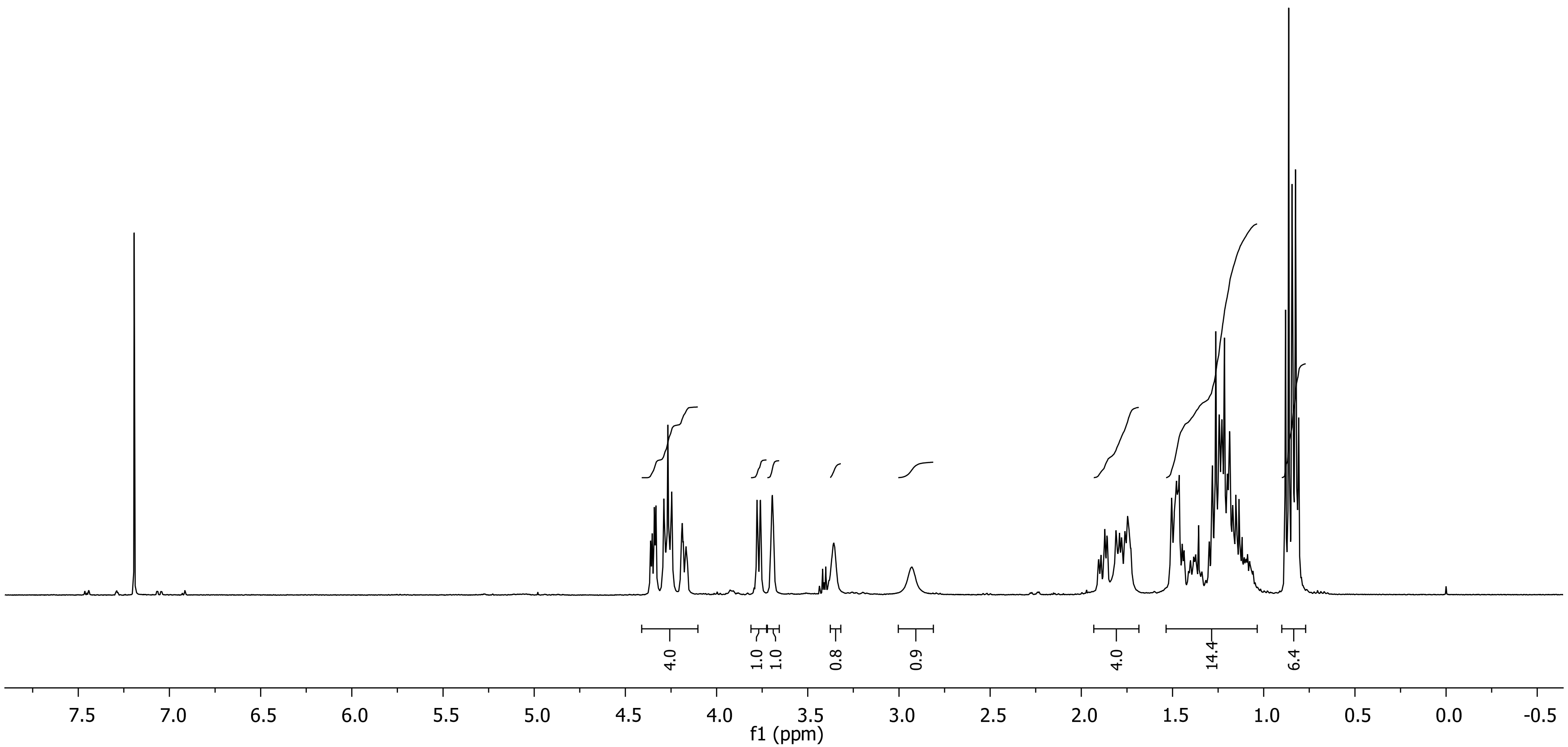

^{13}C NMR of compound 5-*endo* (100 MHz, $CDCl_3$, 300K)

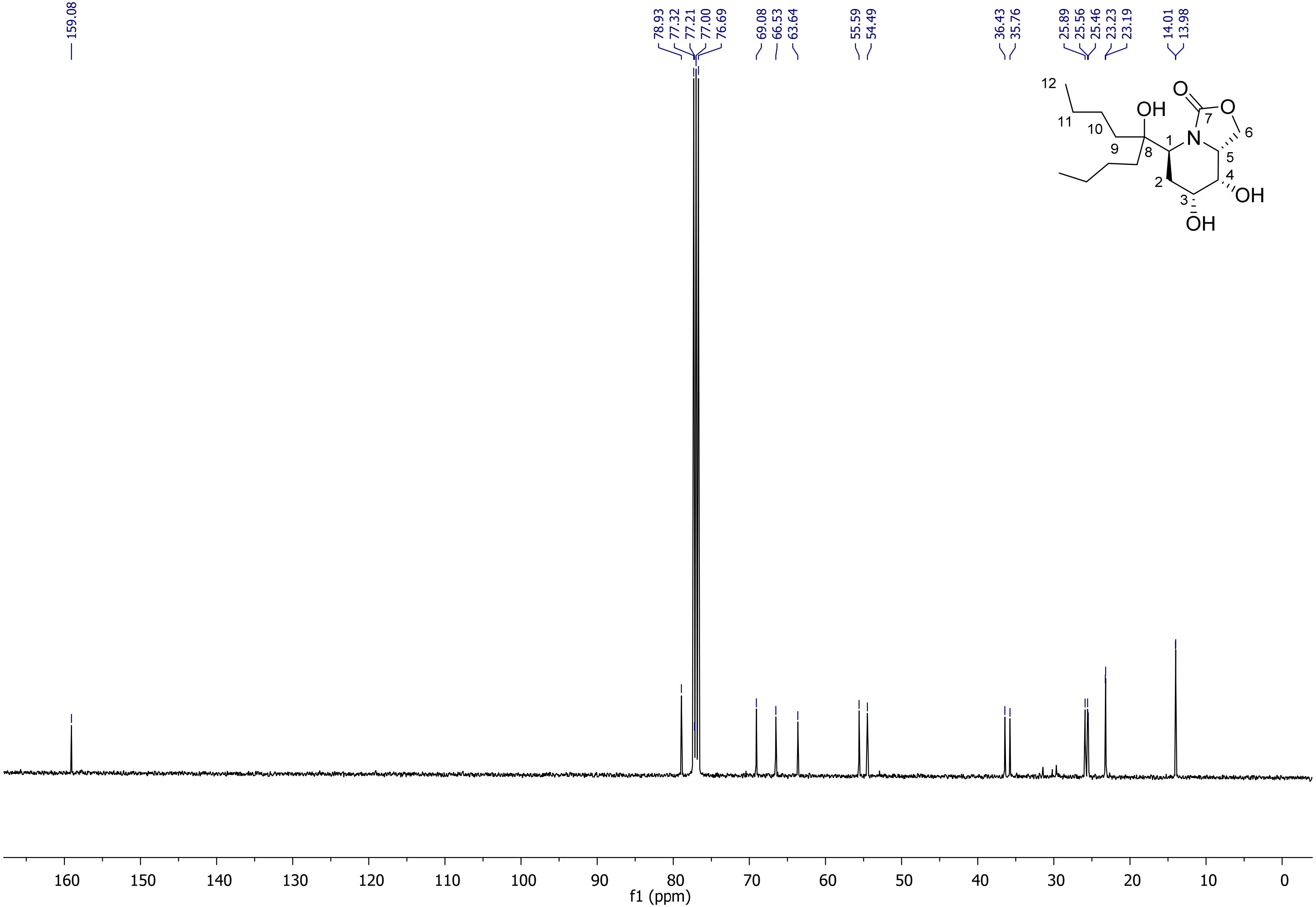

^{1}H NMR of compound **6-exo** (300 MHz, $CDCl_3$, 300K)

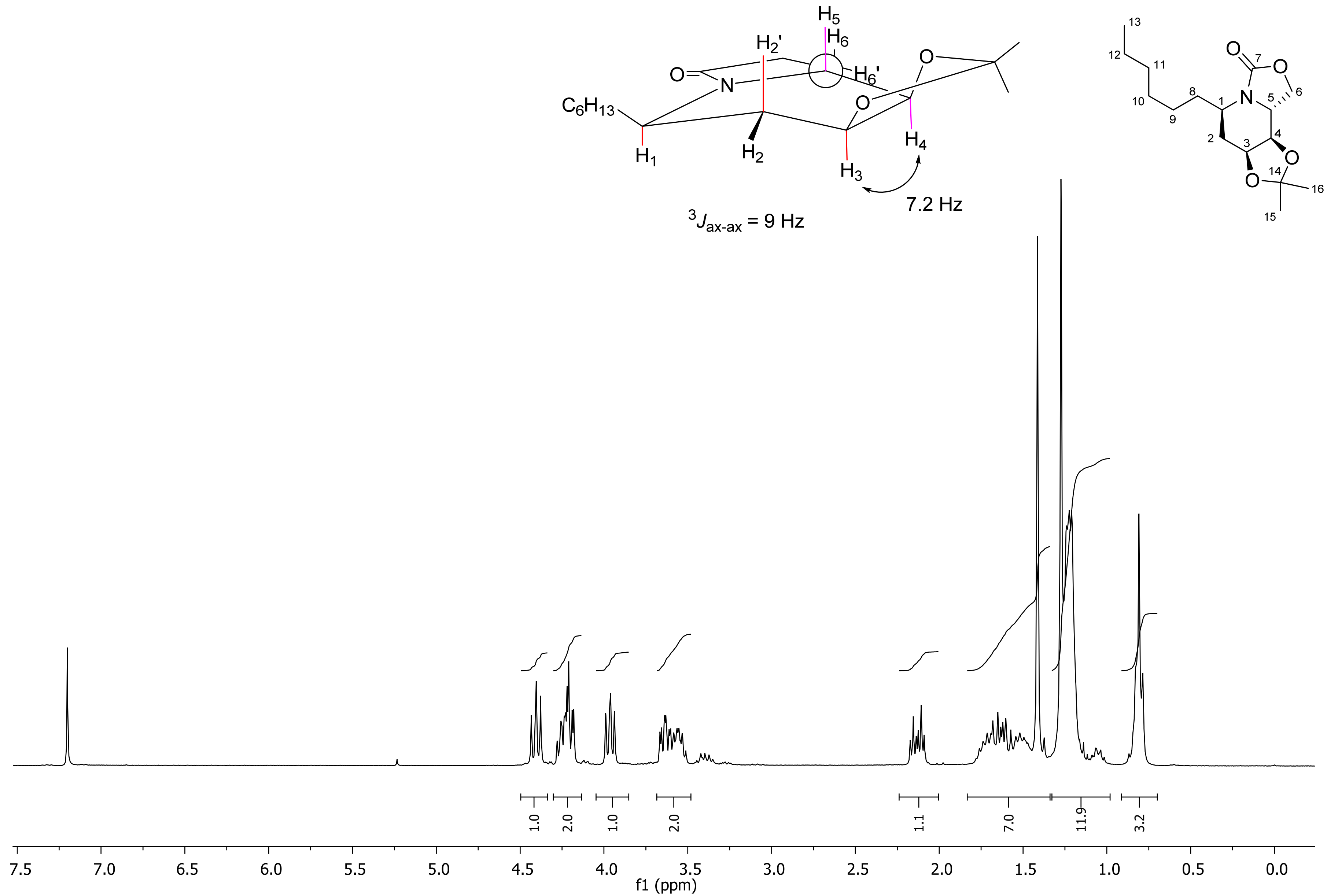

^{13}C NMR of compound **6-*exo*** (75 MHz, $CDCl_3$, 300K)

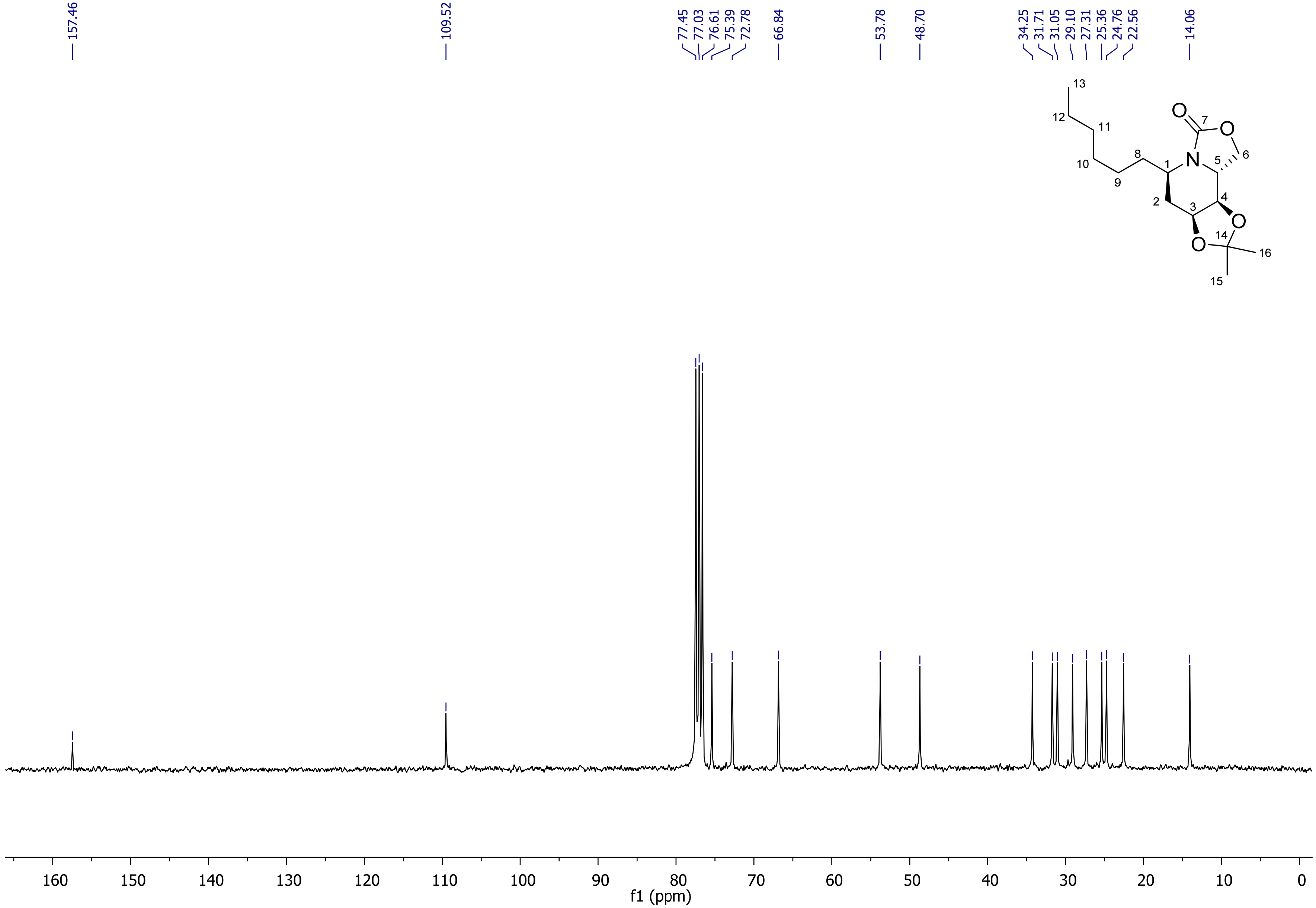

^{1}H NMR of compound **6-*endo*** (300 MHz, $CDCl_3$, 300K)

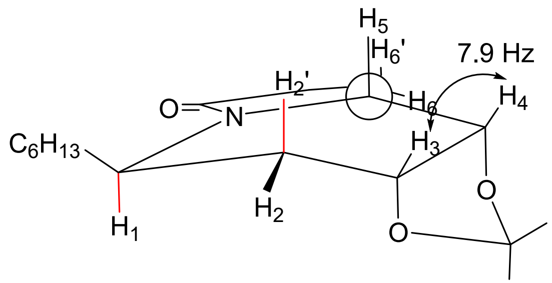

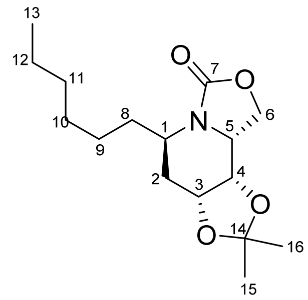

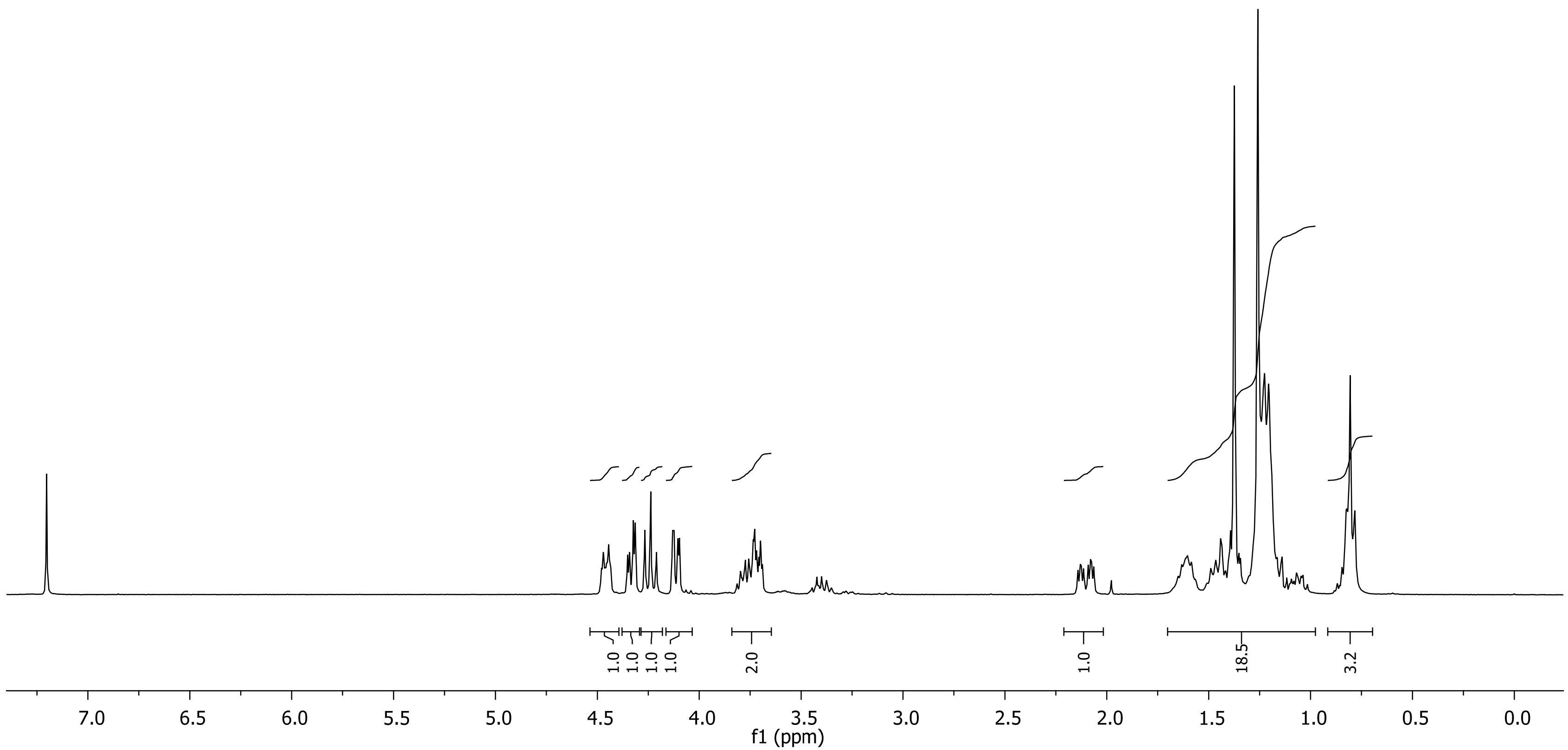

^{13}C NMR of compound **6-*endo*** (75 MHz, $CDCl_3$, 300K)

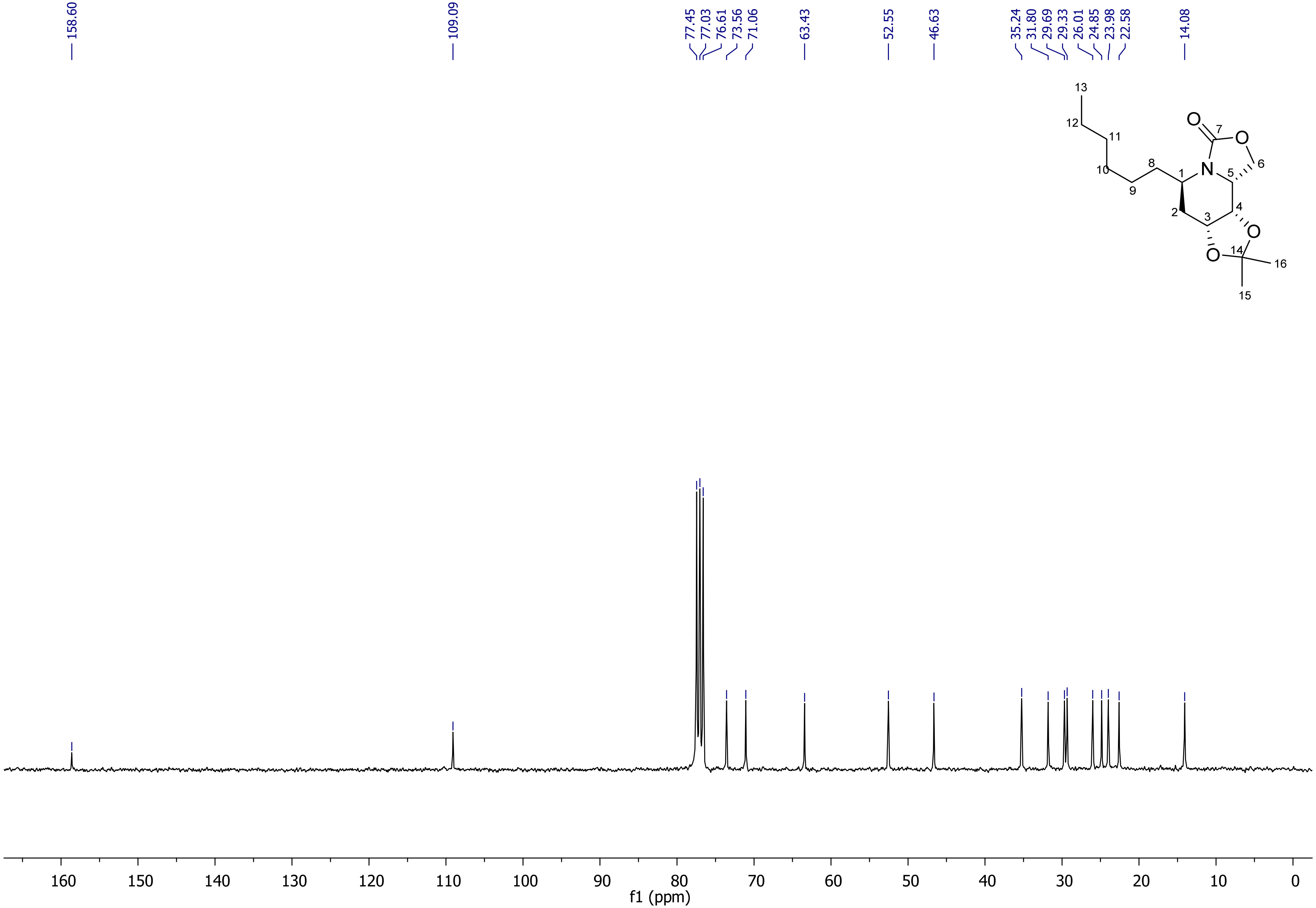

^{1}H NMR of compound **9** (400 MHz, $CDCl_3$, 300K)

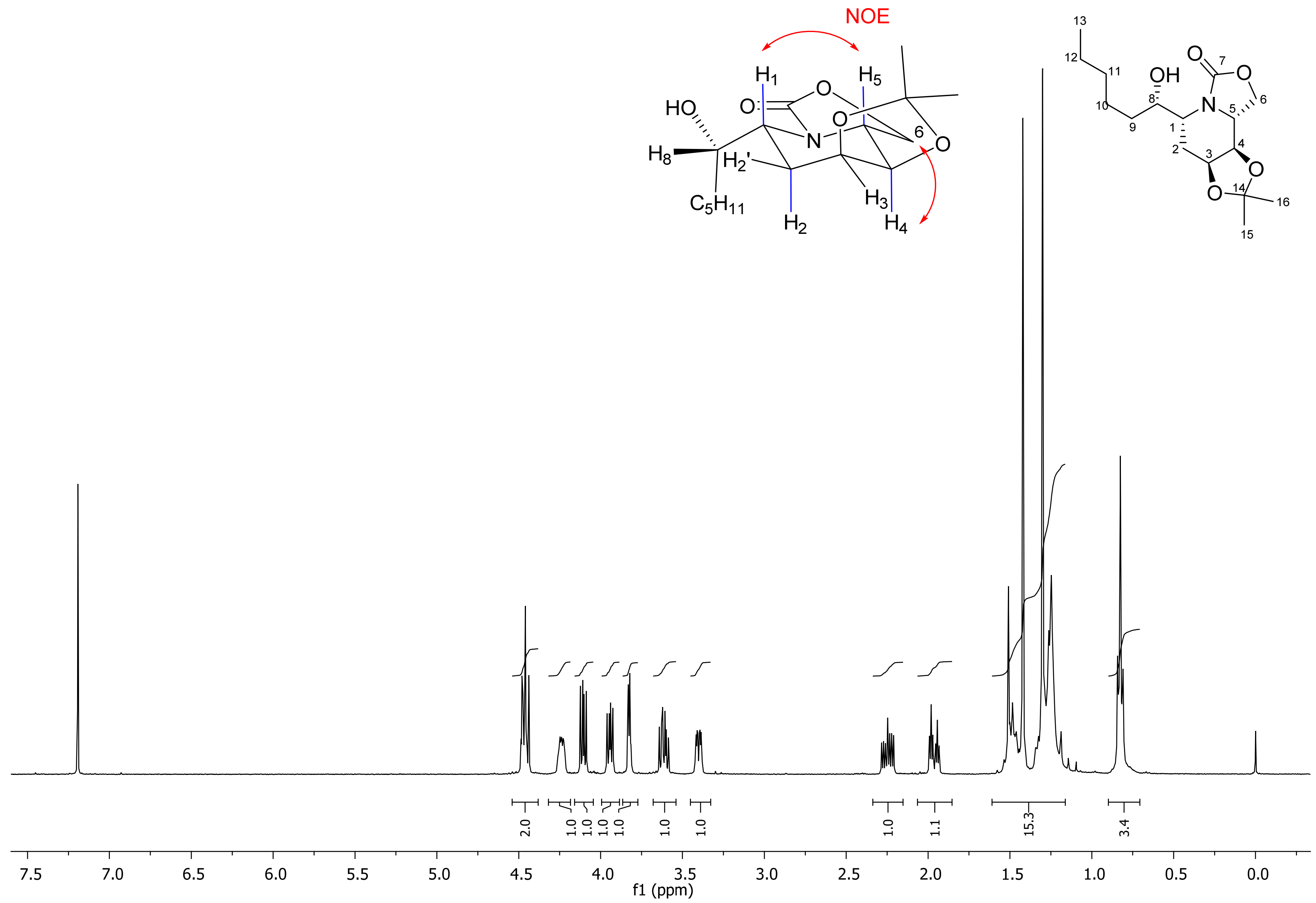

^{13}C NMR of compound **9** (100 MHz, $CDCl_3$, 300K)

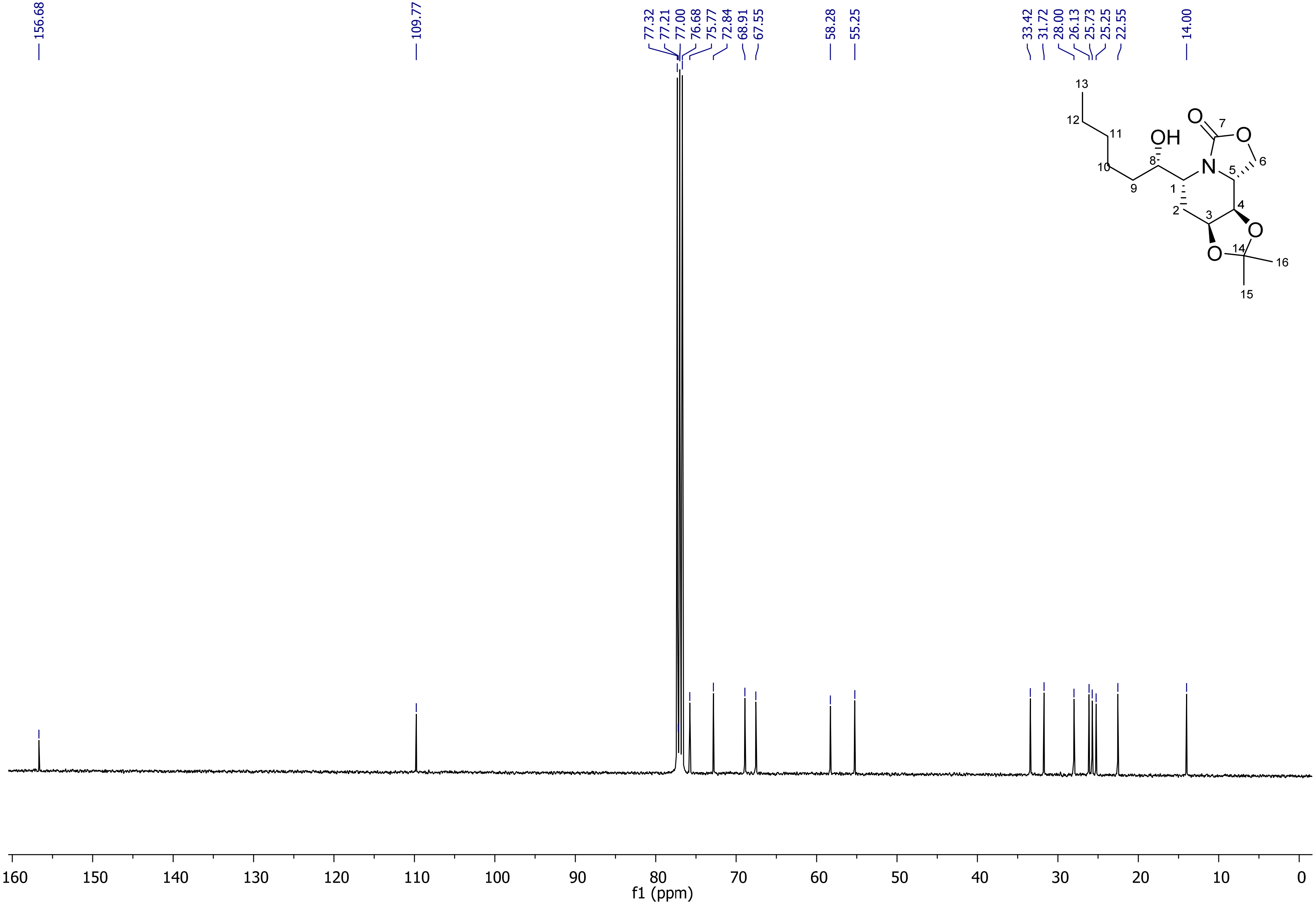

^{1}H NMR of compound **10** (400 MHz, $CDCl_3$, 300K)

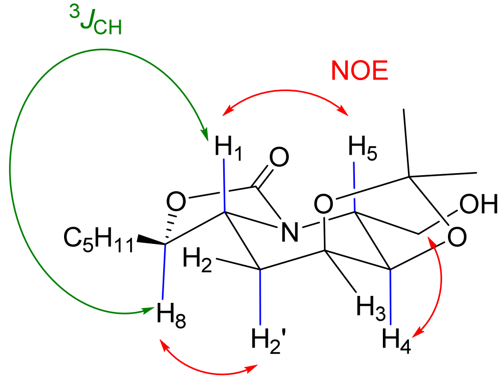

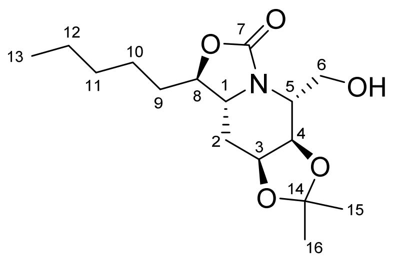

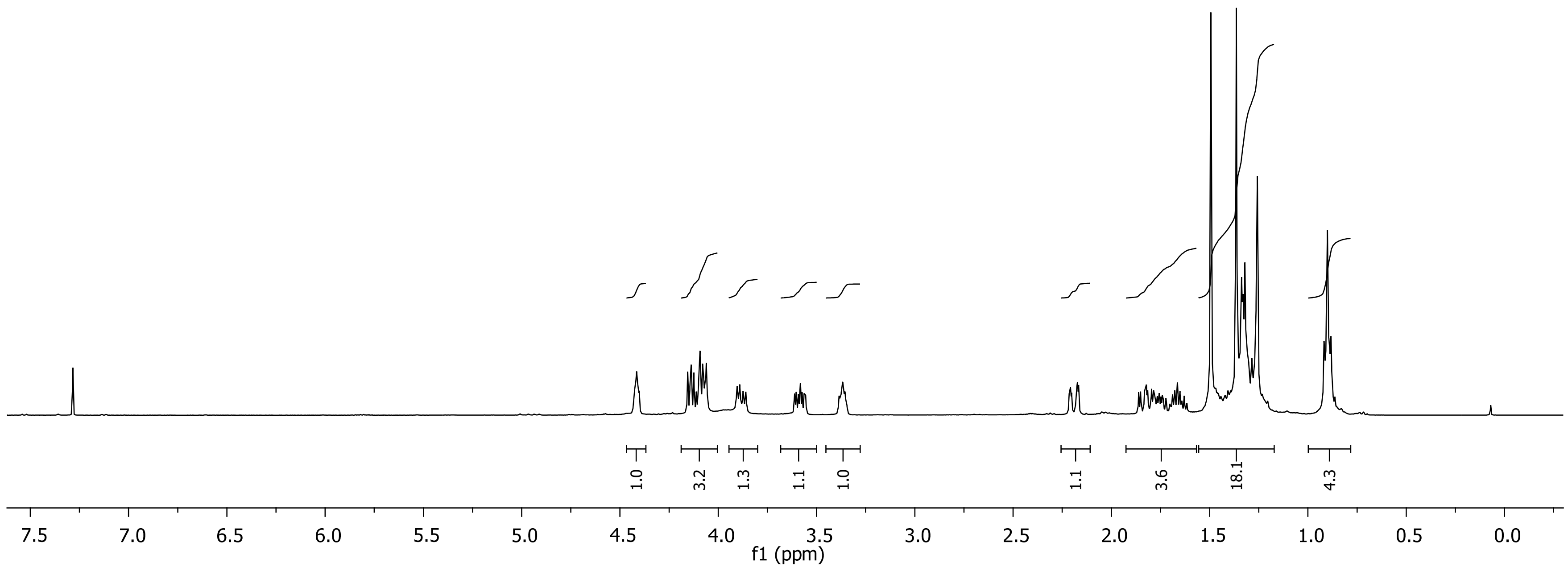

^{13}C NMR spectrum of compound **10** (100 MHz, $CDCl_3$, 300K)

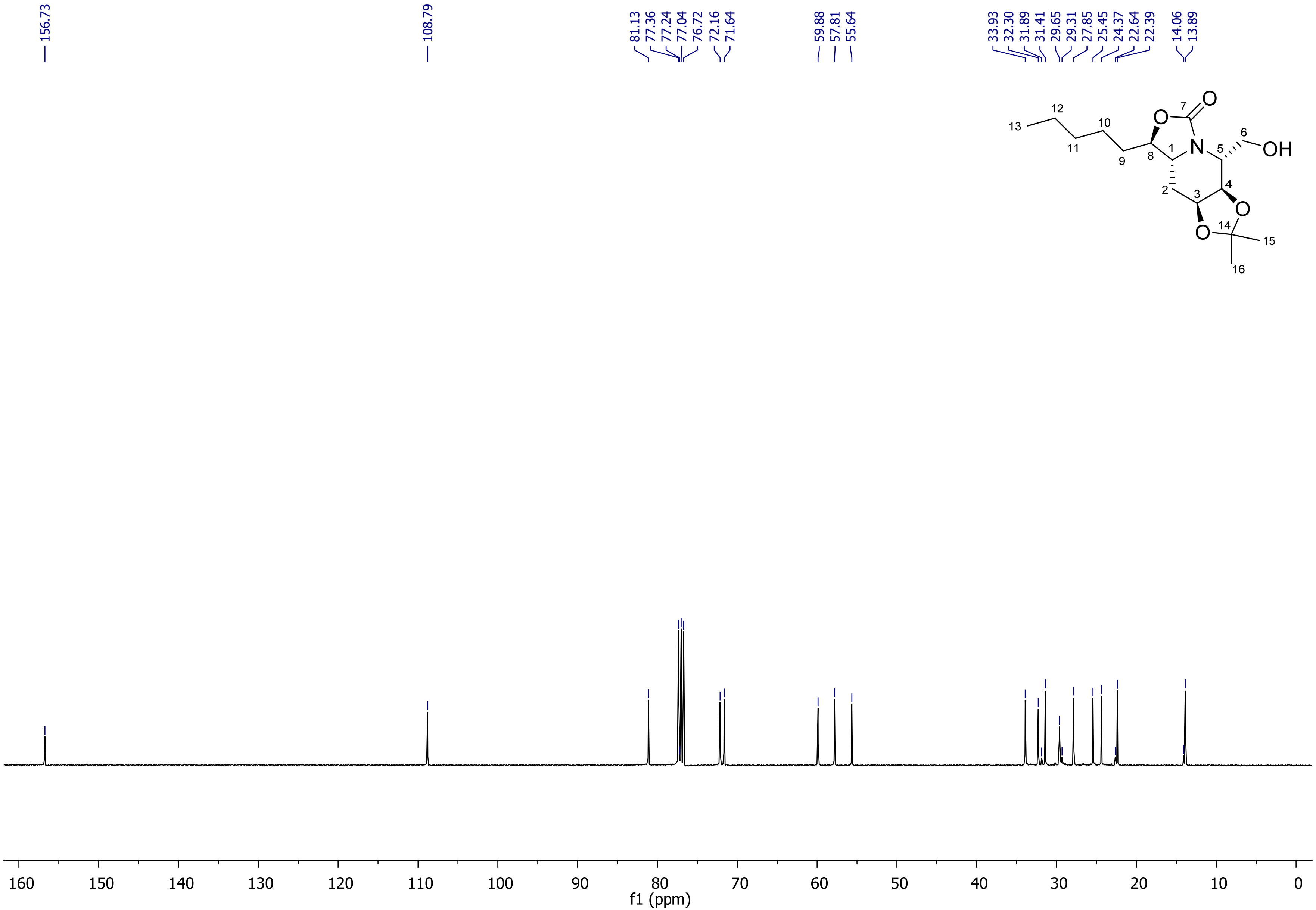

[1]H NMR of compound **11** (400 MHz, $CDCl_3$, 300K)

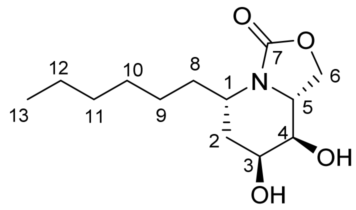

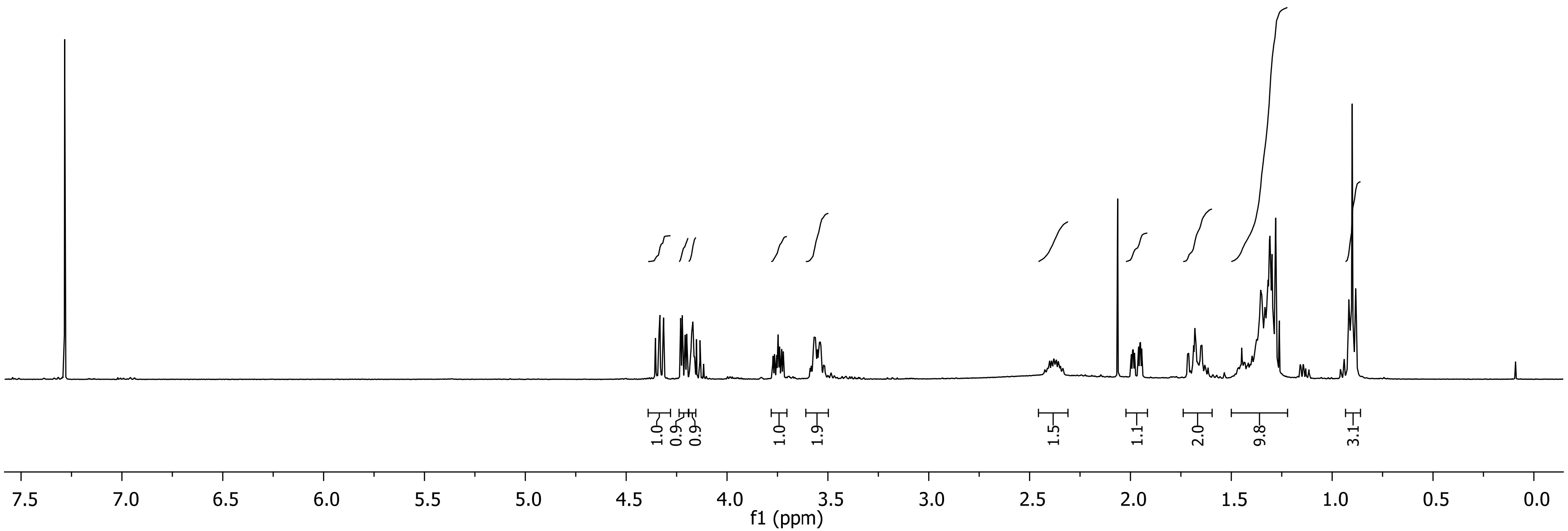

^{13}C NMR compound **11** (100 MHz, $CDCl_3$, 300K)

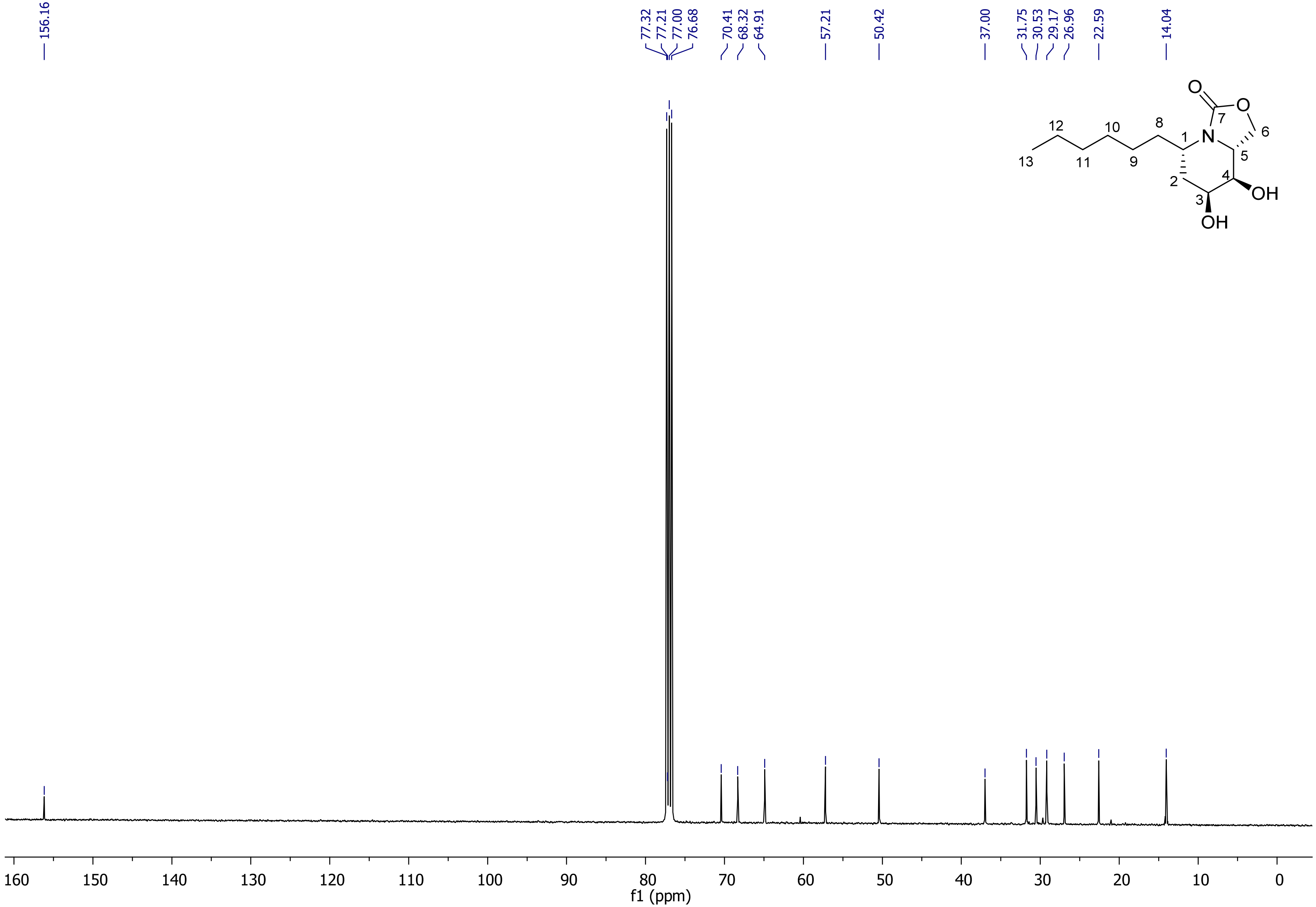

[1]H NMR of compound **12** (300 MHz, $CDCl_3$, 300K)

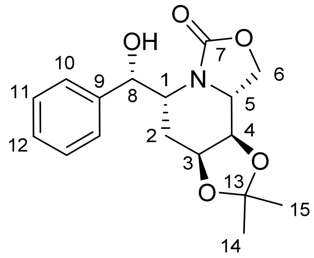

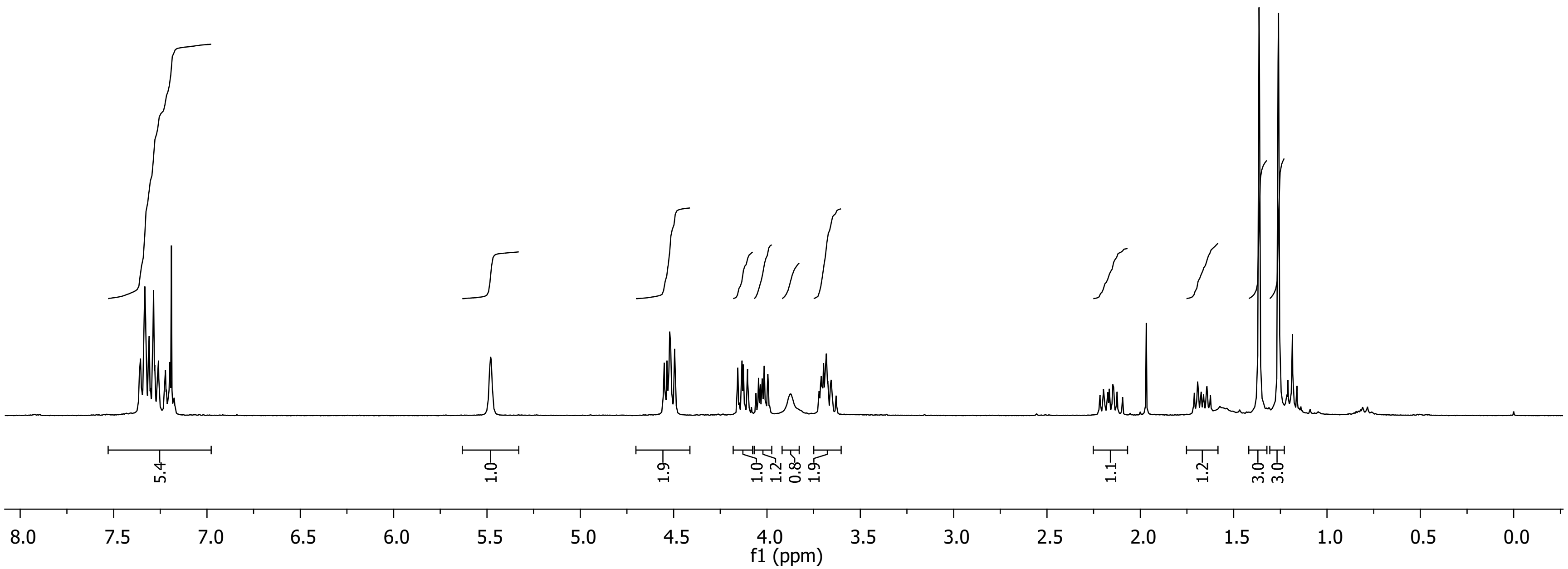

^{13}C NMR of compound **12** (75 MHz, $CDCl_3$, 300K)

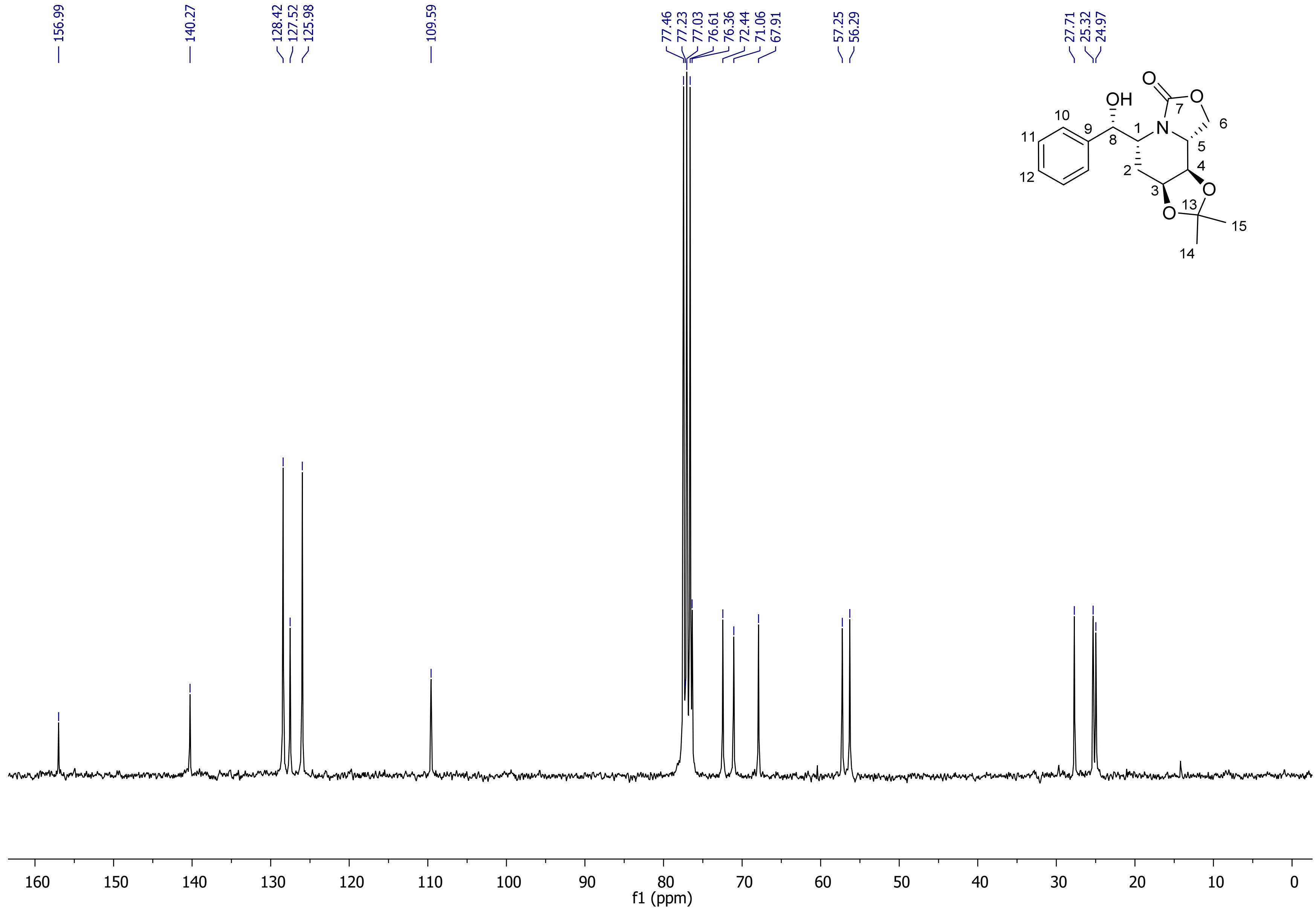

^{1}H NMR of compound **13** in (300 MHz, $CDCl_3$, 300K)

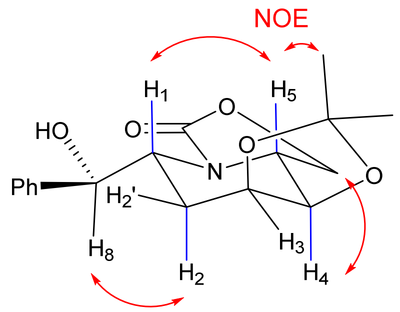

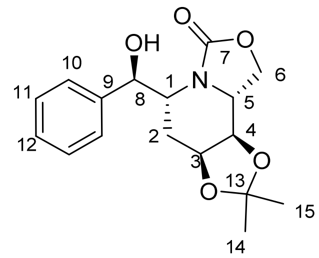

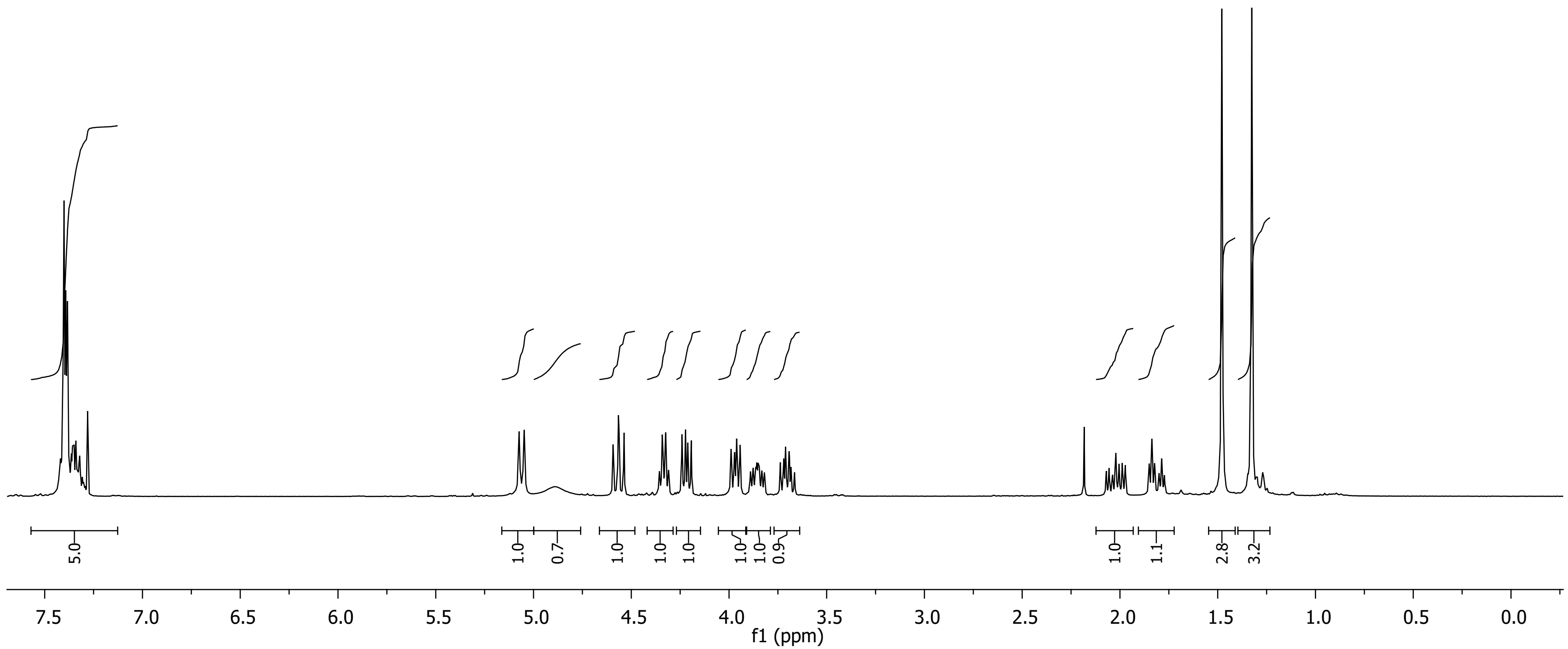

^{13}C NMR of compound **13** (75 MHz, $CDCl_3$, 300K)

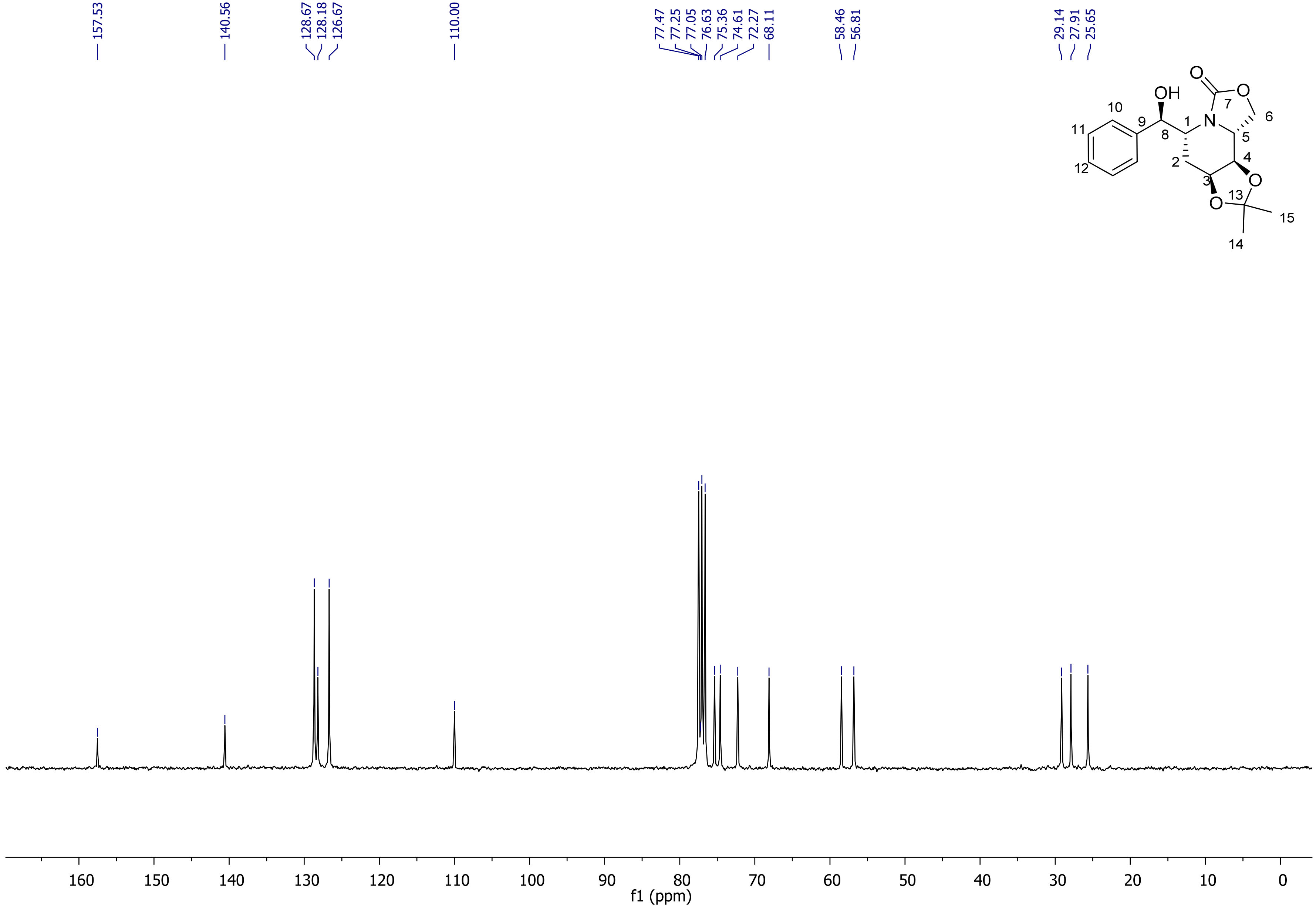

^{1}H NMR of compound **14** (400 MHz, $CDCl_3$, 300K)

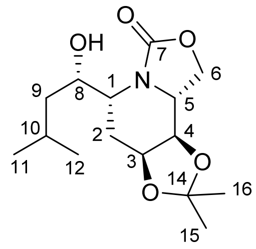

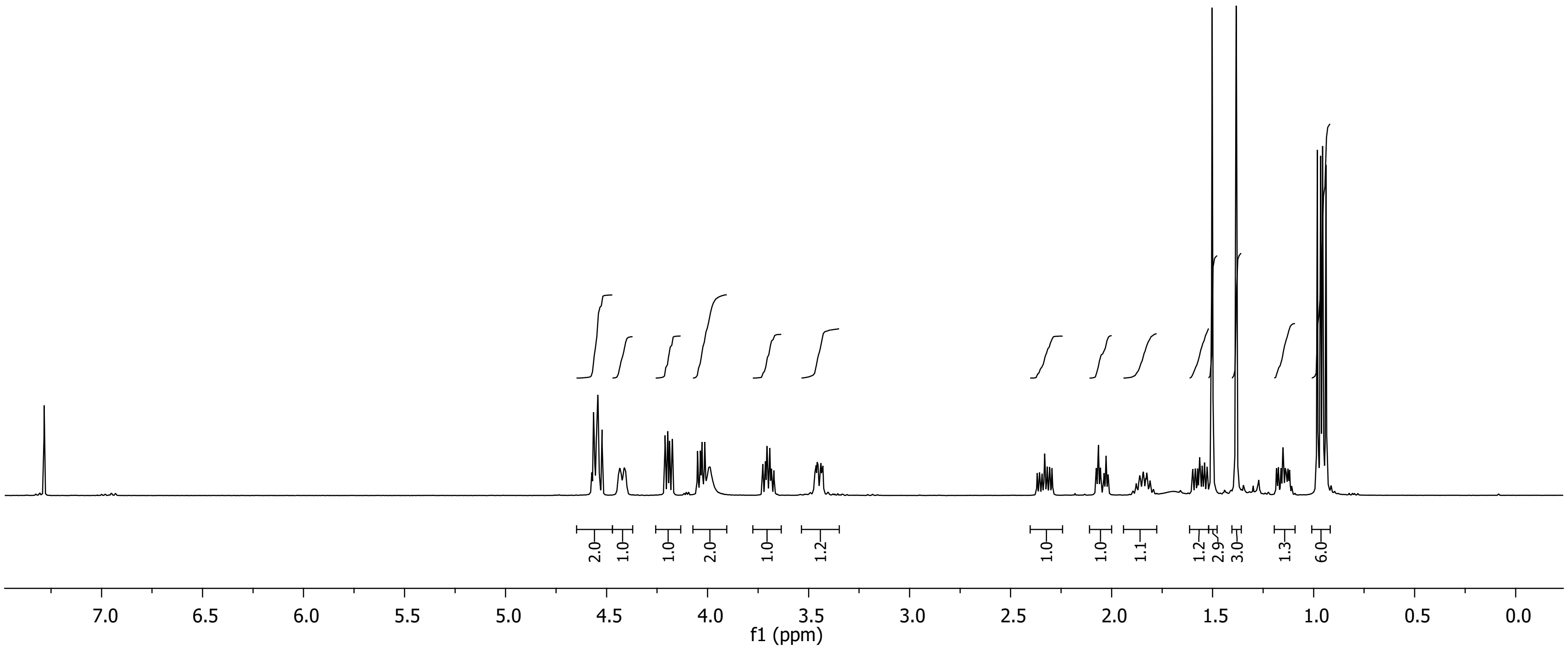

^{13}C NMR of compound **14** (100 MHz, $CDCl_3$, 300K)

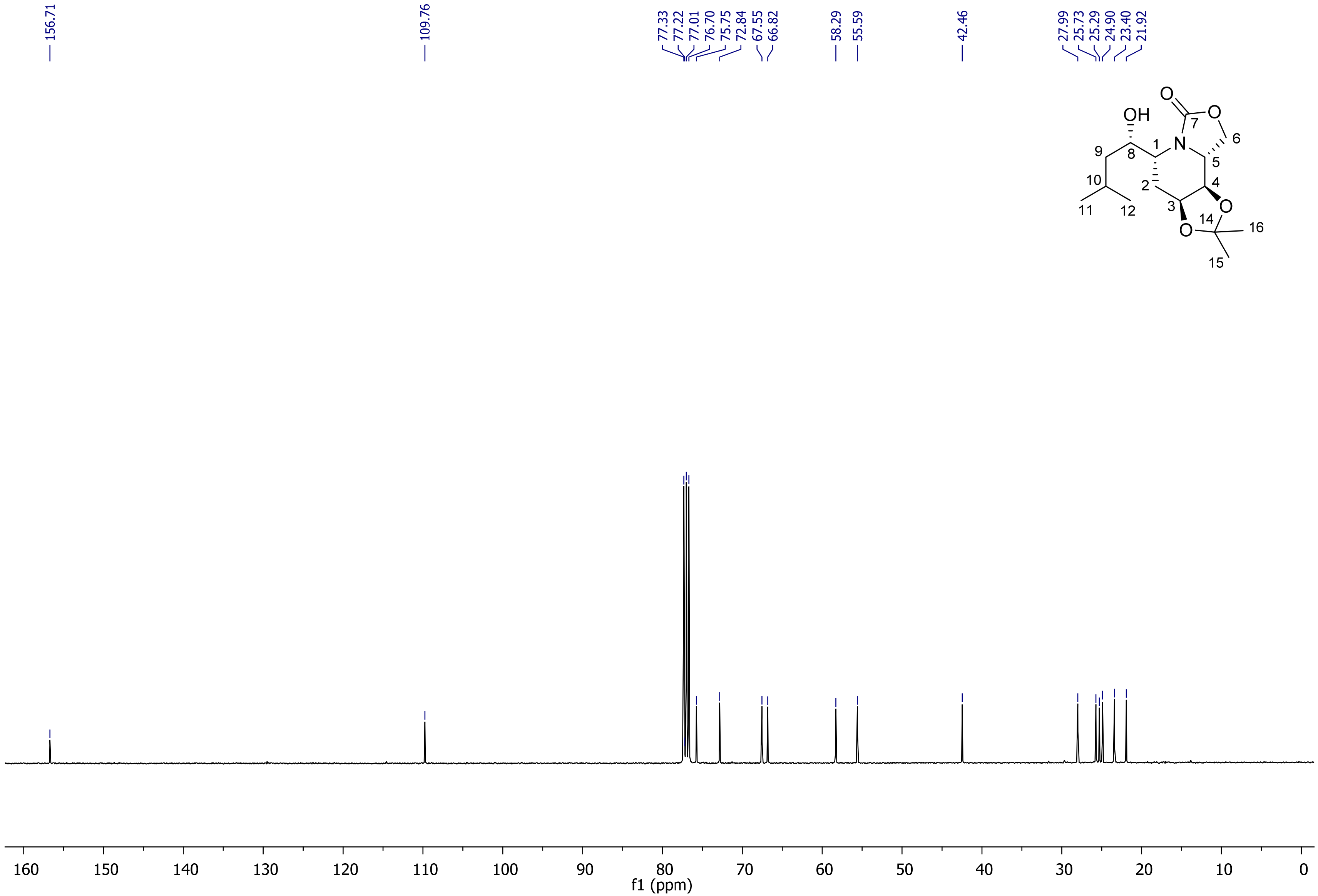

^{1}H NMR of compound **15** (400 MHz, CD_3OD, 300K)

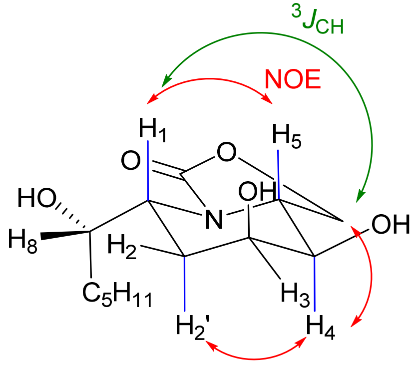

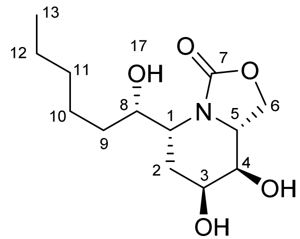

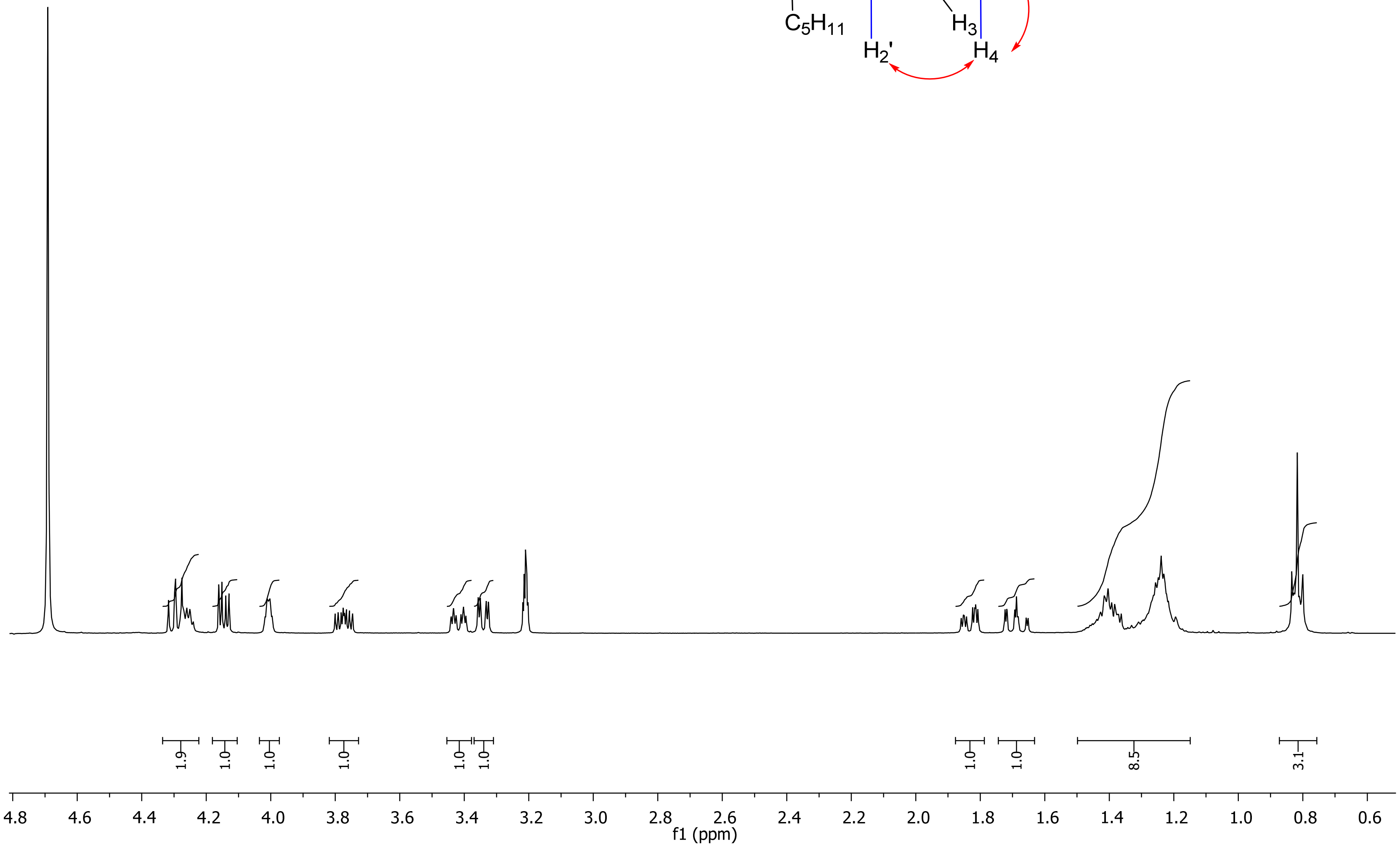

^{13}C NMR of compound **15** (100 MHz, CD_3OD, 300K)

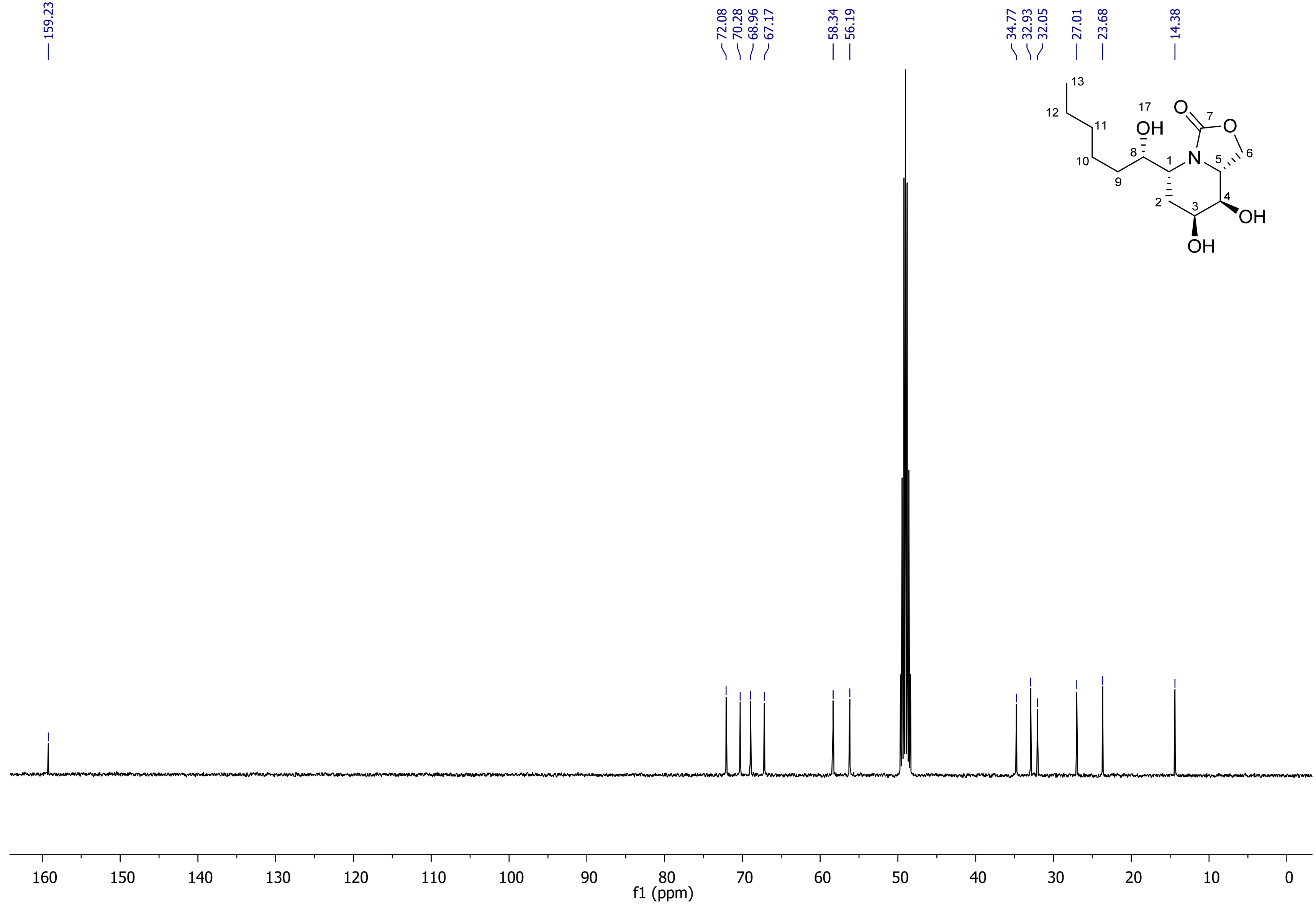

^{1}H NMR of compound **16** (400 MHz, CD_3OD, 300K)

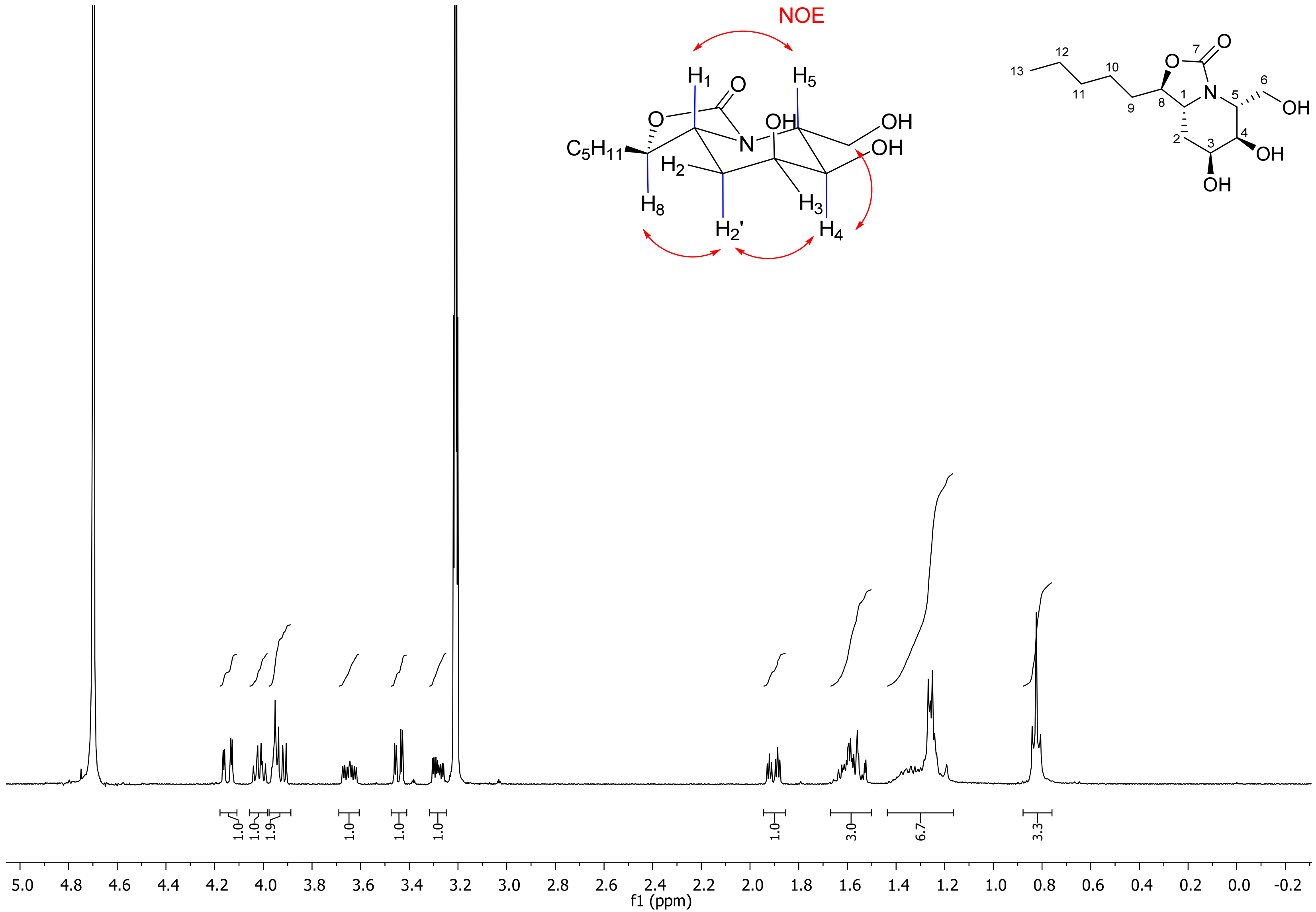

^{13}C NMR of compound **16** (100 MHz, CD_3OD, 300K)

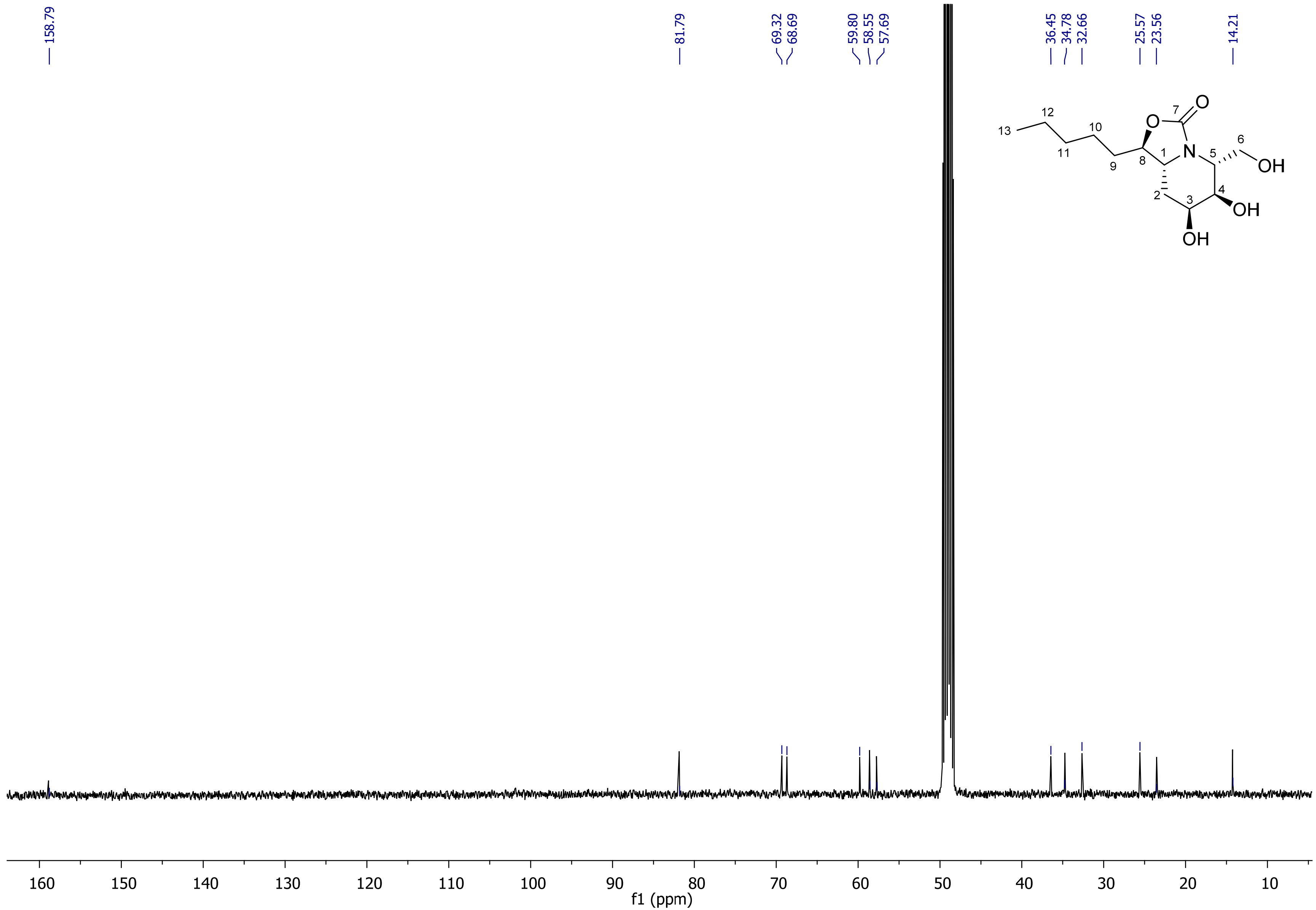

[1]H NMR of compound **17** (*dr* = 67/33) in (300 MHz, $CDCl_3$, 300K)

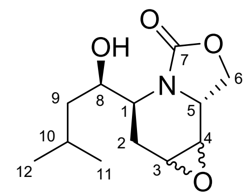

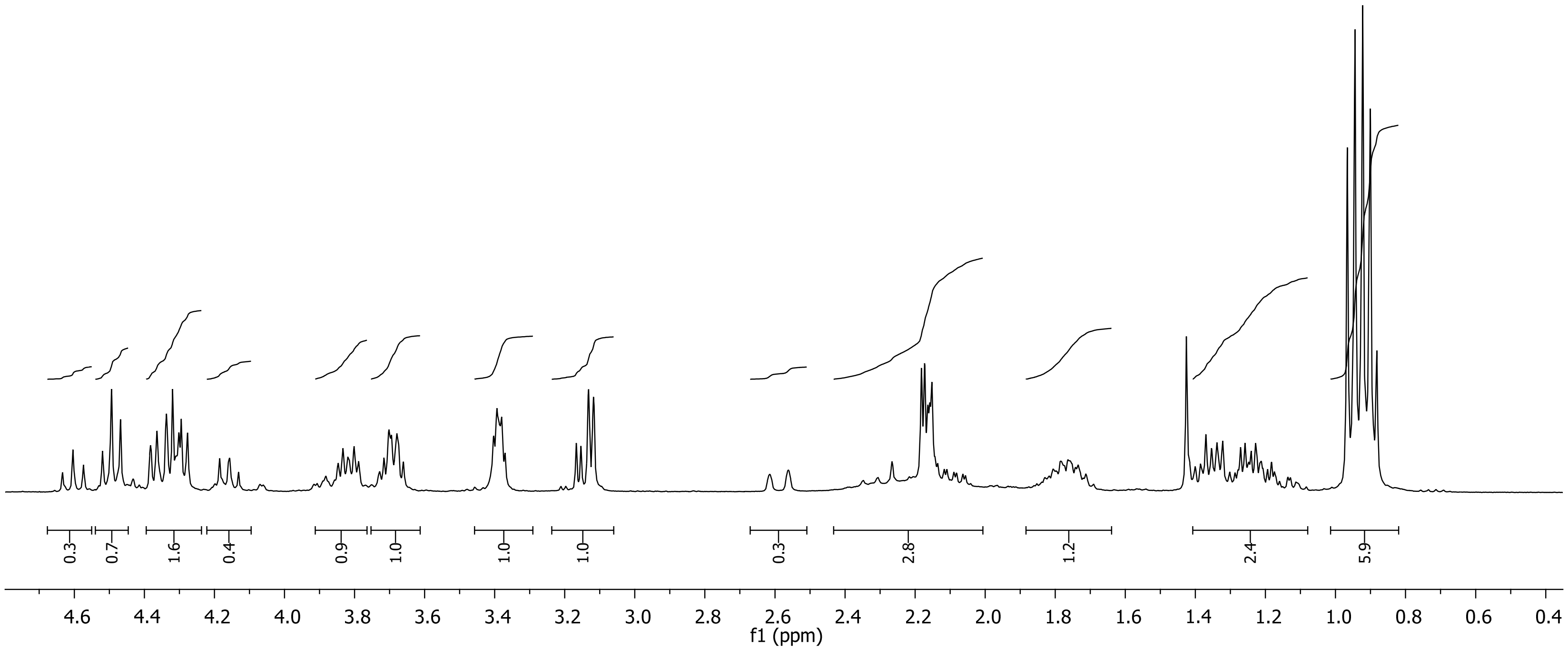

^{13}C NMR of compound **17** (*dr* = 67/33) (75 MHz, $CDCl_3$, 300K)

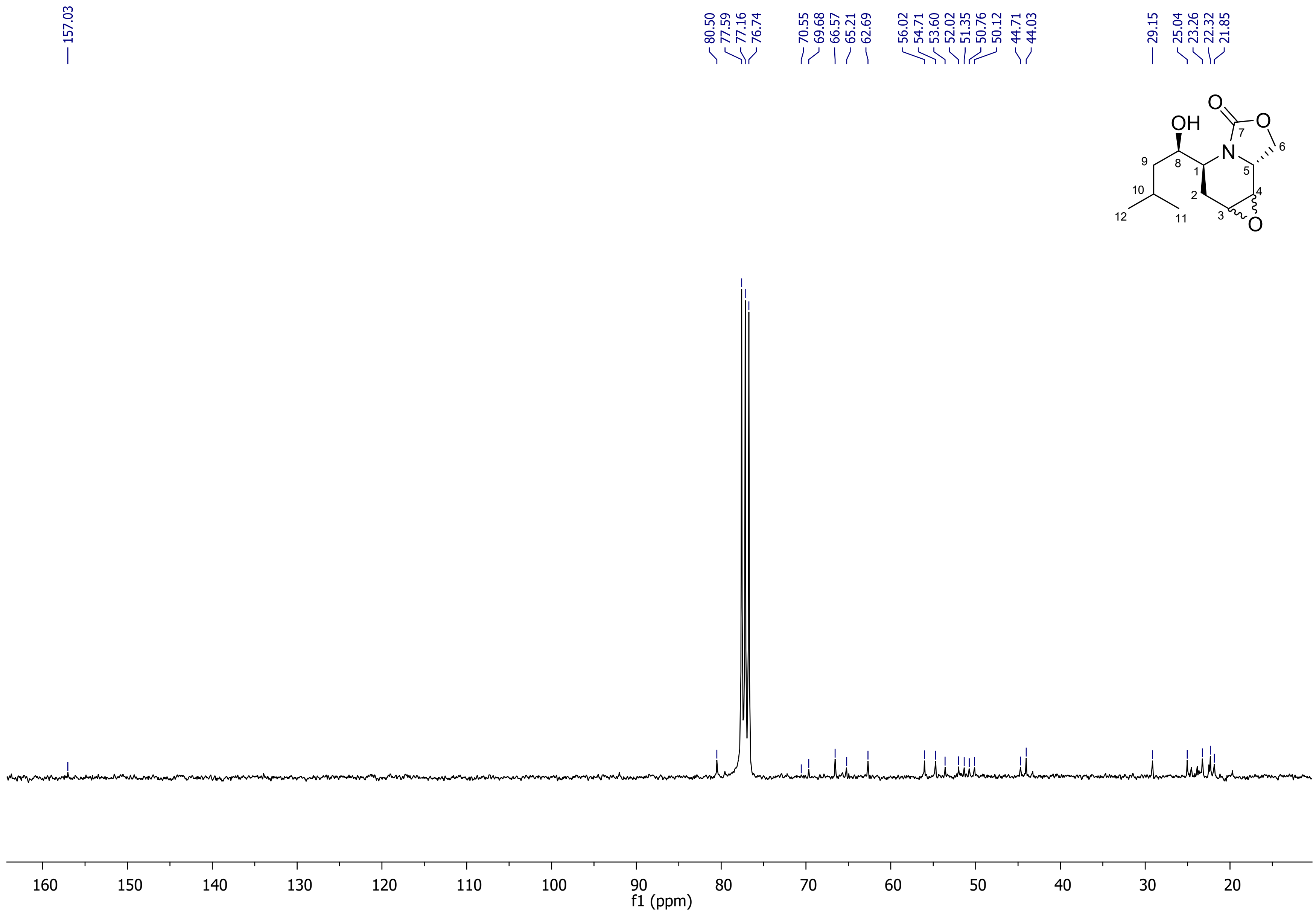

^{1}H NMR of compound **18** in (300 MHz, $CDCl_3$, 300K)

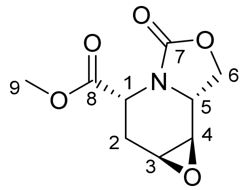

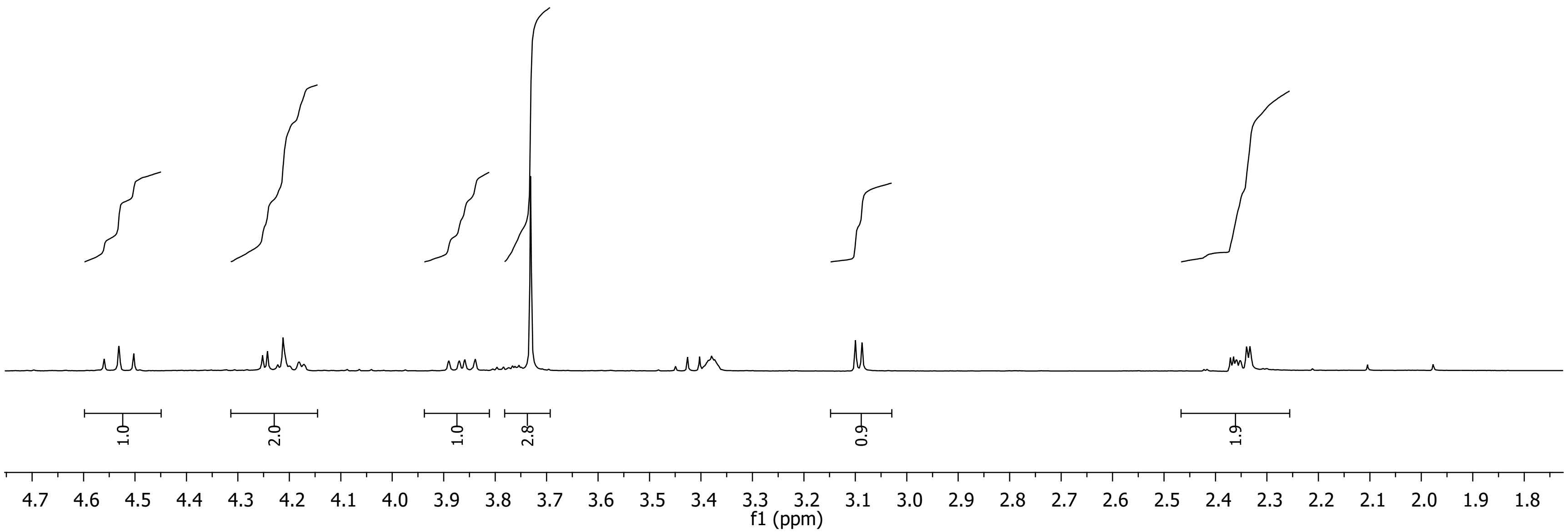

^{13}C NMR of compound **18** (75 MHz, $CDCl_3$, 300K)

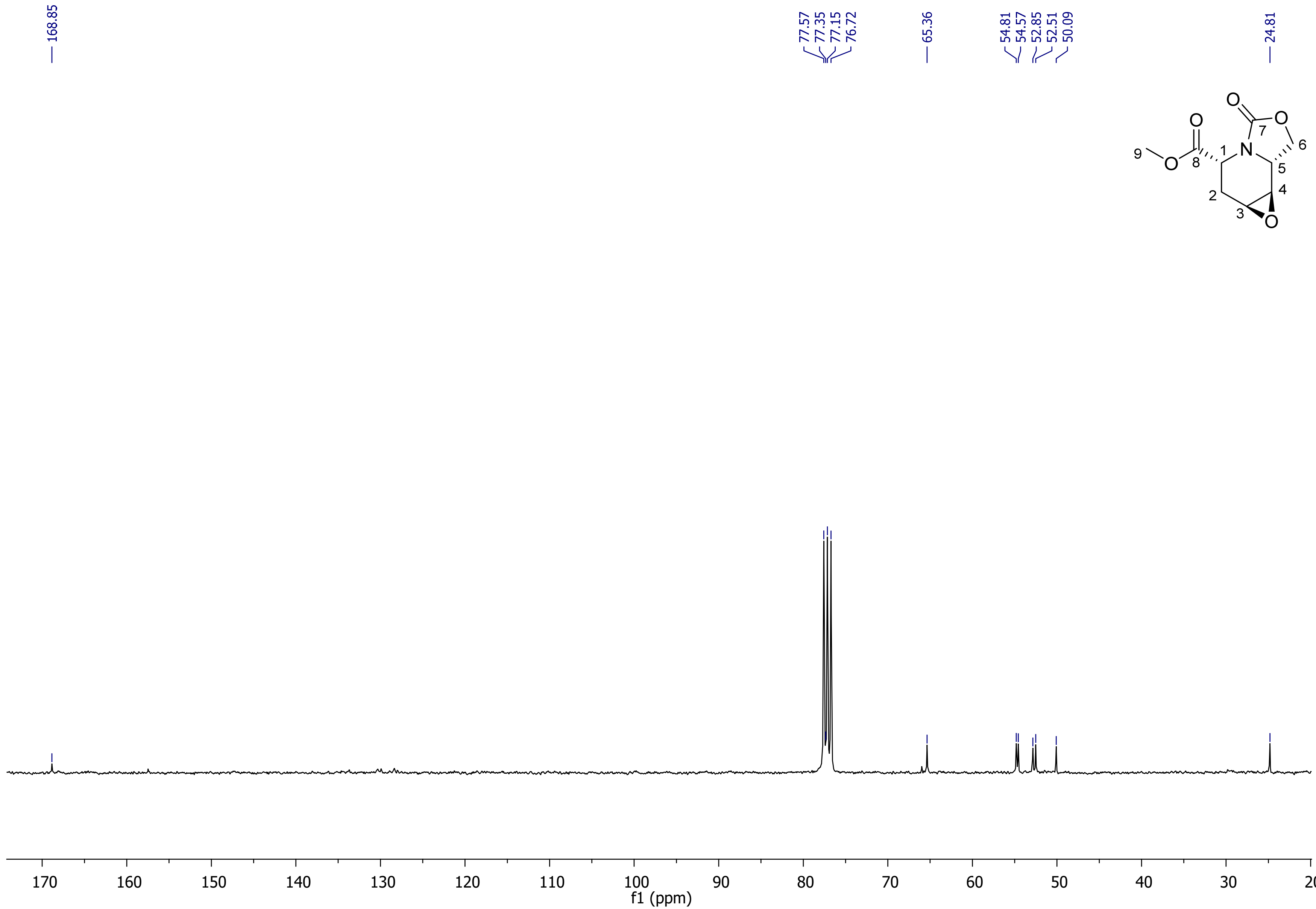

^{1}H NMR of compound **19’** (400 MHz, $CDCl_3$, 300K) obtained from **19**-*exo*

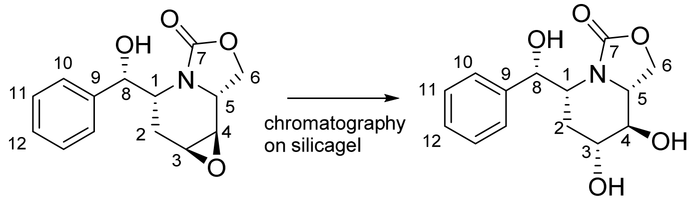

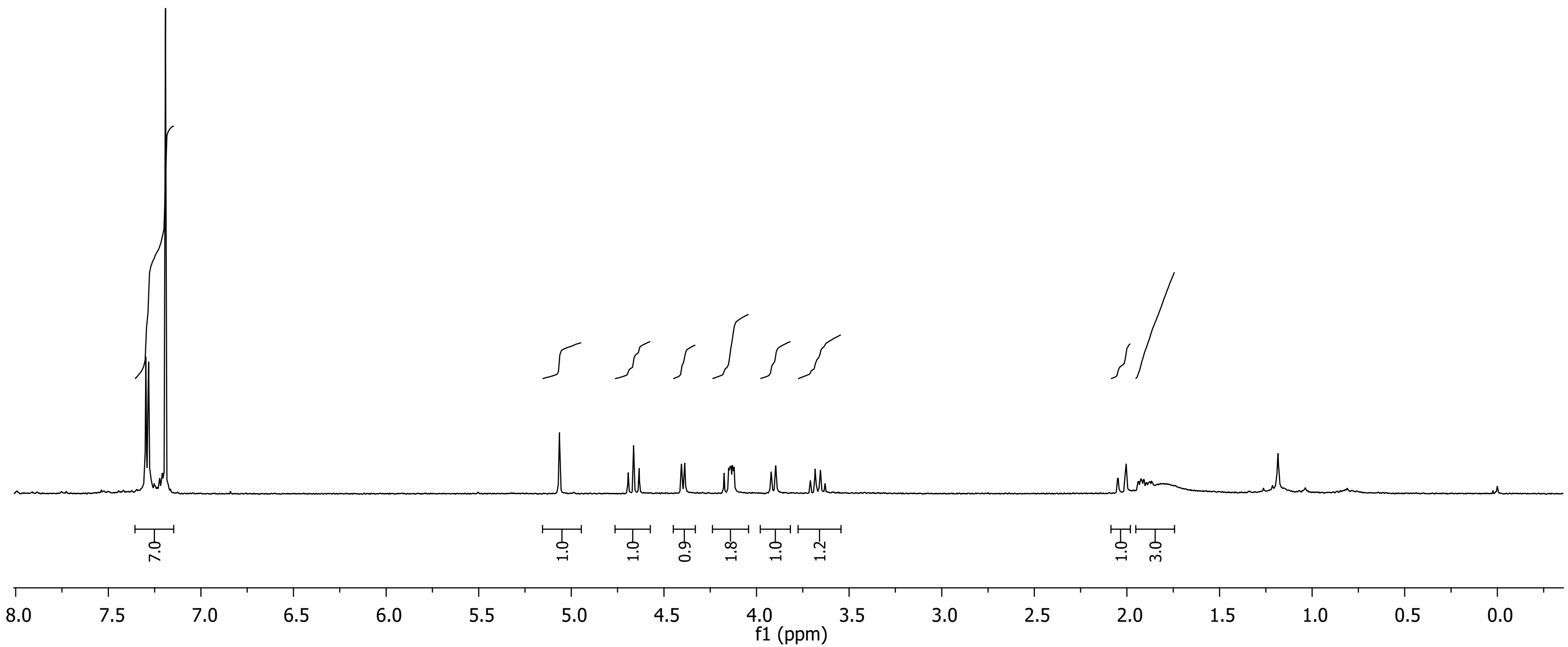

[13]C NMR of compound **19’** (100 MHz, $CDCl_3$, 300K) obtained from **19**-*exo*

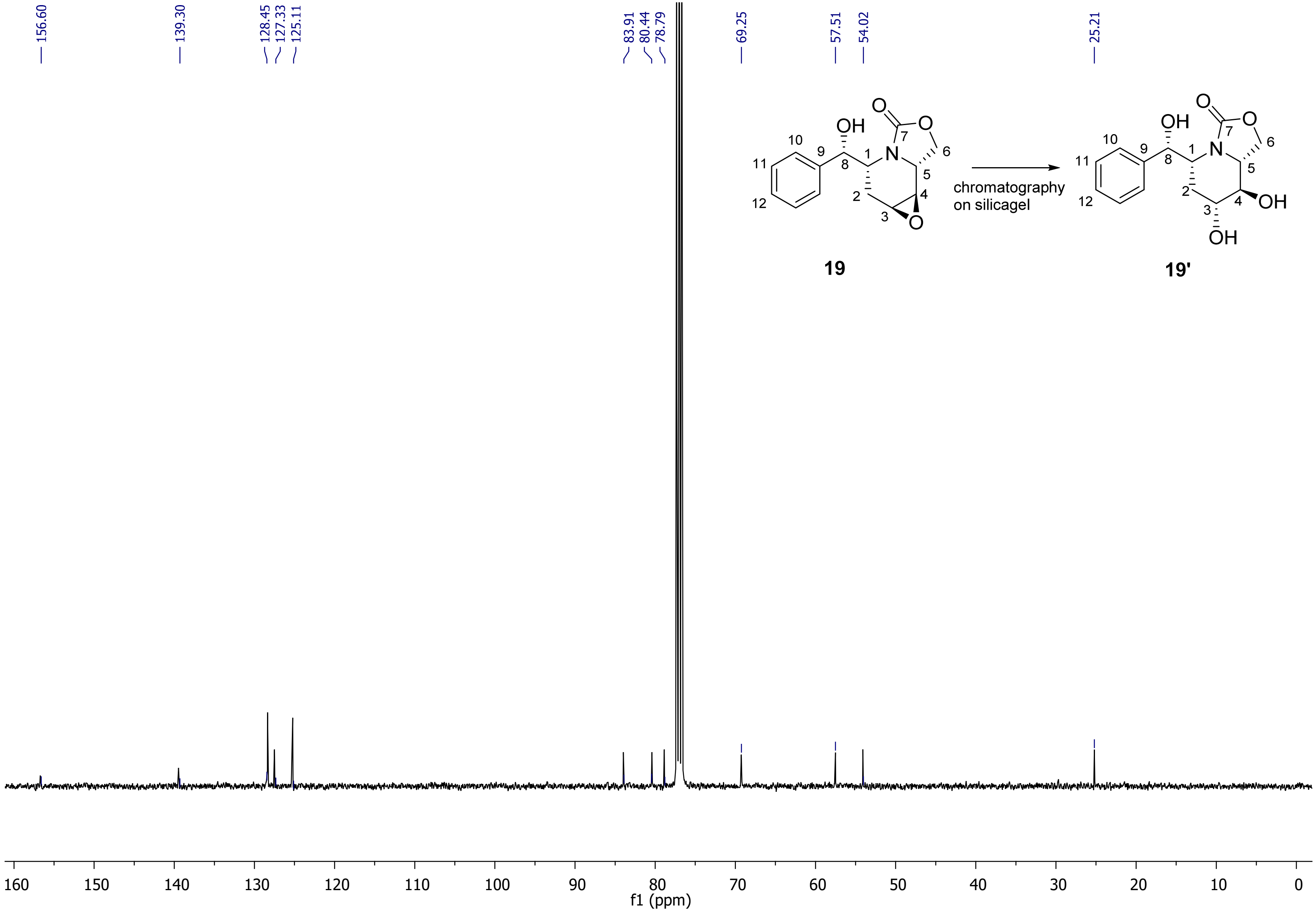

^{1}H NMR compound **19-*endo*** (300 MHz, $CDCl_3$, 300K)

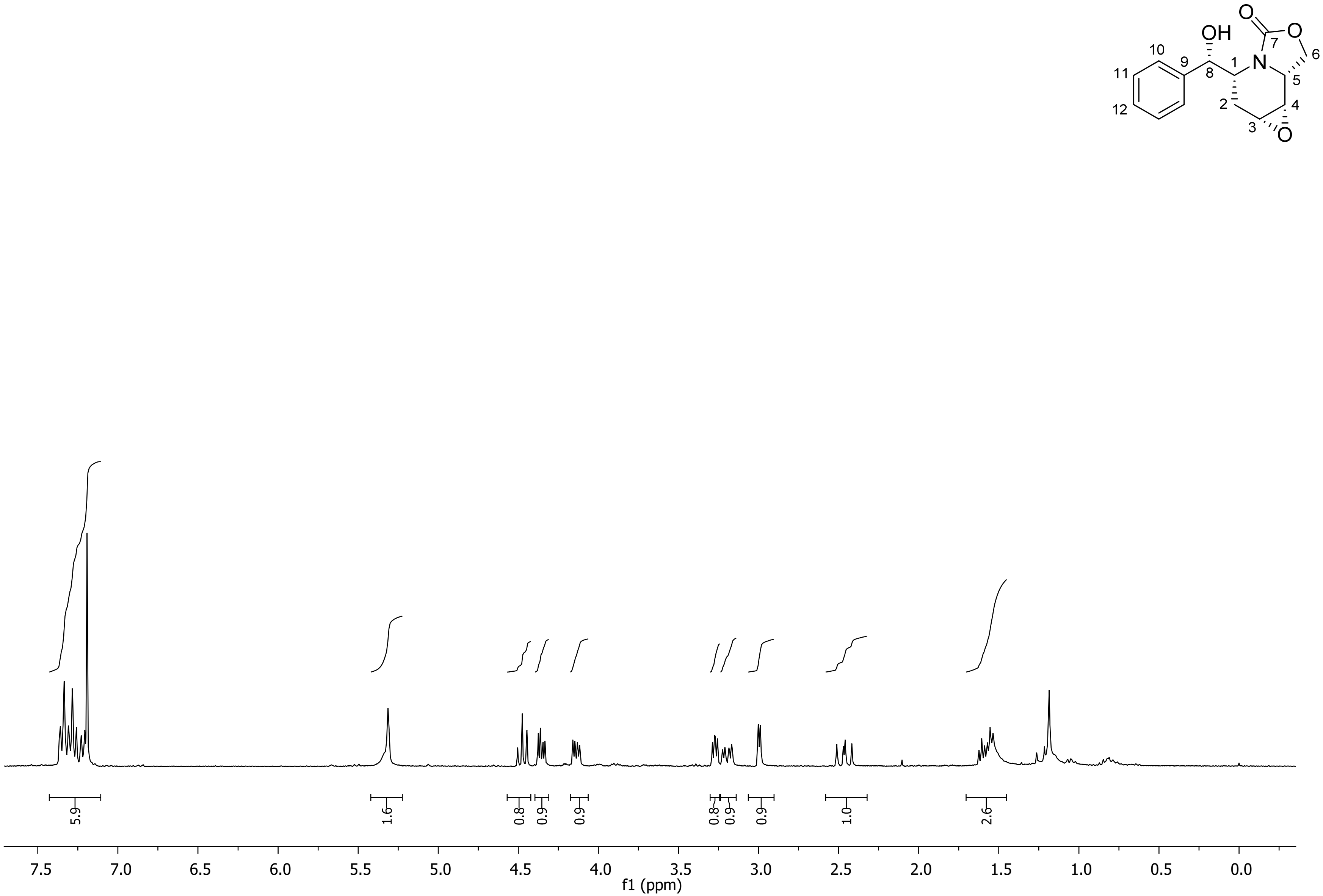

^{13}C NMR compound **19**-*endo* (75 MHz, $CDCl_3$, 300K)

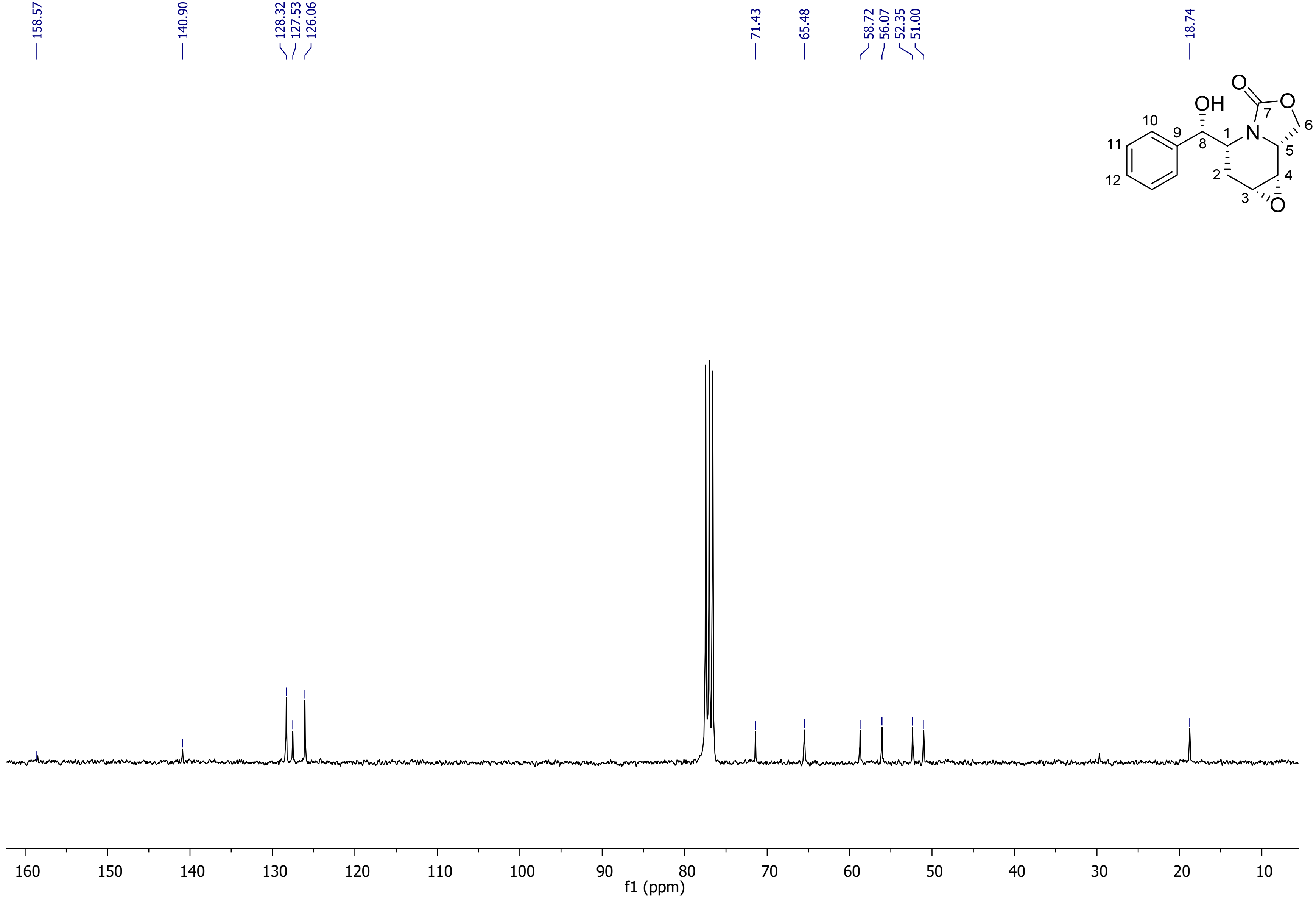

^{1}H NMR of compound **20-*exo*** (400 MHz, $CDCl_3$, 300K)

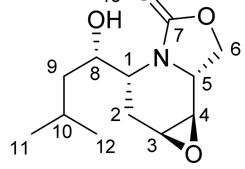

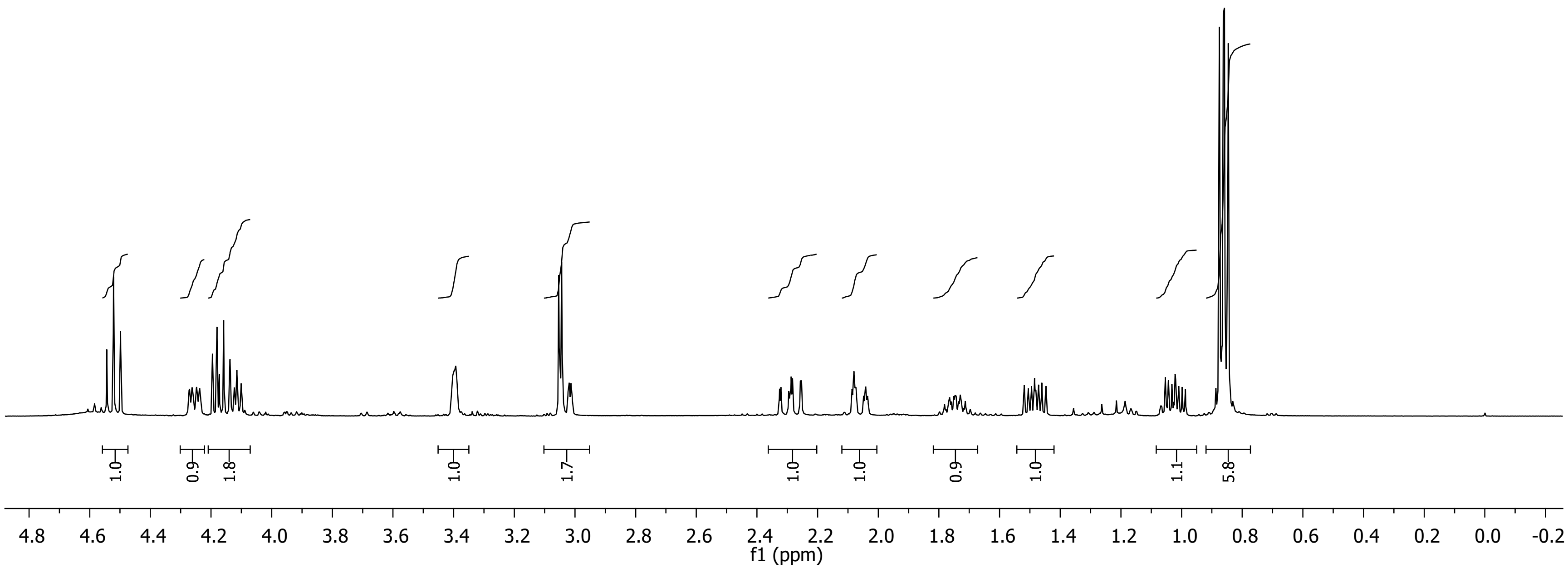

^{13}C NMR of compound **20-*exo*** (100 MHz, $CDCl_3$, 300K)

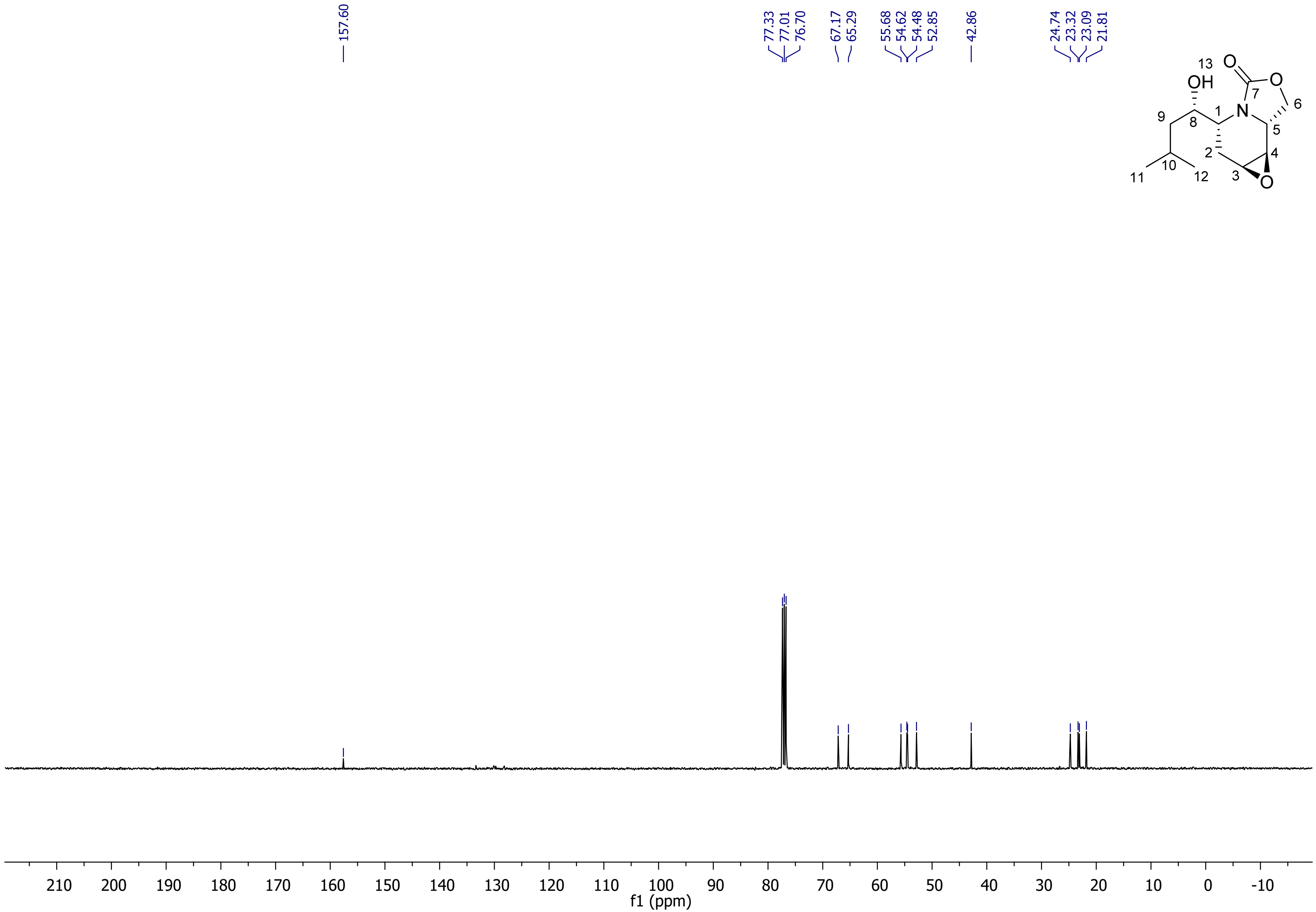

^{1}H NMR of compound **20-*endo*** (300 MHz, $CDCl_3$ 300K)

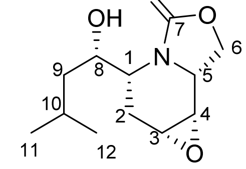

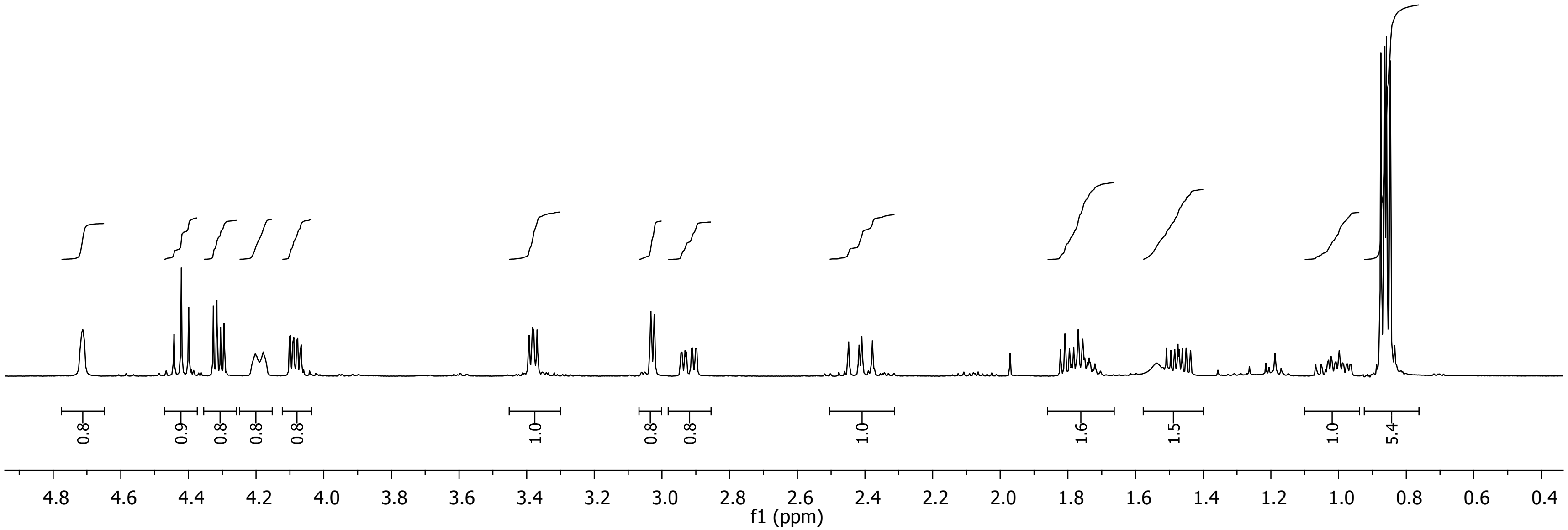

^{13}C NMR of compound **20-*endo*** (100 MHz, $CDCl_3$, 300K)

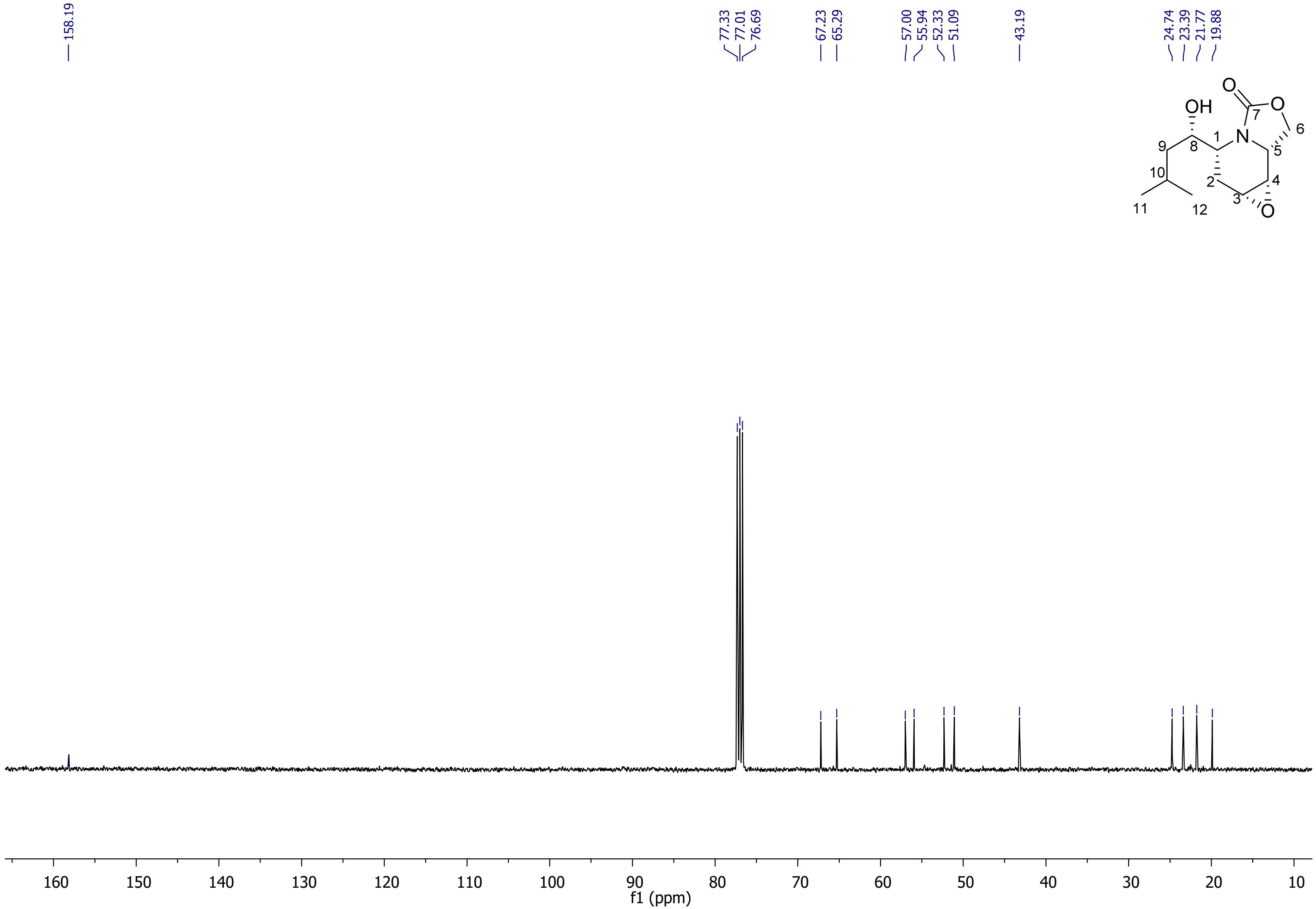

Discrimination between *exo* and *endo* epoxides

Having in hand the radiocrystallographic structure of **18-*exo***, the assignment of the *exo* or *endo* epoxide was established on the basis of NMR spectra, including chemical shift of epoxide carbons in ^{13}C NMR spectrometry and meaningful vicinal coupling constants or meaningful NOE effects as indicated on the following schemes.

Major (18-*exo*)

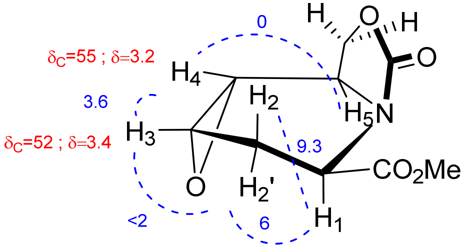

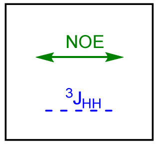

Conformation and configuration corroborated by radiocrystallographic structure

Major (19-*endo*)

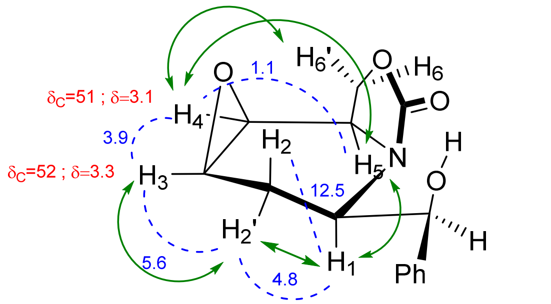

Minor (20-*exo*)

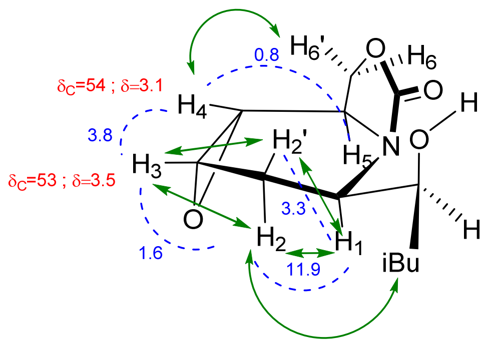

Major (20-*endo*)

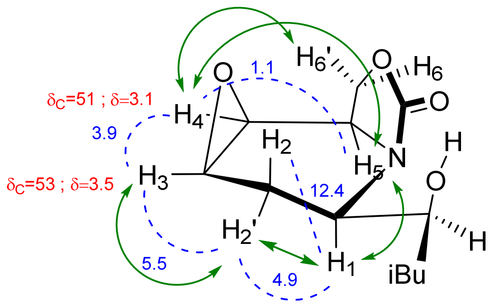

^{1}H NMR of compound **21** (300 MHz, $CDCl_3$, 300K)

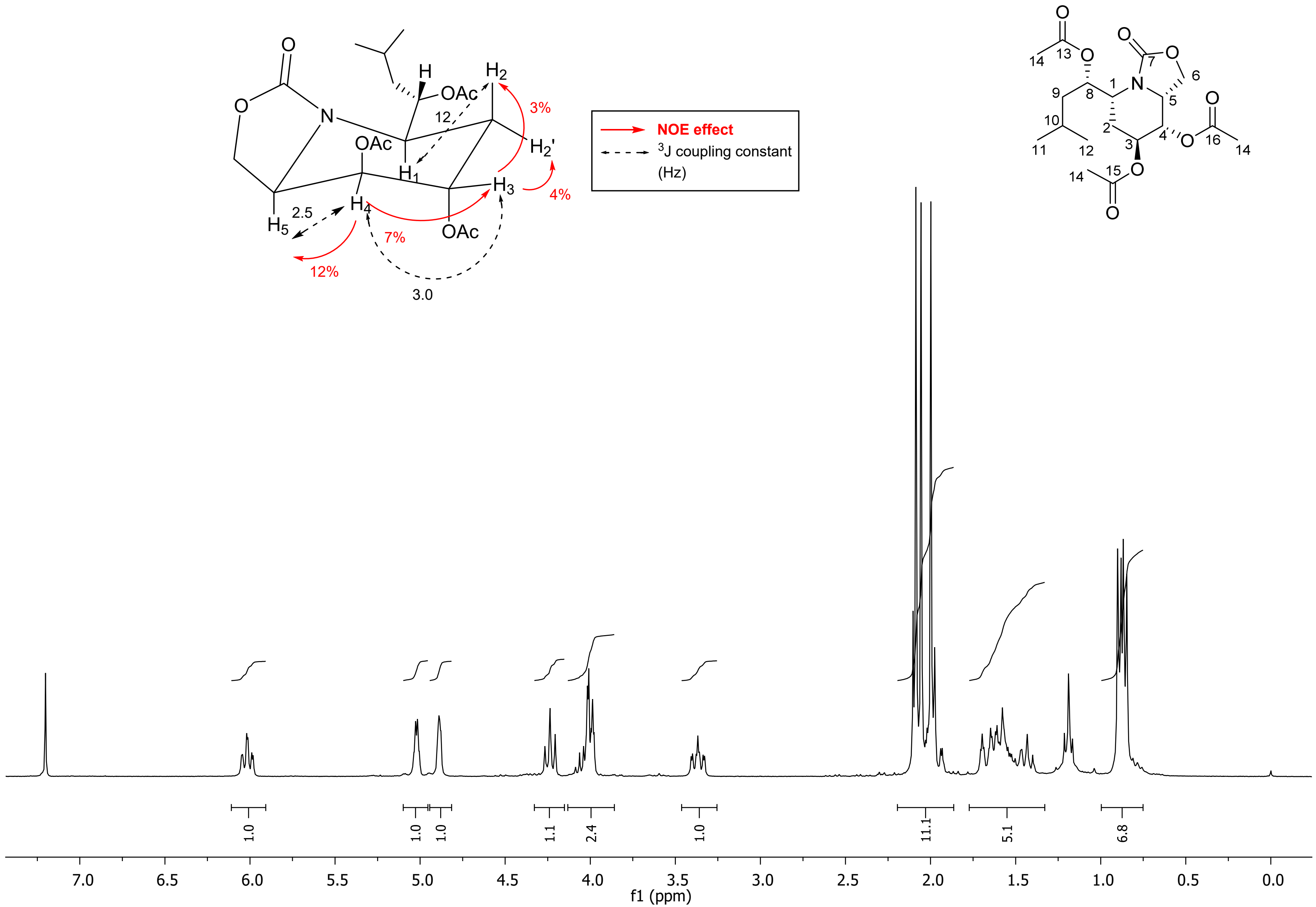

^{13}C NMR of compound **21** (75 MHz, $CDCl_3$, 300K)

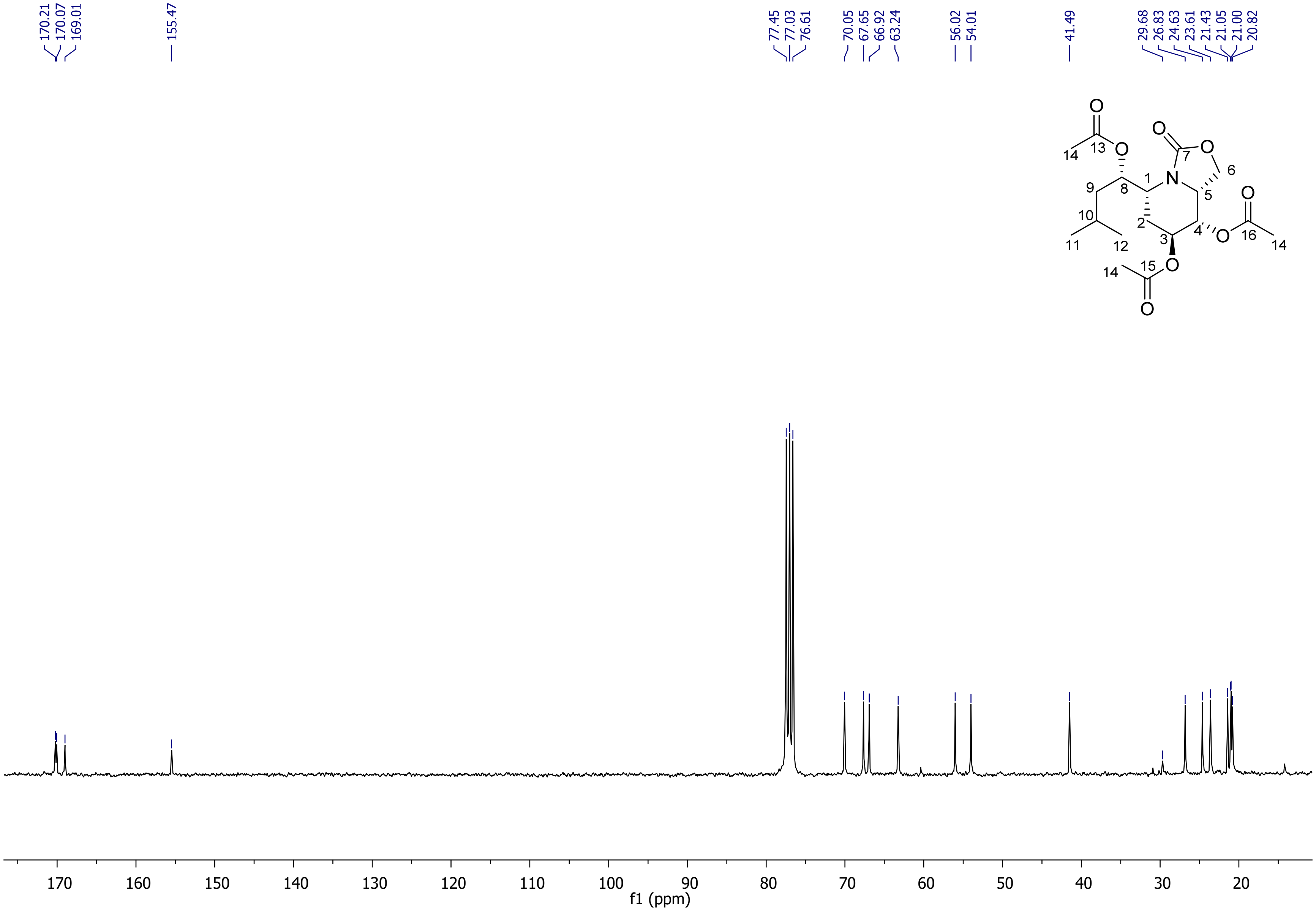

^{1}H NMR spectrum of compound **22** (400 MHz, $CDCl_3$, 300K)

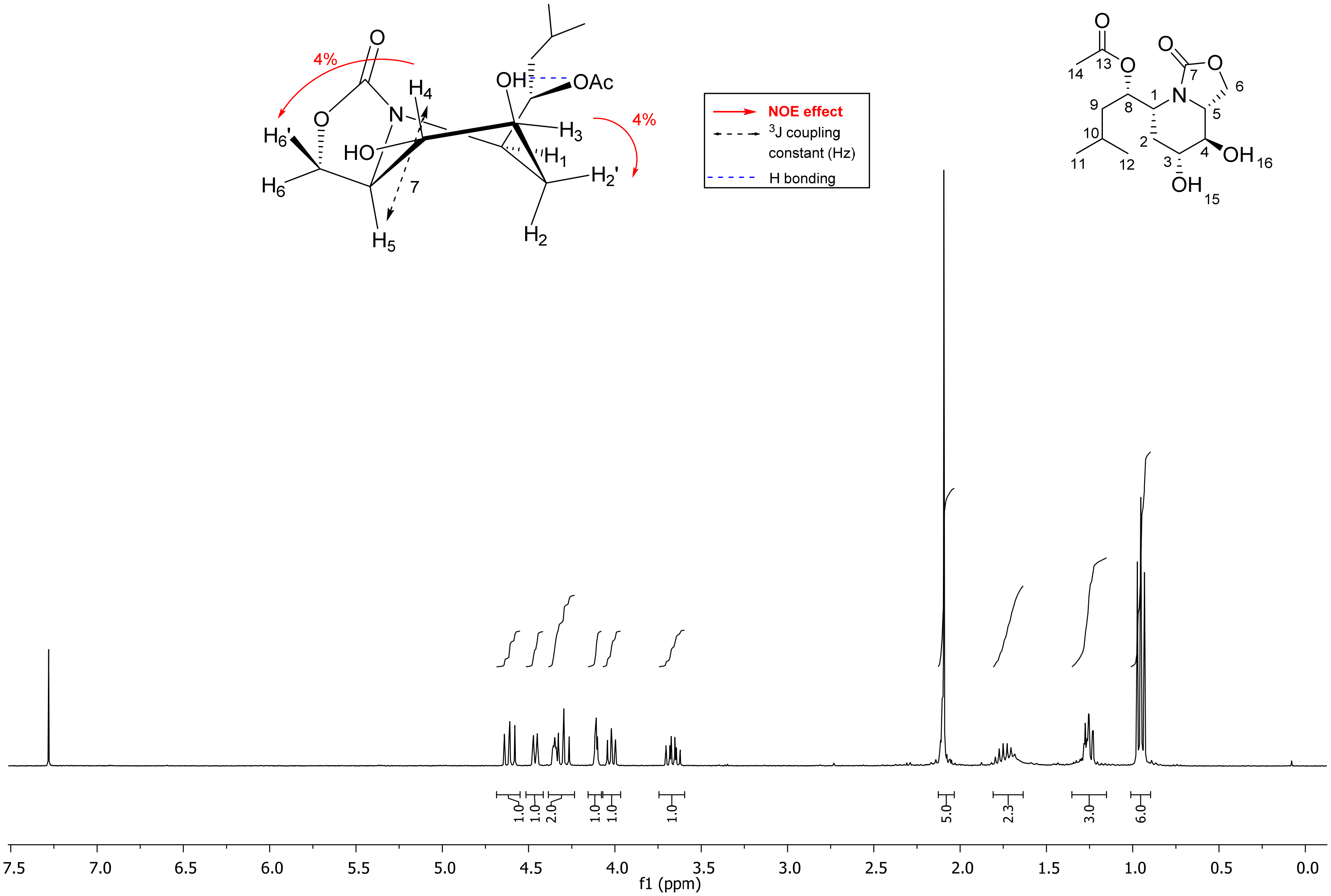

^{13}C NMR of compound **22** (100 MHz, $CDCl_3$, 300K)

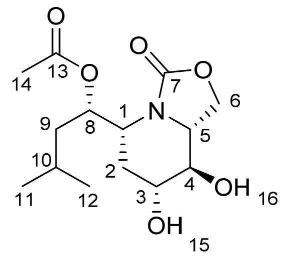

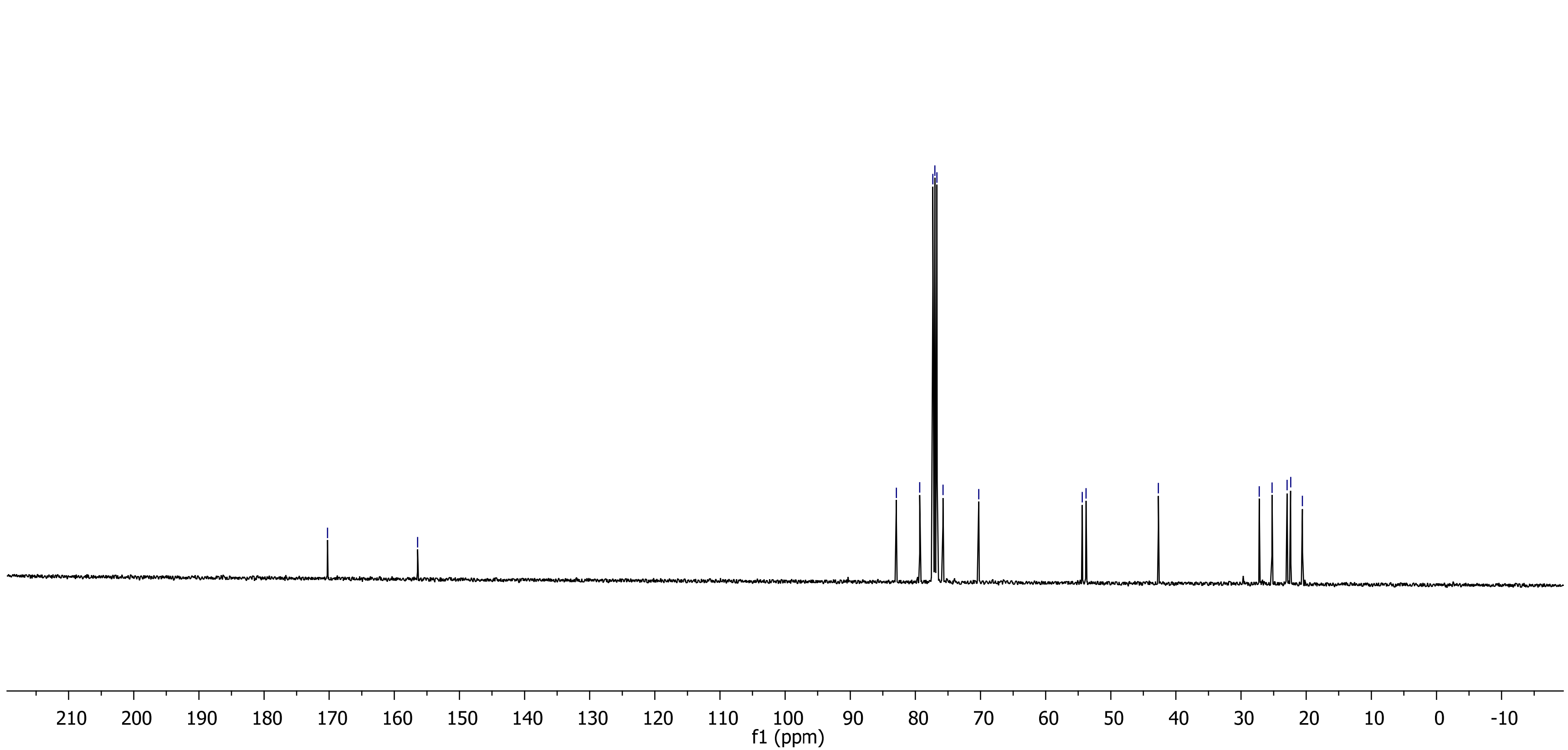

^{1}H NMR of compound **23** (400 MHz, CD_3OD, 300K)

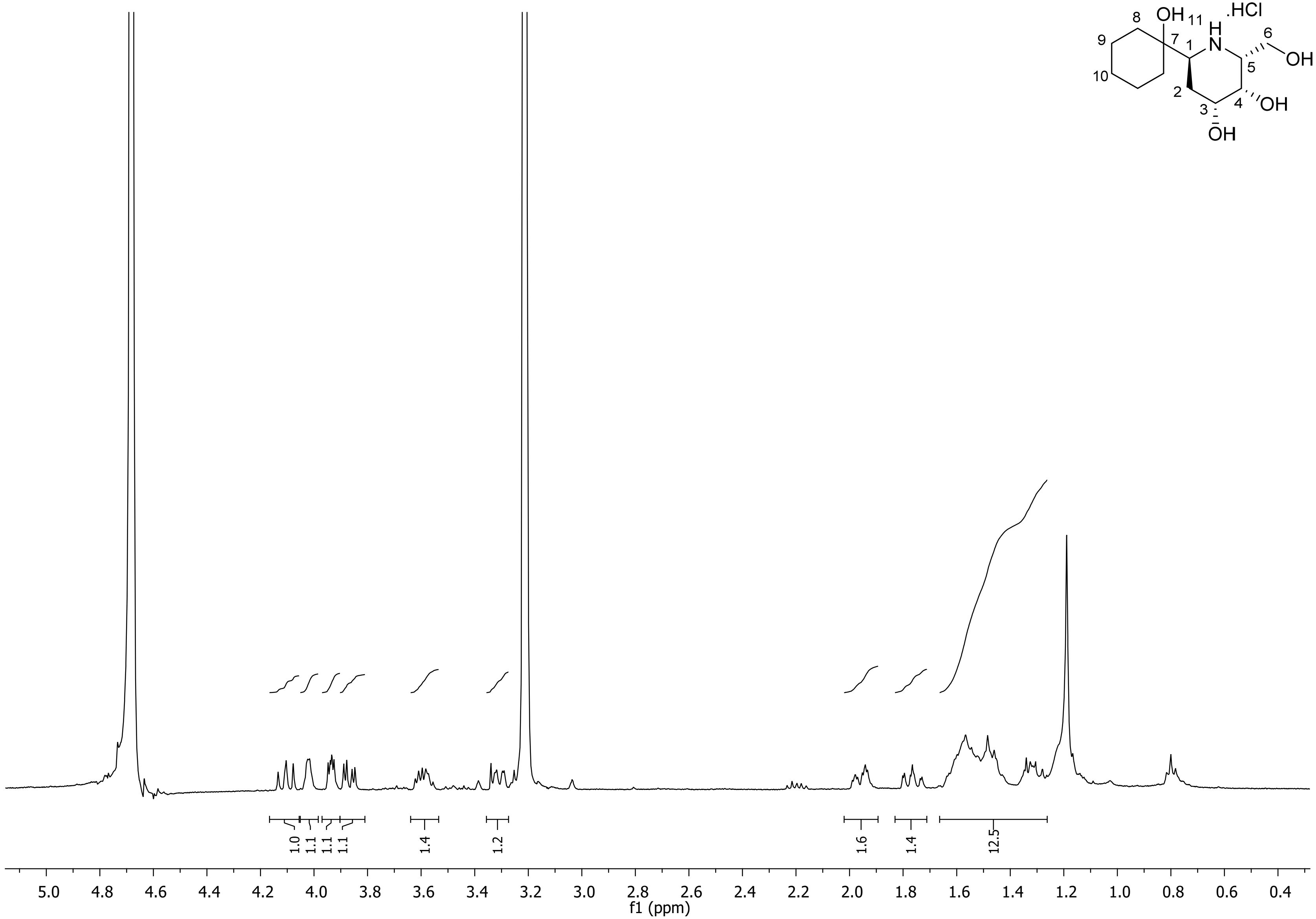

^{13}C NMR of compound **23** (100 MHz, CD_3OD, 300K)

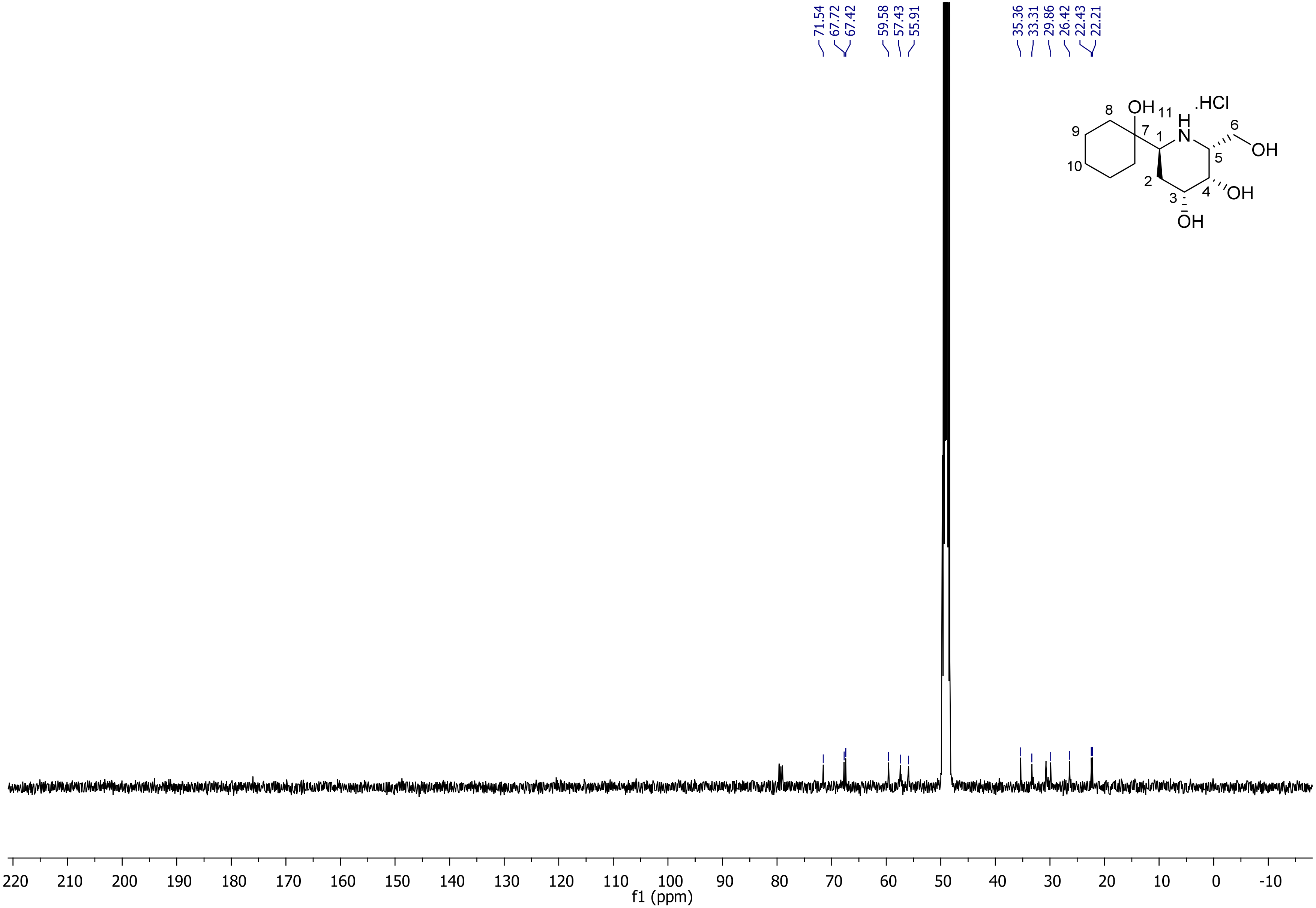

[1]H NMR spectrum of compound **24** (400 MHz, CH_3OD, 300K)

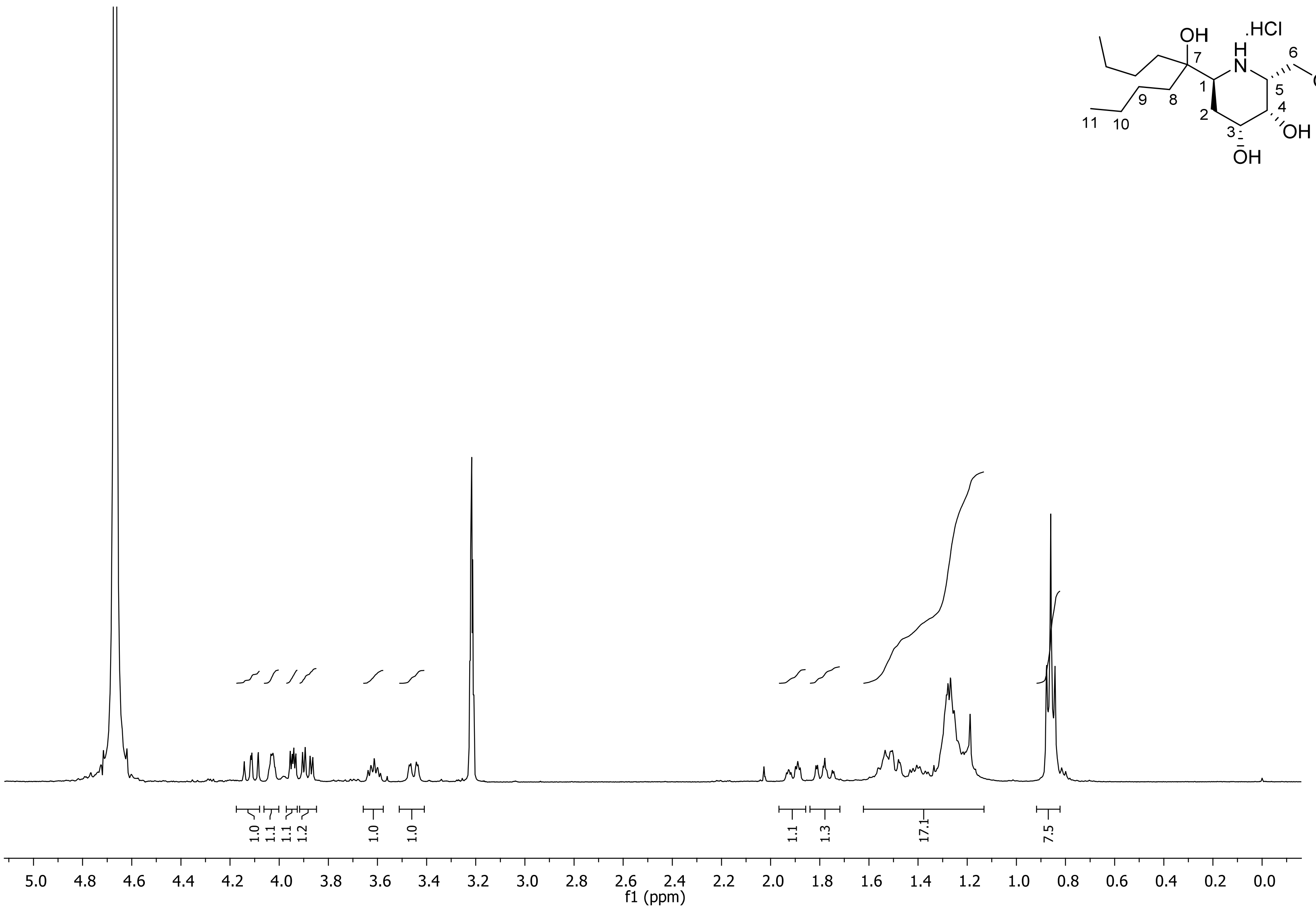

[13]C NMR of compound **24** (100 MHz, CH_3OD, 300K)

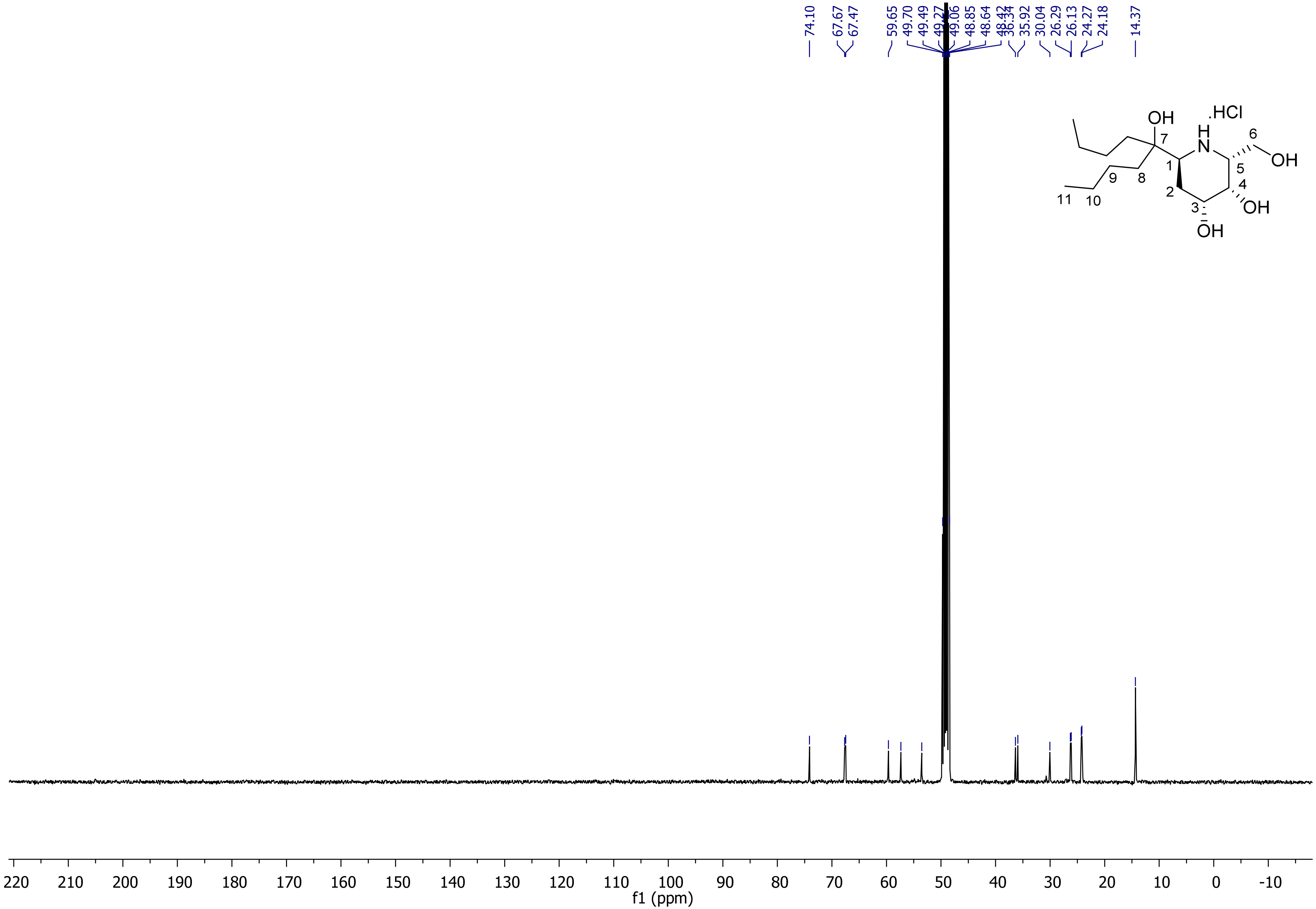

[1]H NMR of compound **25** (400 MHz, CD_3OD, 300K)

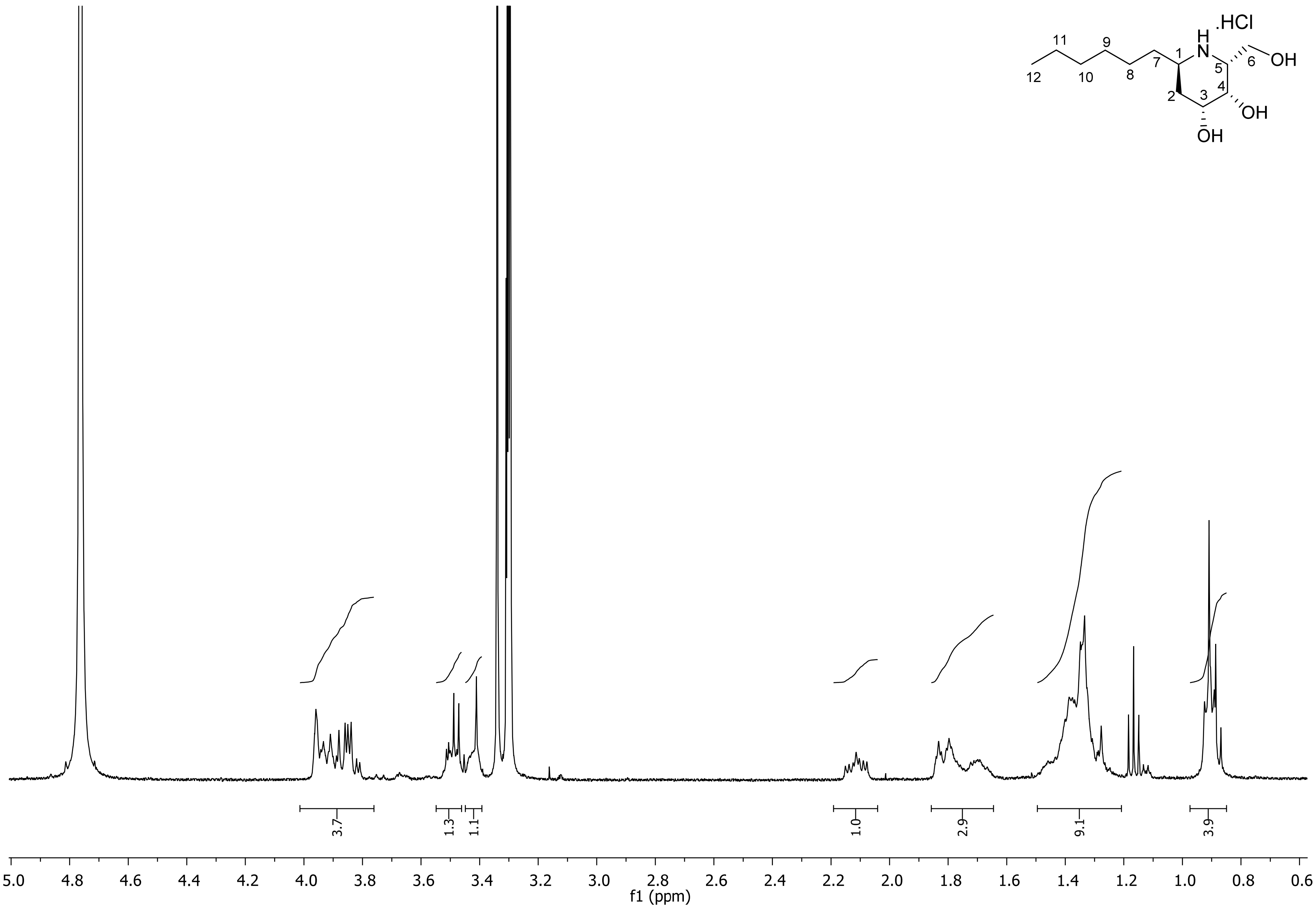

^{13}C NMR of compound **25** (100 MHz, CD_3OD, 300K)

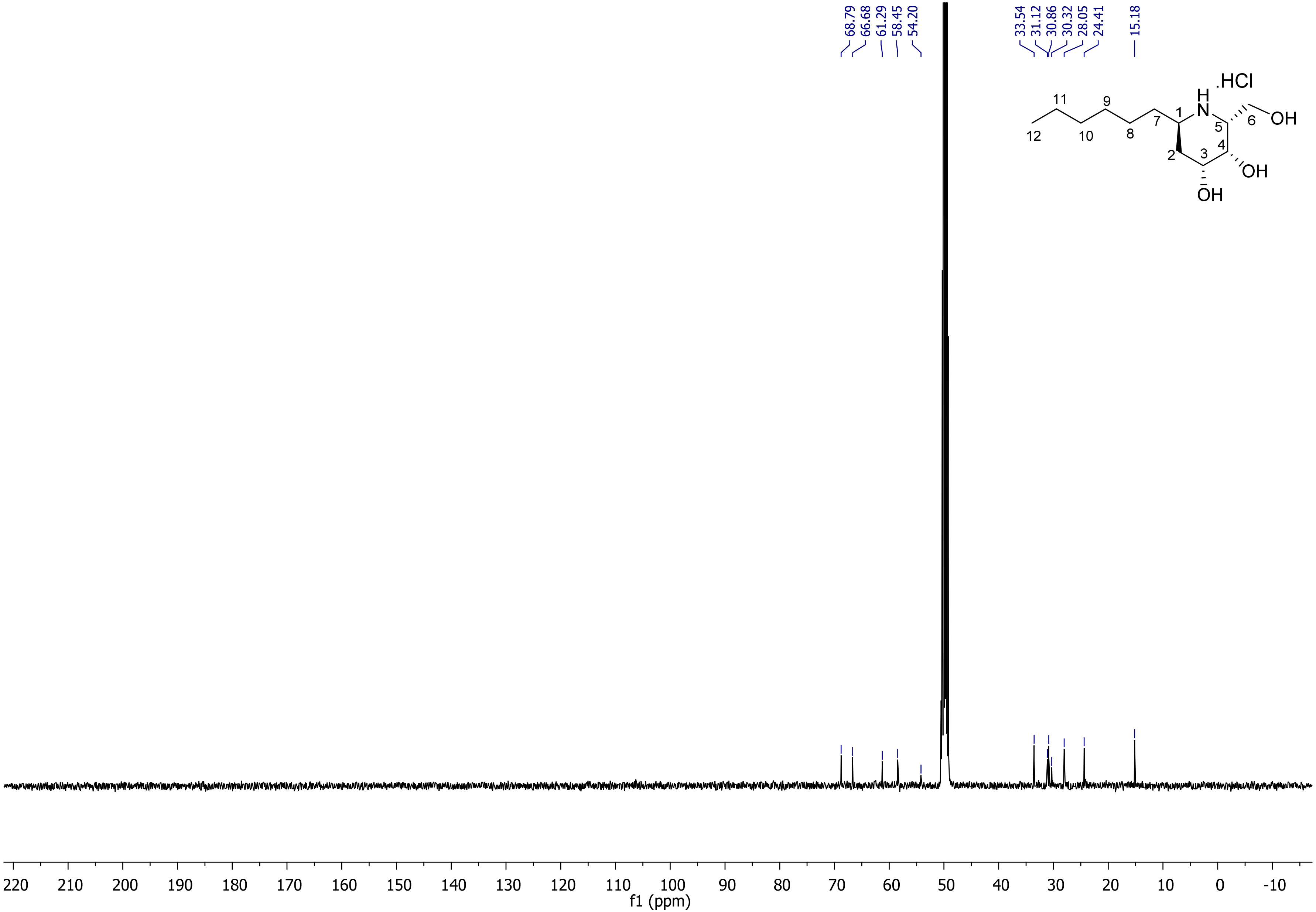

^{1}H NMR of compound **26** (300 MHz, CD_3OD, 300K)

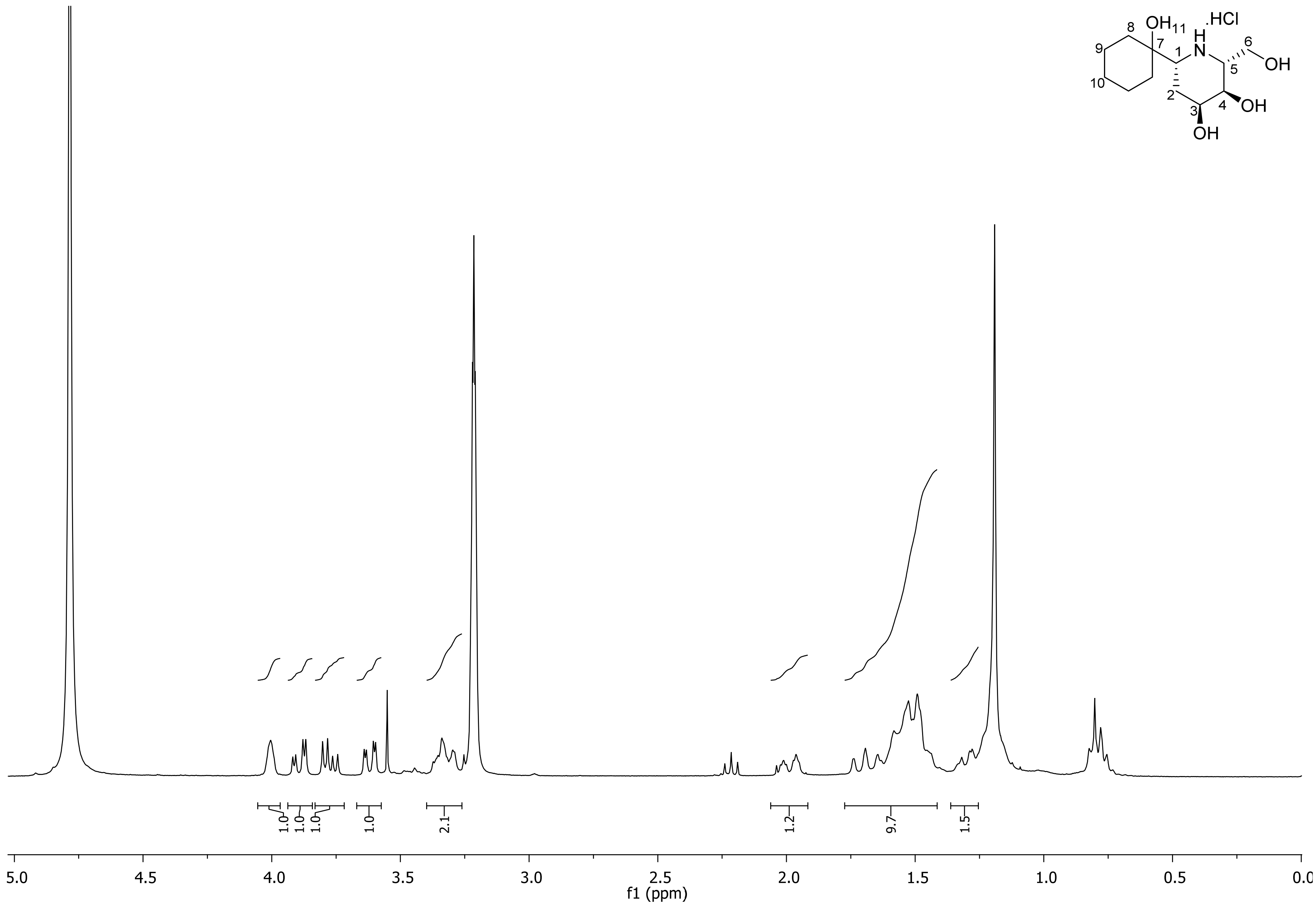

^{13}C NMR of compound **26** (75 MHz, CD_3OD, 300K)

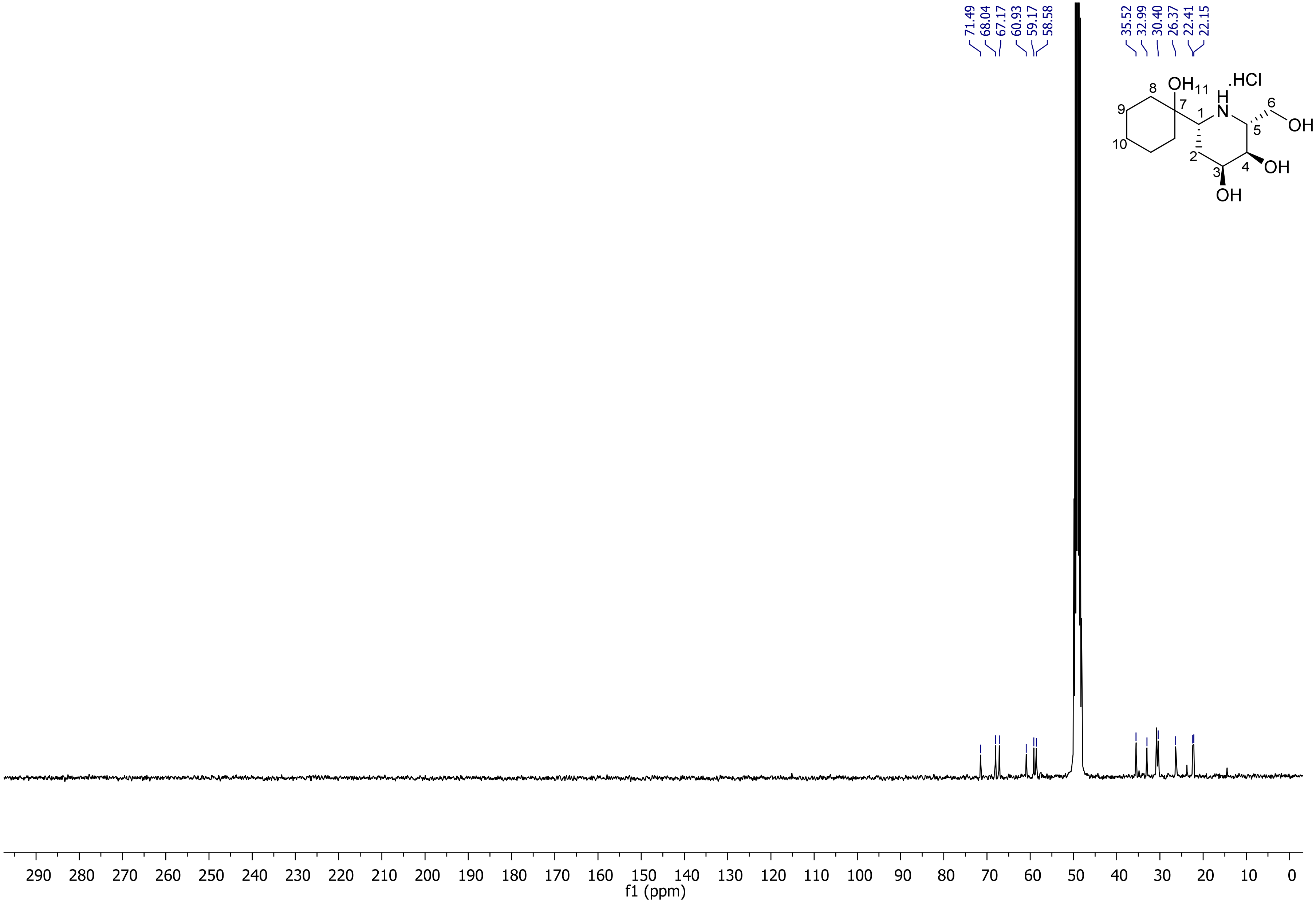

[1]H NMR of compound **27** (400MHz, CD_3OD, 300K)

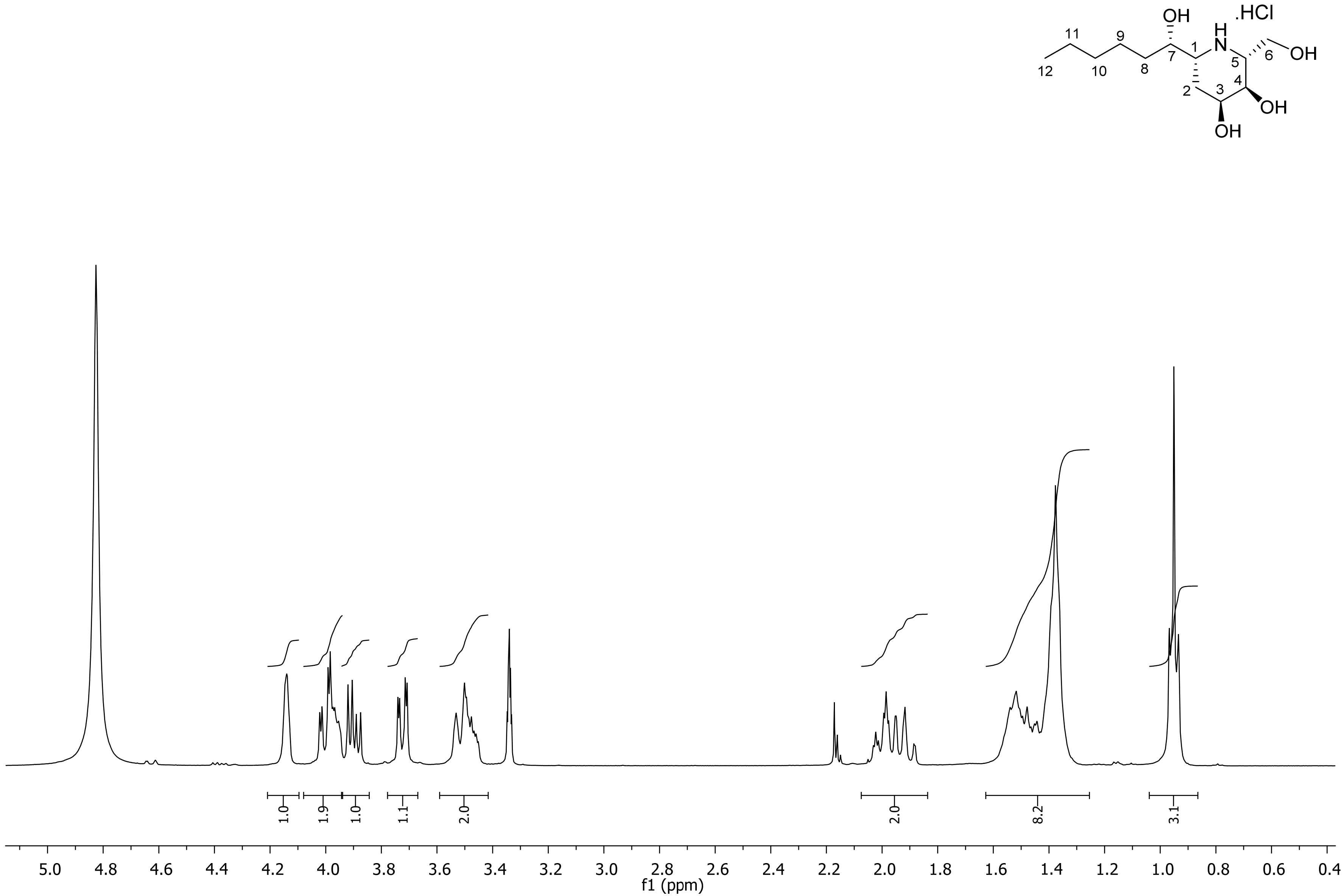

^{13}C NMR of compound **27** (100 MHz, CD_3OD, 300K)

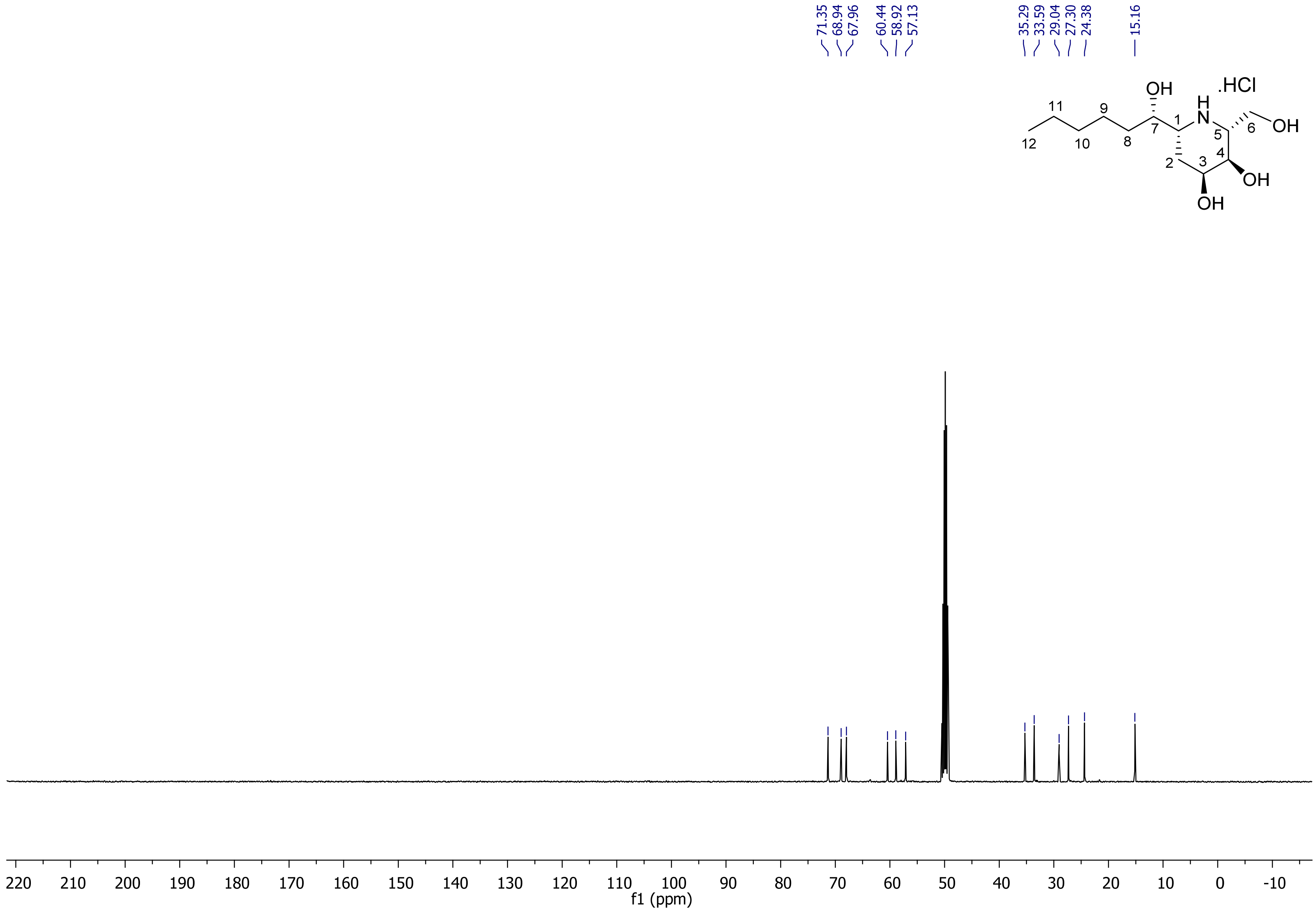

[1]H NMR of compound **28** (400MHz, CD_3OD, 300K)

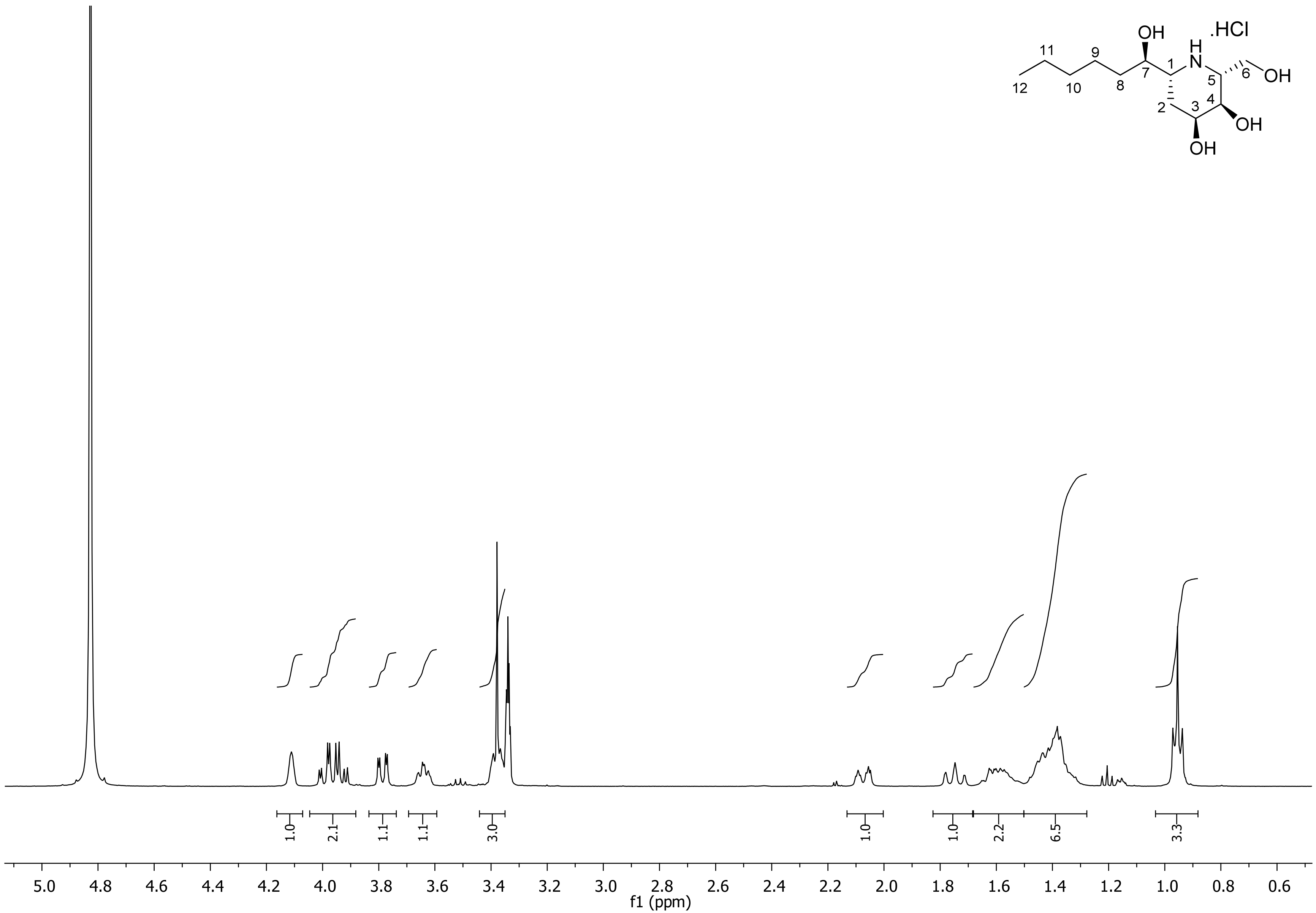

^{13}C NMR of compound **28** (100 MHz, CD_3OD, 300K)

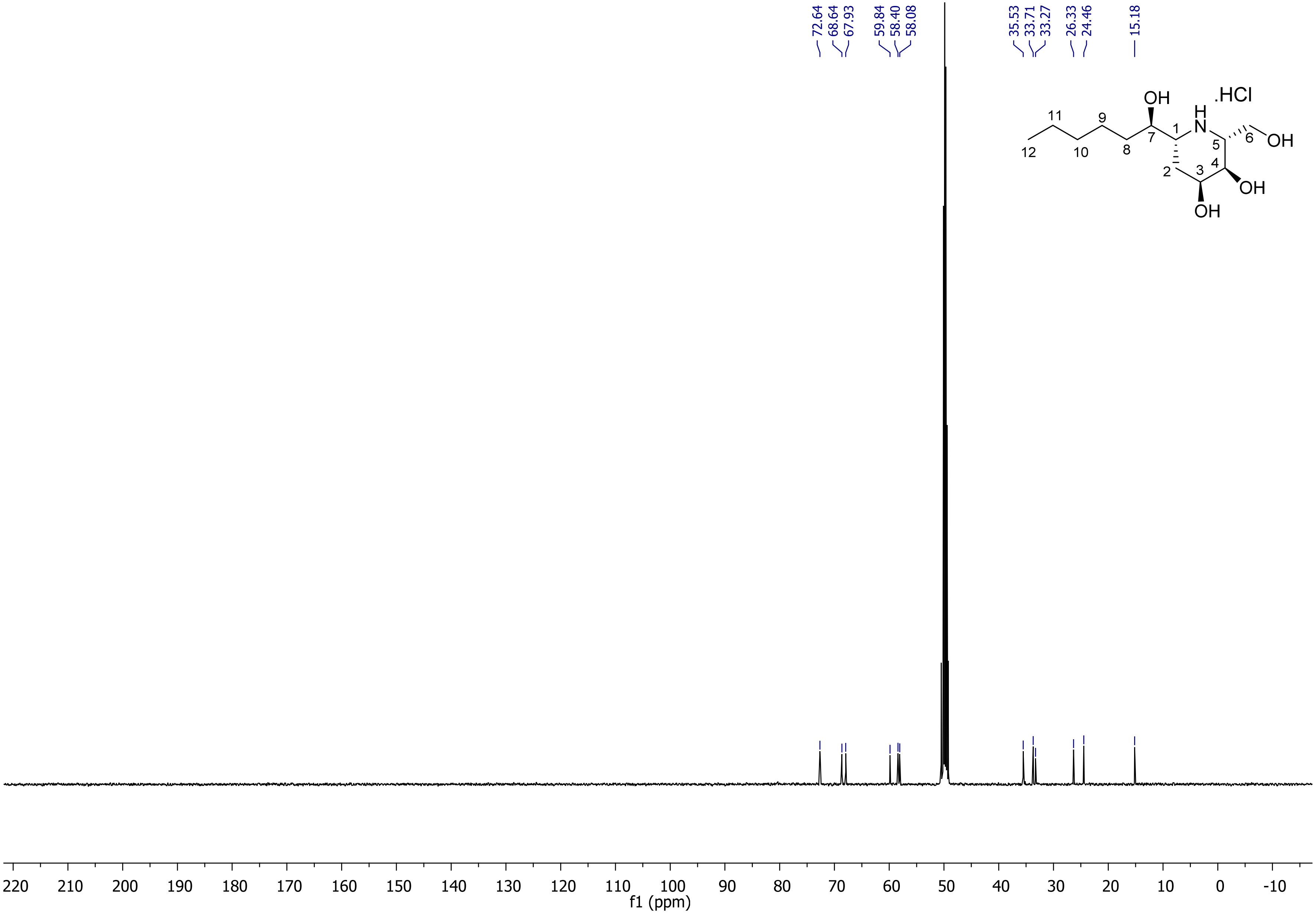

[1]H NMR of compound **29** (400 MHz, CD_3OD, 300K)

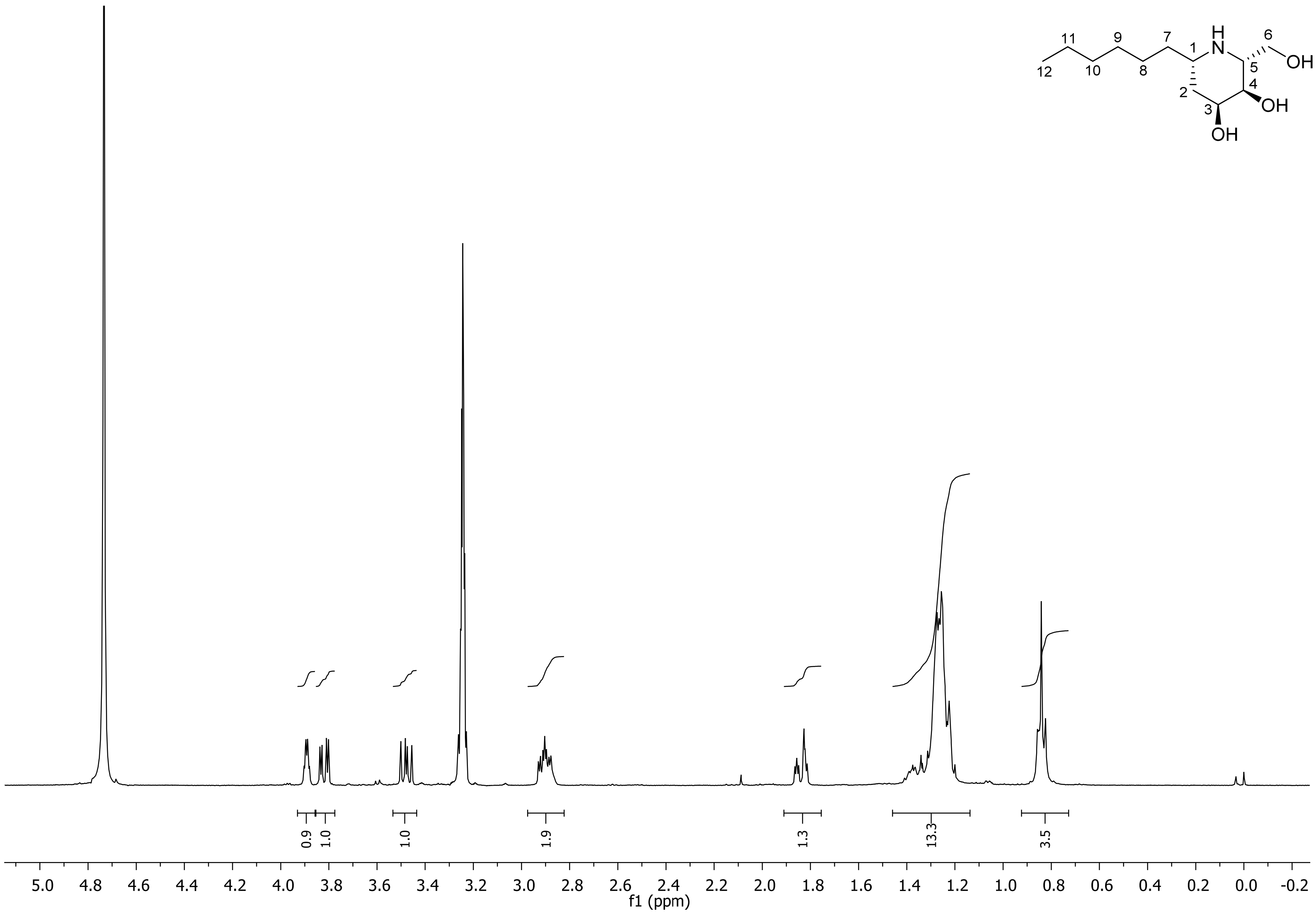

^{13}C NMR of compound **29** (100 MHz, CD_3OD, 300K)

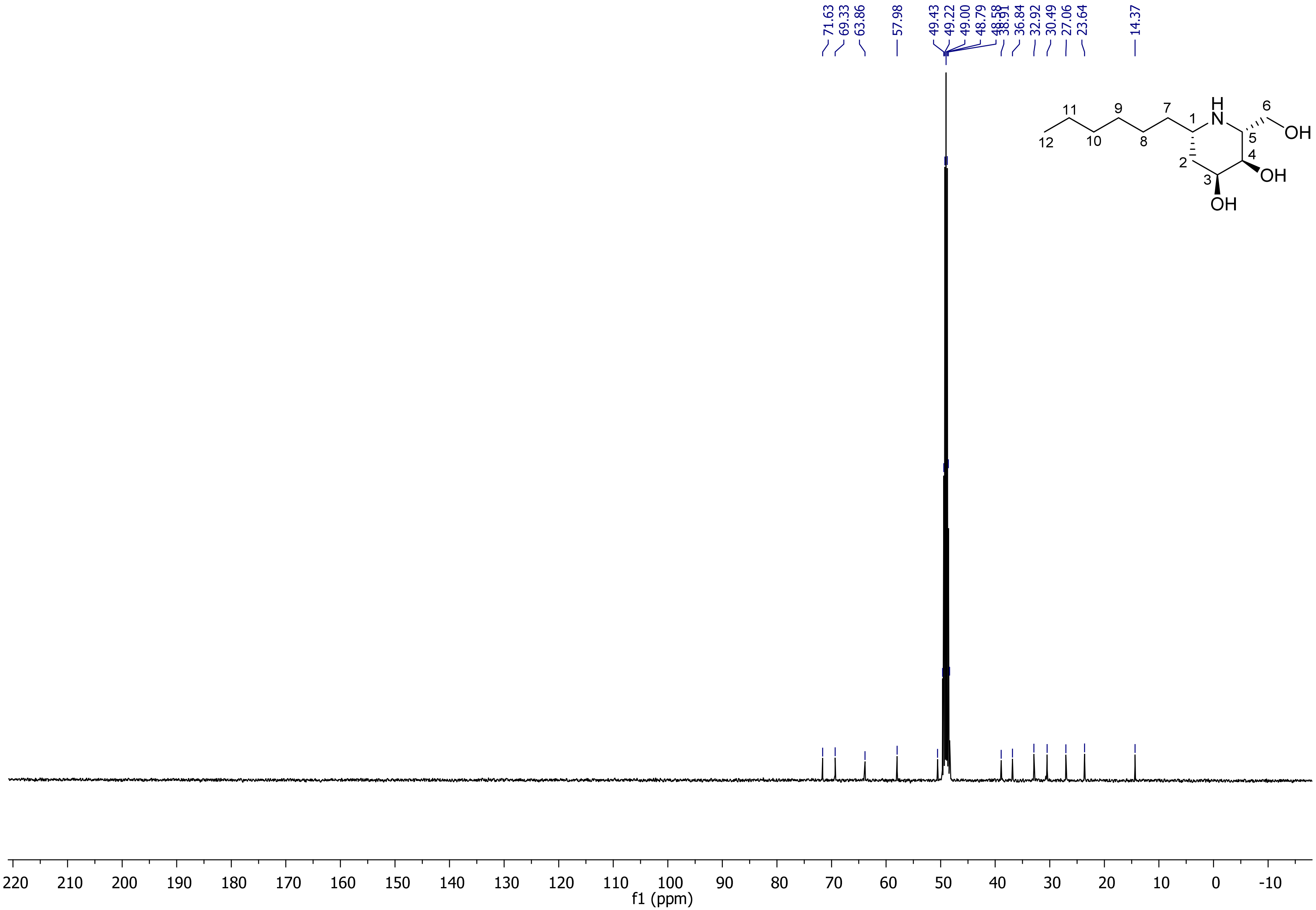

^{1}H NMR of compound **30** (300 MHz, CD_3OD, 300K)

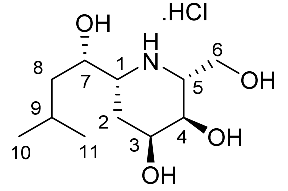

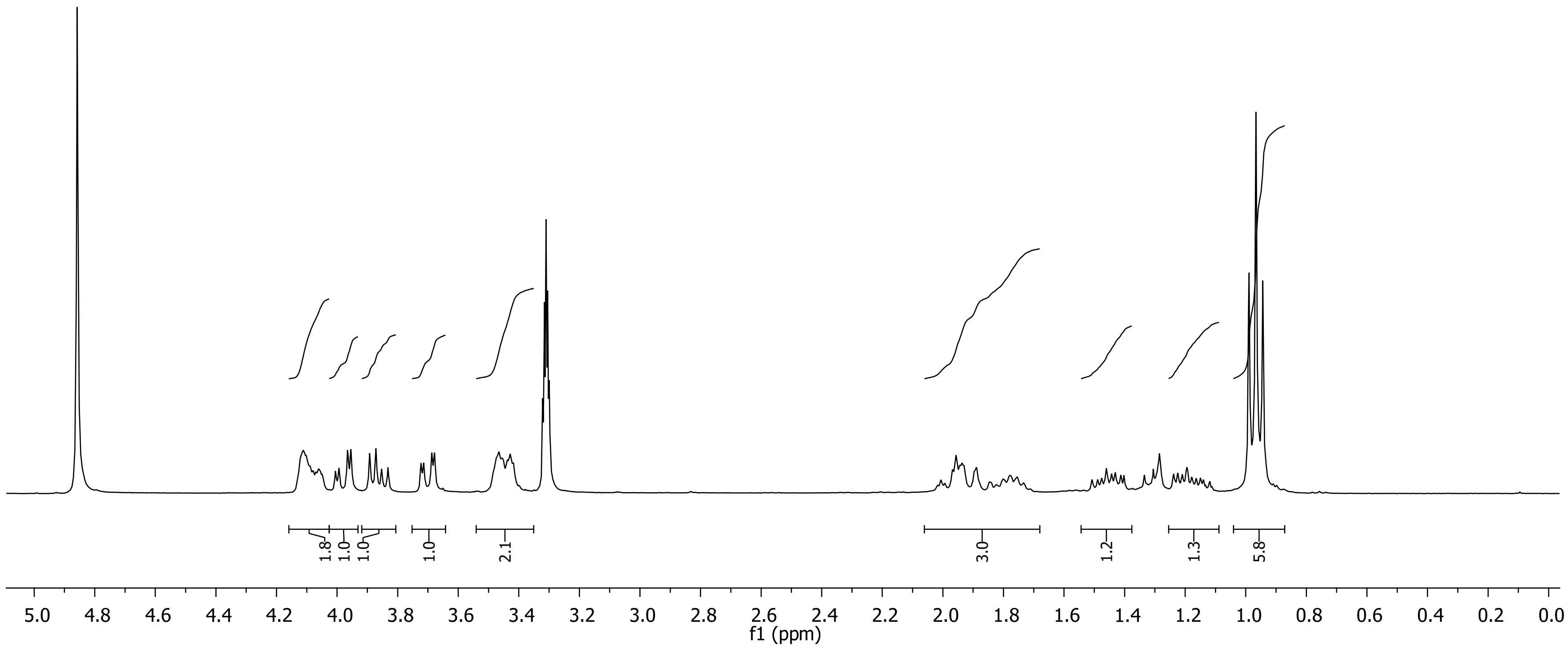

^{13}C NMR of compound **30** (75 MHz, CD_3OD, 300K)

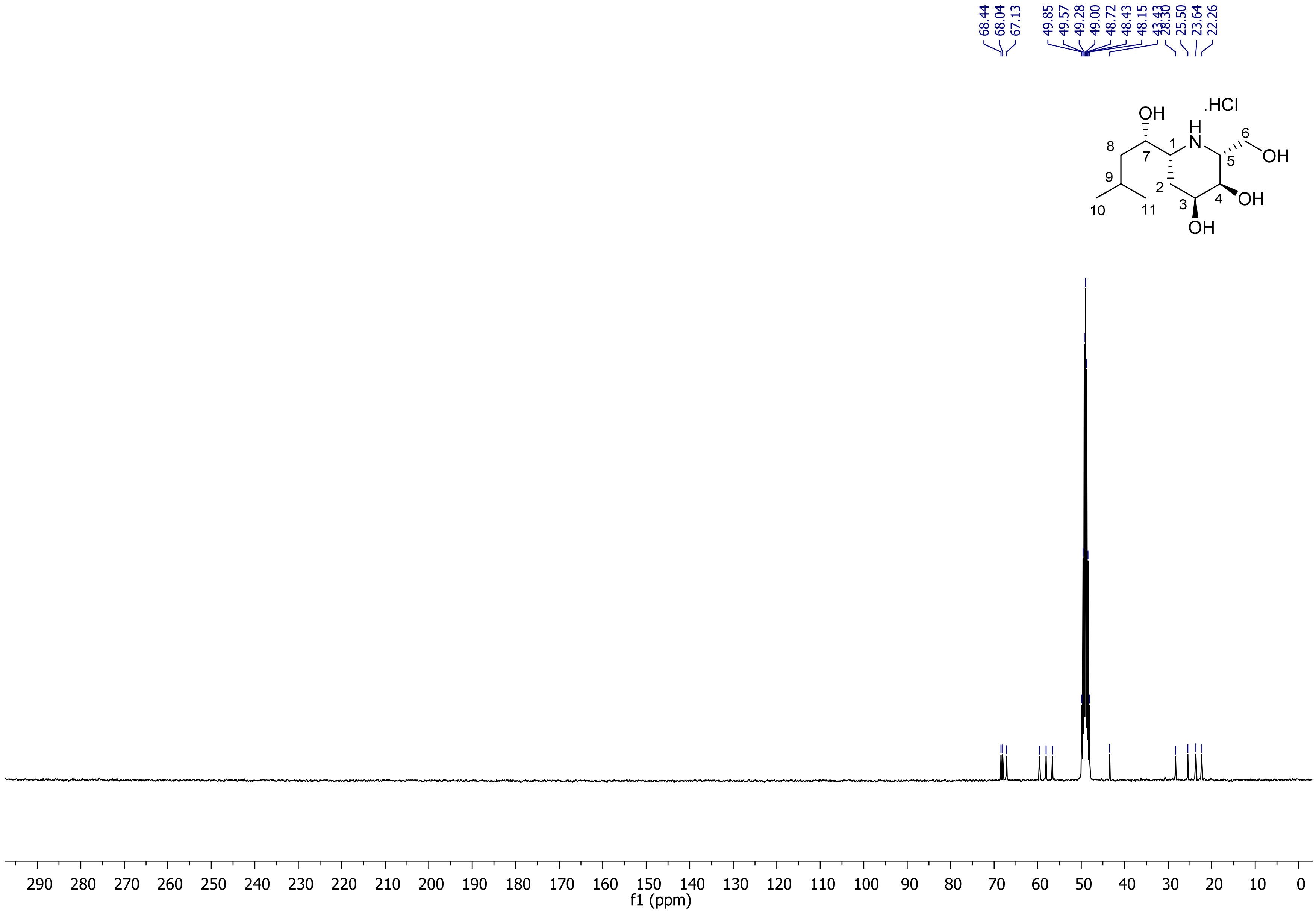

[1]H NMR of compound **31** (400 MHz, CD_3OD, 300K)

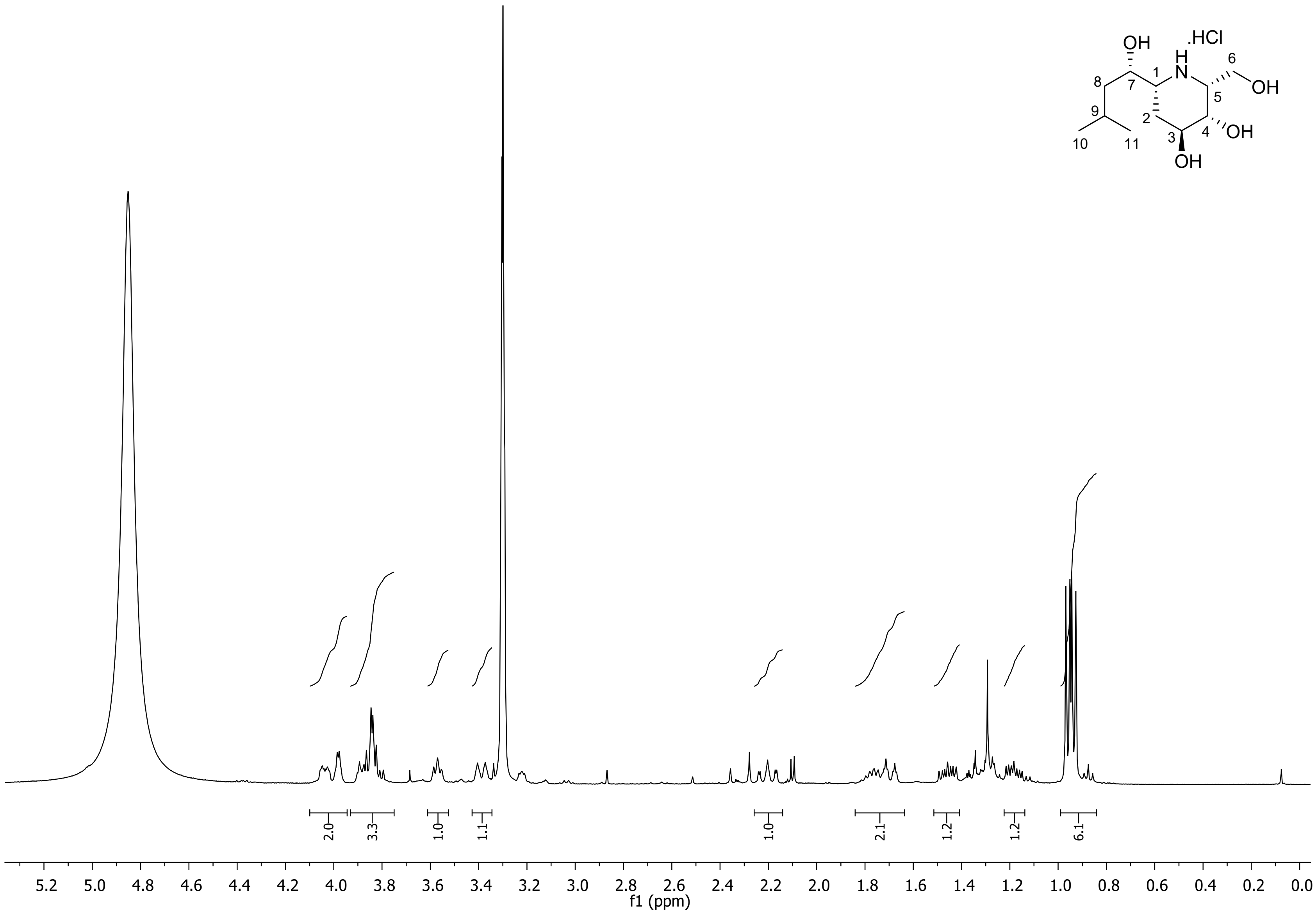

[13]C NMR of compound **31** (100 MHz, CD_3OD, 300K)

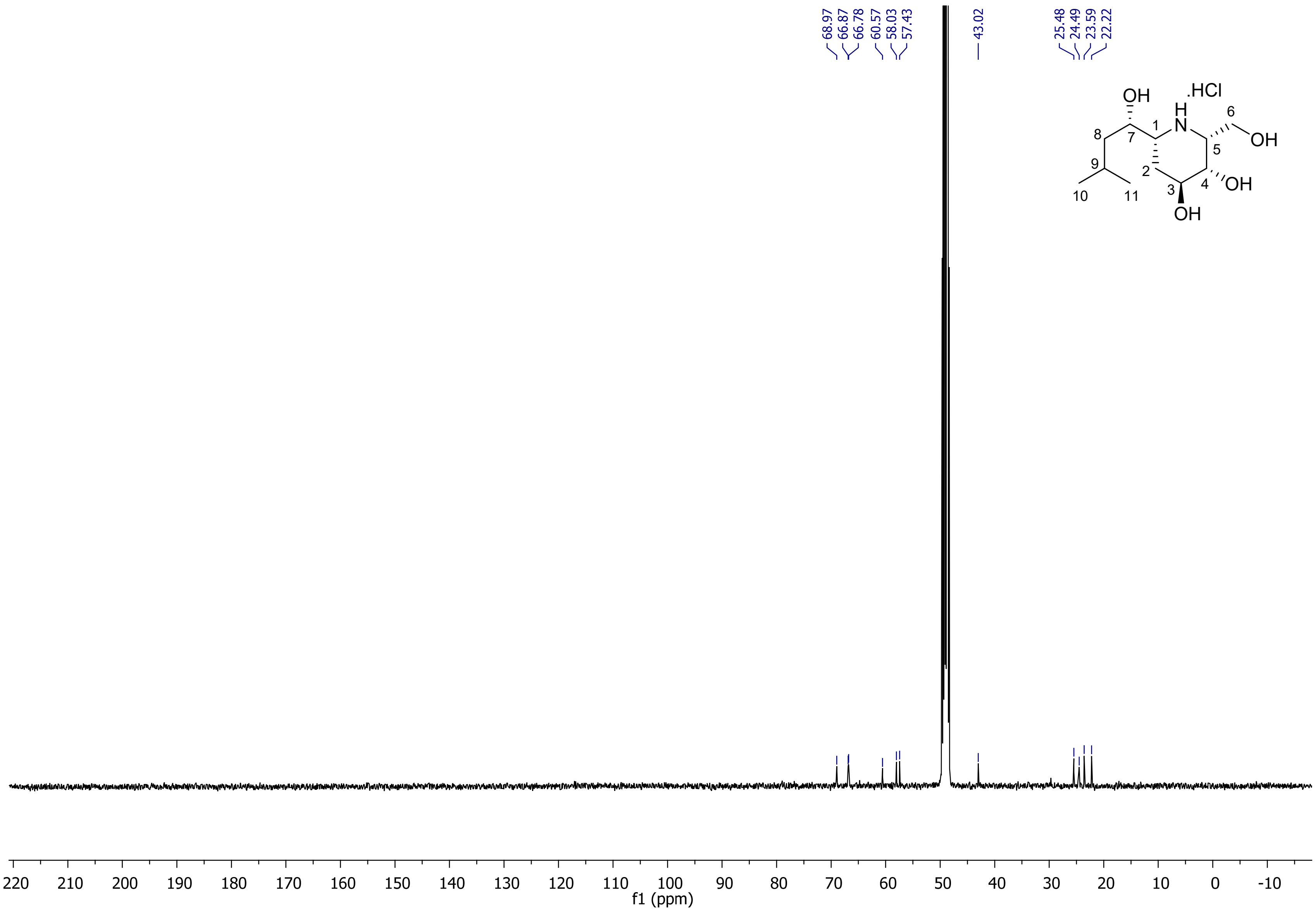

[1]H NMR of compound **32** (400 MHz, CD_3OD, 300K)

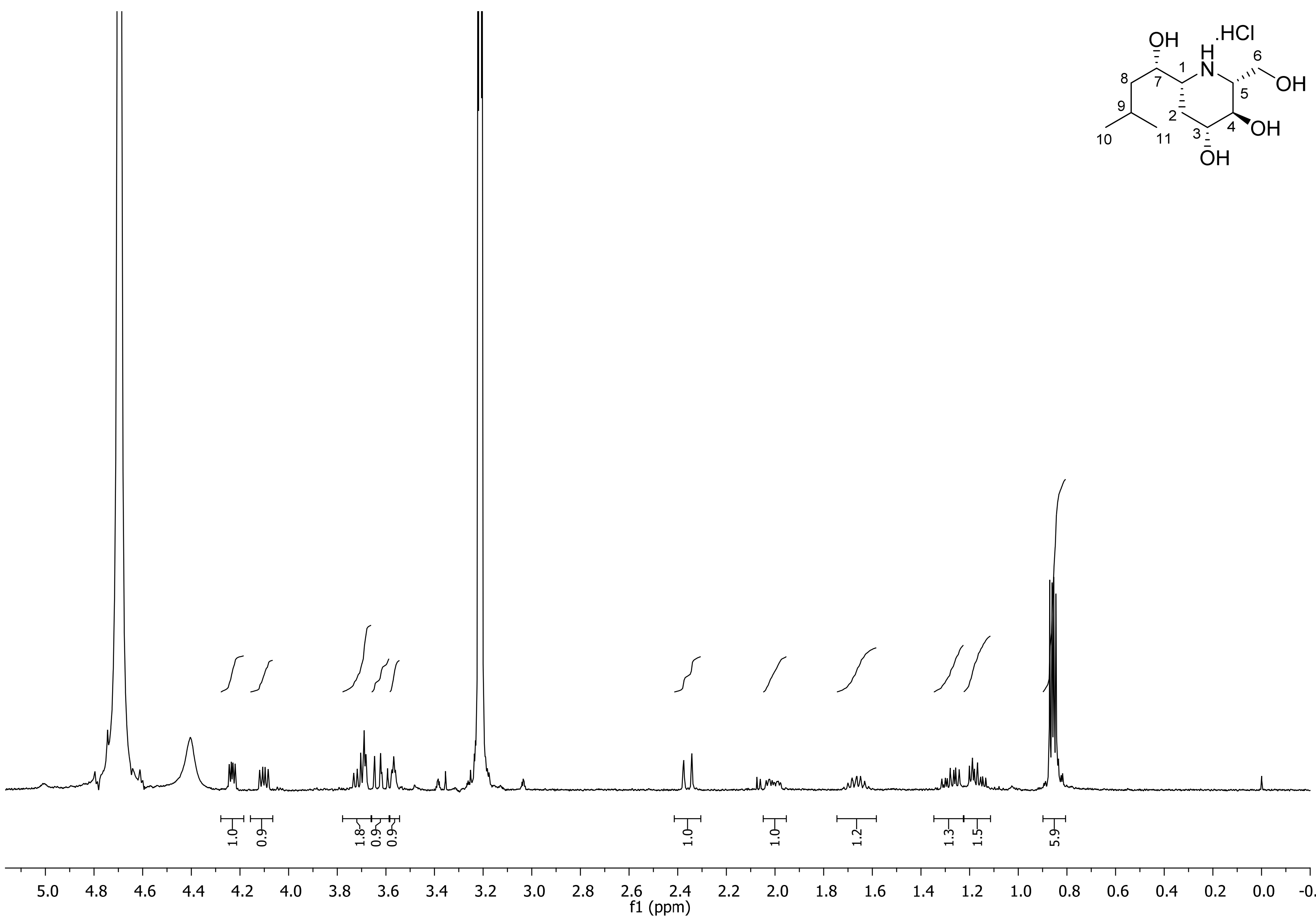

^{13}C NMR of compound **32** (100 MHz, CD_3OD, 300K)

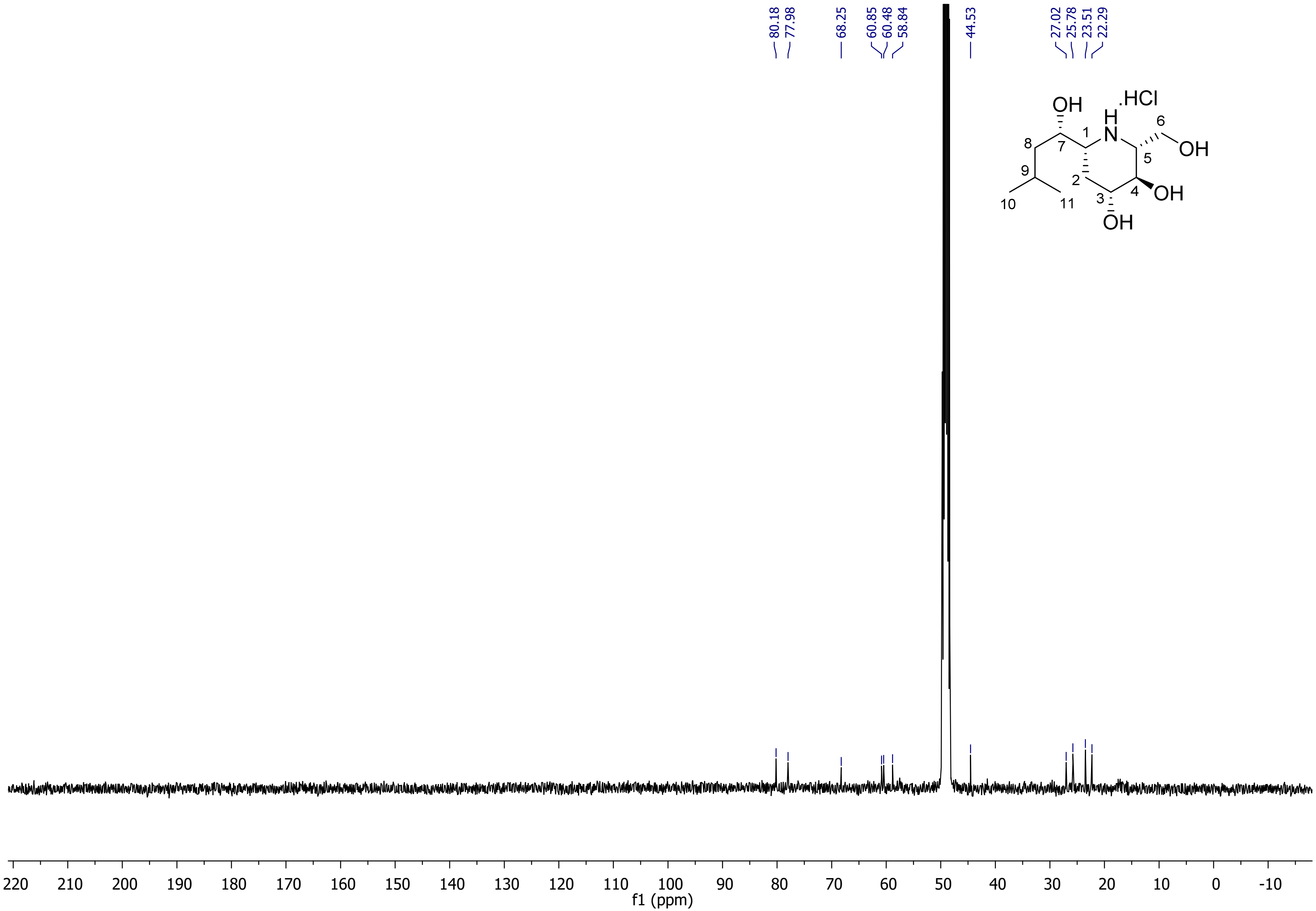

^{1}H NMR of compound **35** (400 MHz, CD_3OD, 300K)

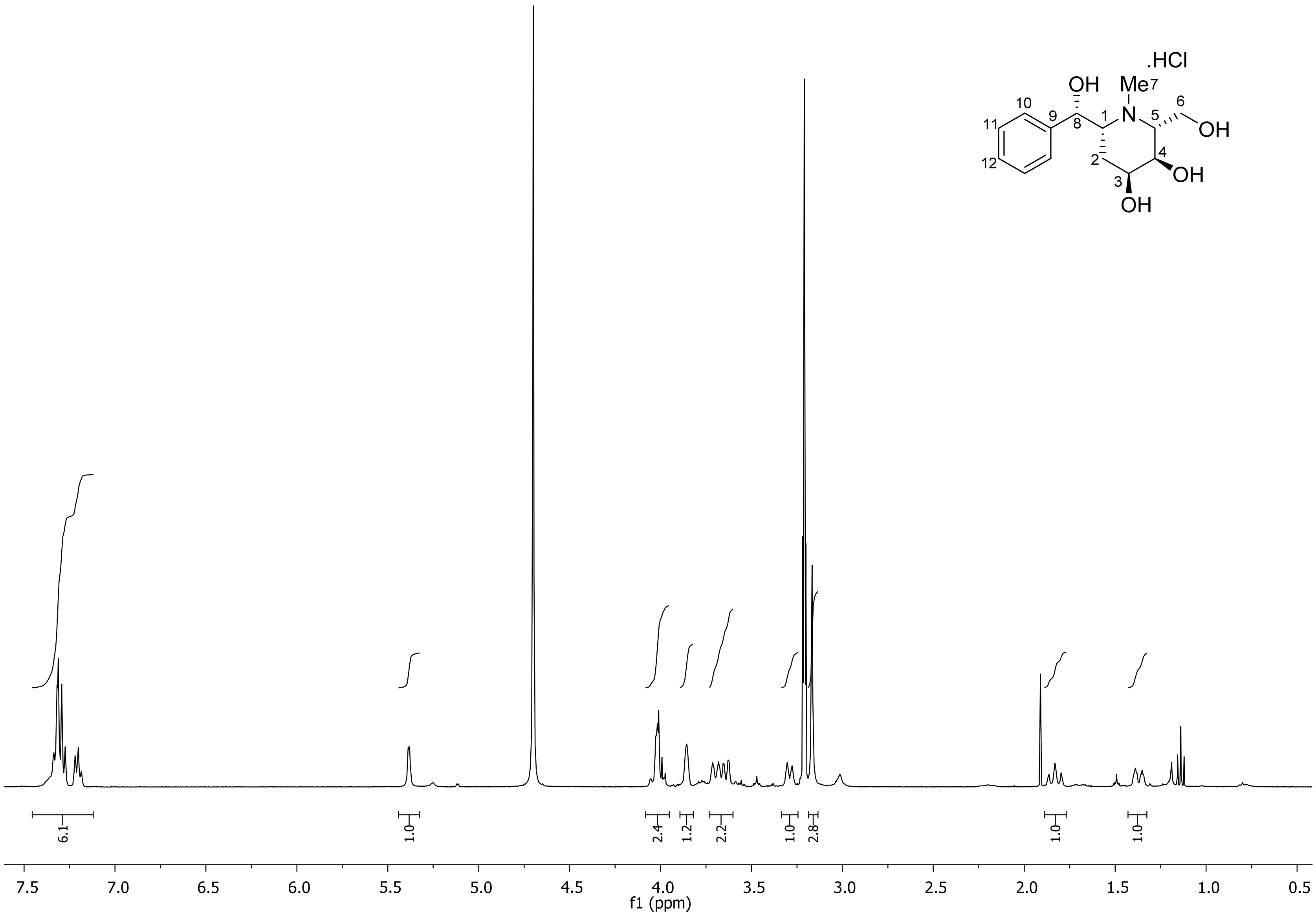

^{13}C NMR of compound **35** (100 MHz, CD_3OD, 300K)

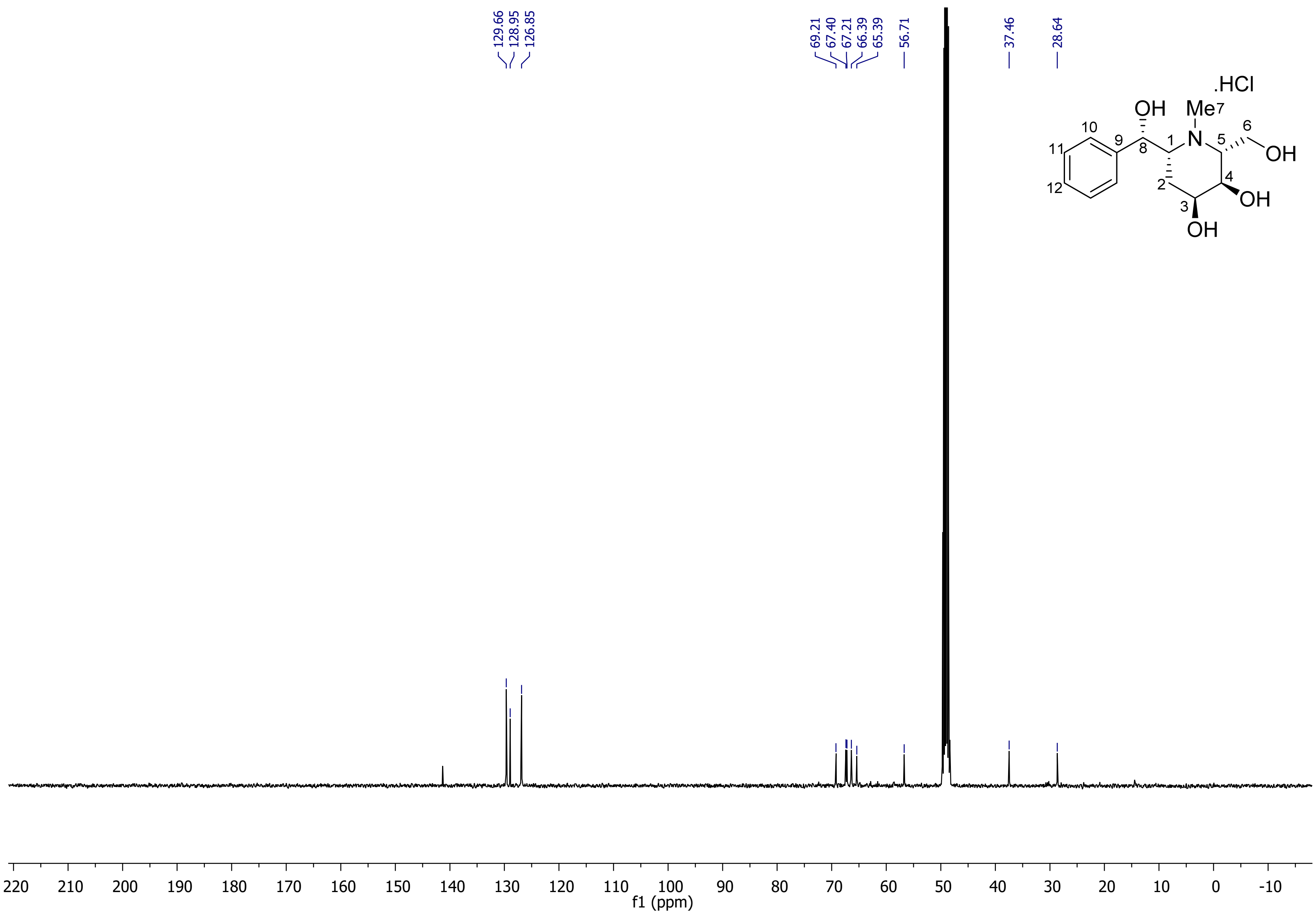

II- Dixon and Lineweaver-Burk plots for Ki determination

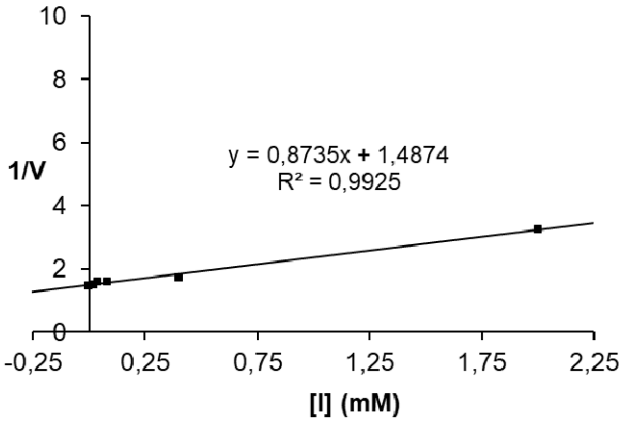

Figure S1. Dixon Plot for K_i determination (473 ± 50 μM) of 23 against *bovine liver* β-galactosidase.

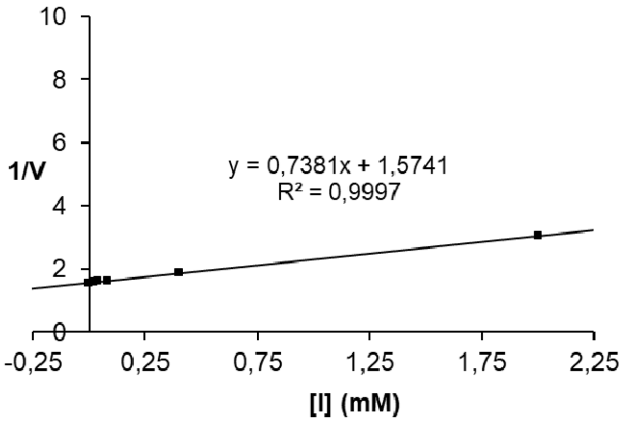

Figure S2. Dixon Plot for K_i determination (652 ± 55 μM) of 24 against *bovine liver* β-galactosidase.

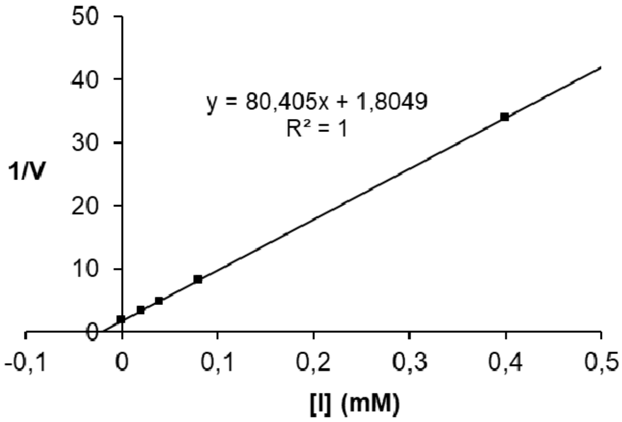

Figure S3. Dixon Plot for K_i determination (10 ± 0.2 μM) of 25 against *bovine liver* β-galactosidase.

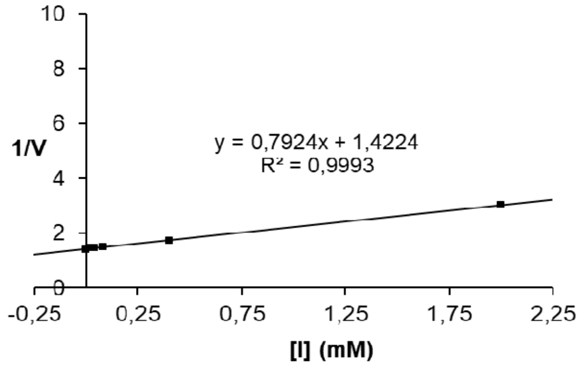

Figure S4. Dixon Plot for K_i determination (475 ± 45 μM) of **33** against *bovine liver* β-galactosidase.

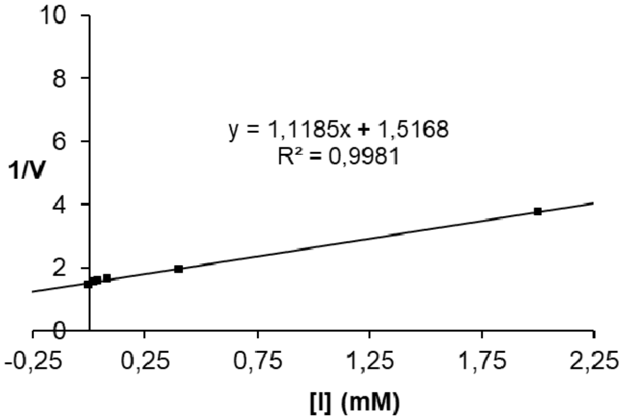

Figure S5. Dixon Plot for K_i determination (301 ± 25 μM) of **26** against *bovine liver* β-galactosidase.

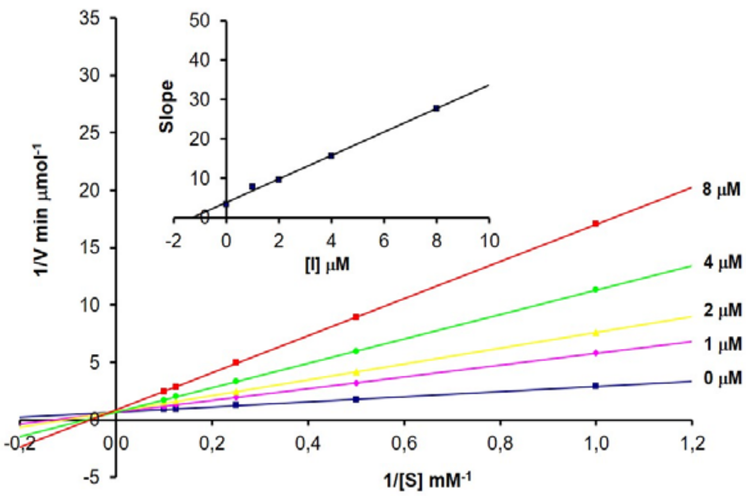

Figure S6. Lineweaver-Burk Plot for K_i determination (1.3 ± 0.1 μM) of **27** against *bovine liver* β-galactosidase/β-glucosidase.

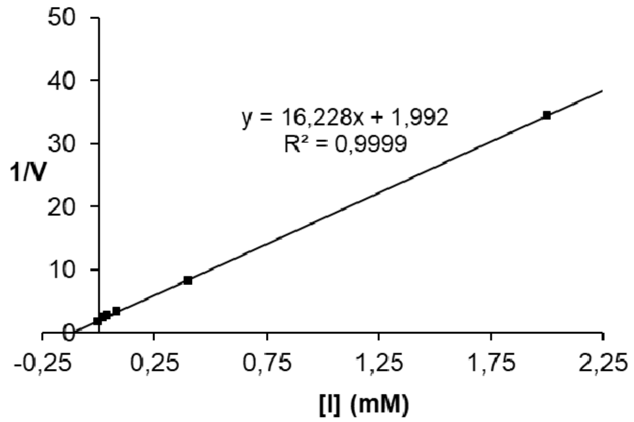

Figure S7. Dixon Plot for K_i determination (42 ± 4 μM) of 28 against *bovine liver* β-galactosidase/β-glucosidase.

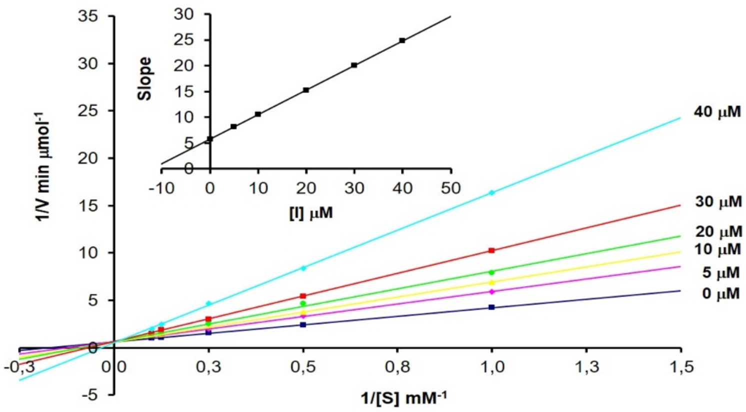

Figure S8. Lineweaver-Burk Plot for K_i determination (12.1 ± 2 μM) of 29 against *bovine liver* β-galactosidase/β-glucosidase.

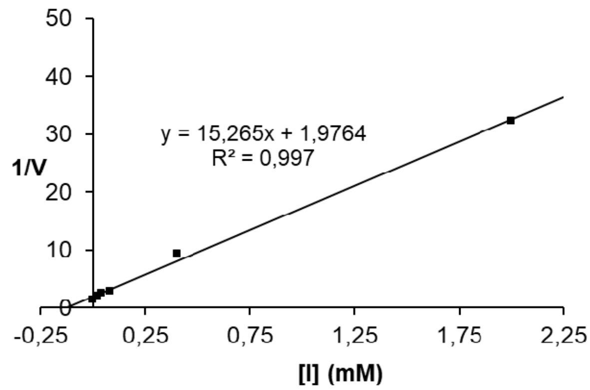

Figure S9. Dixon Plot for K_i determination (58 ± 6 μM) of 30 against *bovine liver* β-galactosidase.

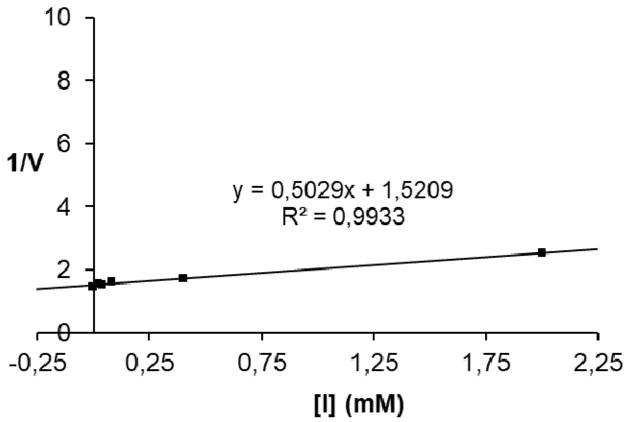

Figure S10. Dixon Plot for K_i determination (594 ± 60 μM) of 34 against *bovine liver* β-galactosidase.

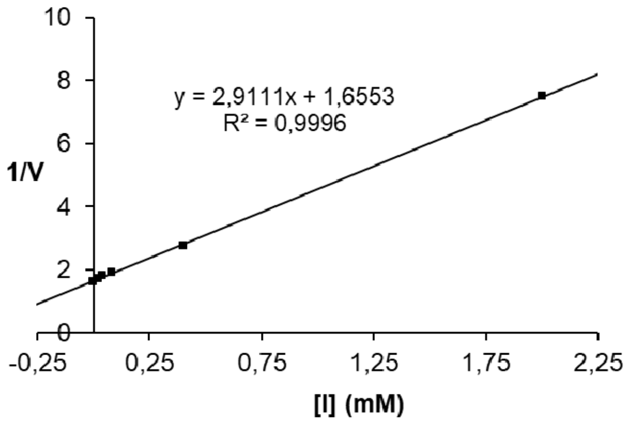

Figure S11. Dixon Plot for K_i determination (195 ± 20 μM) of 35 against *bovine liver* β-galactosidase.

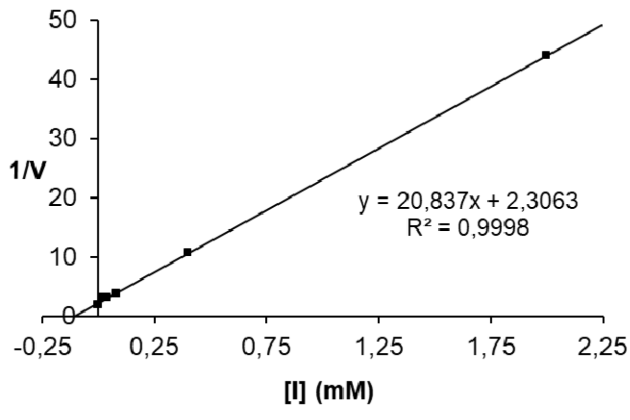

Figure S12. Dixon Plot for K_i determination (46 ± 3 μM) of 24 against *almonds* β-glucosidase.

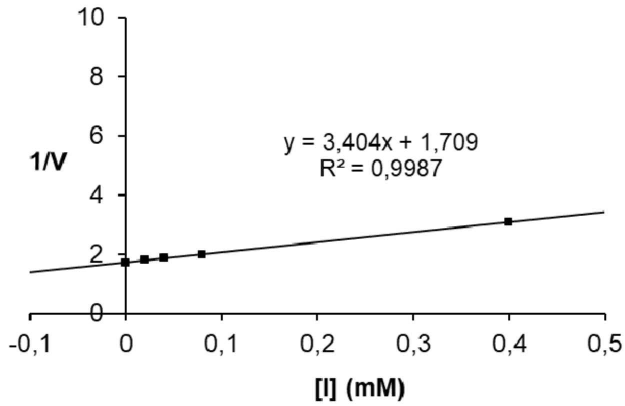

Figure S13. Dixon Plot for K_i determination (252 ± 20 μM) of 25 against *almonds* β-glucosidase.

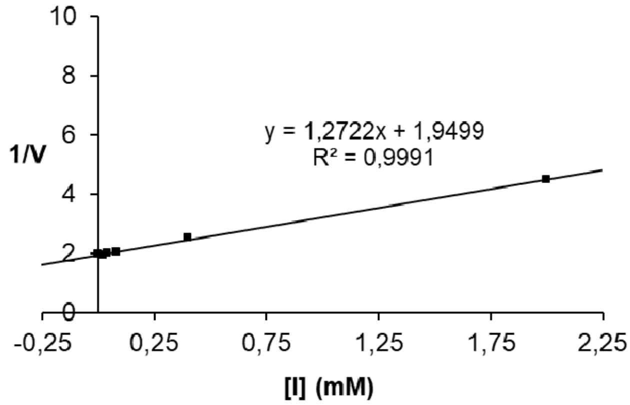

Figure S14. Dixon Plot for K_i determination (693 ± 65 μM) of 26 against *almonds* β-glucosidase.

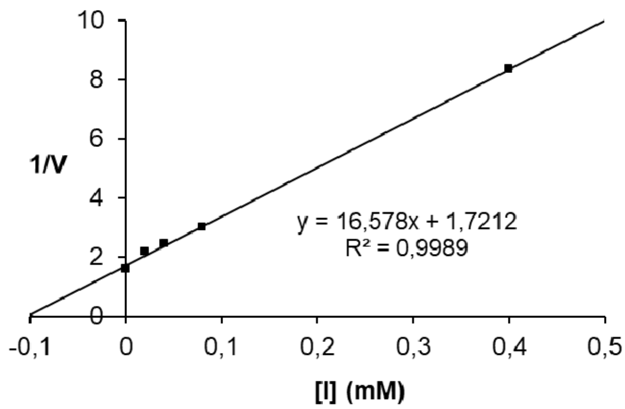

Figure S15. Dixon Plot for Ki determination (36 ± 4 μM) of 27 against almonds β-glucosidase.

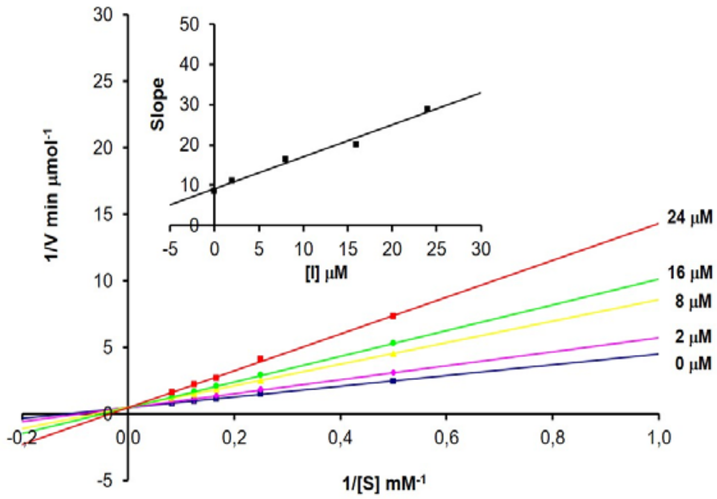

Figure S16. Lineweaver-Burk Plot for K_i determination (11.4 ± 2 μM) of **28** against *almonds* β-glucosidase.

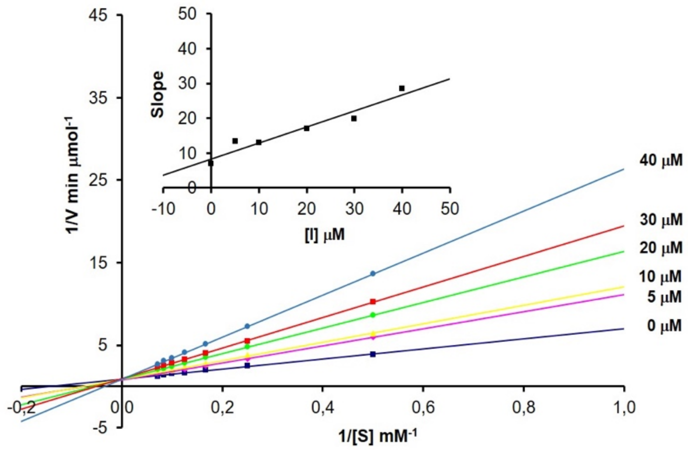

Figure S17. Lineweaver-Burk Plot for K_i determination (18 ± 2 μM) of **29** against *almonds* β-glucosidase.

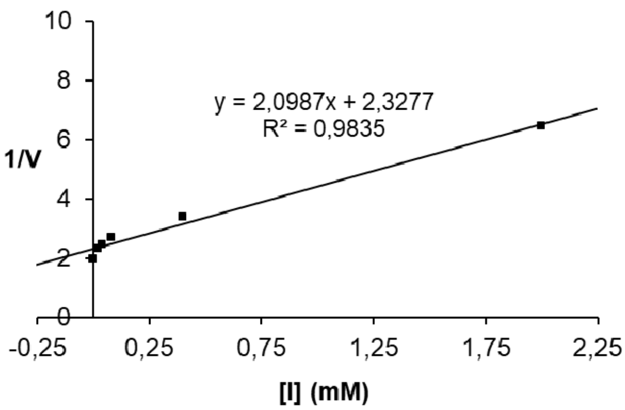

Figure S18. Dixon Plot for K_i determination (436 ± 41 μM) of **30** against *almonds* β-glucosidase.

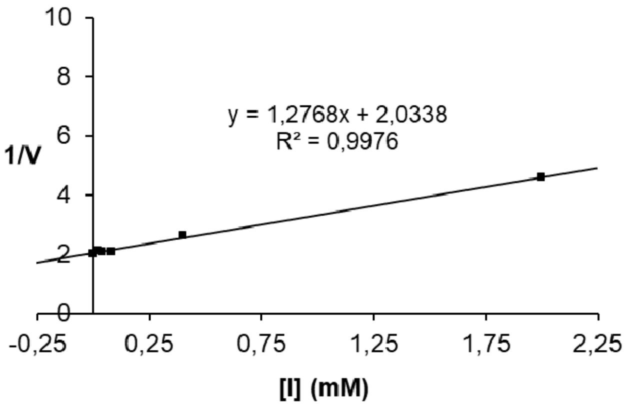

Figure S19. Dixon Plot for K_i determination (537 ± 50 μM) of 34 against *almonds* β-glucosidase.

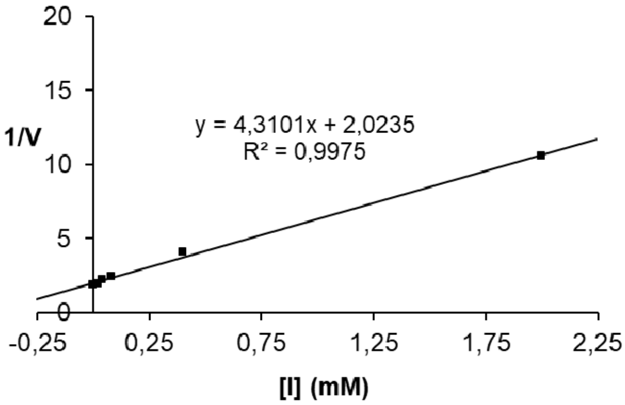

Figure S20. Dixon Plot for K_i determination (140 ± 11 μM) of 35 against *almonds* β-glucosidase.

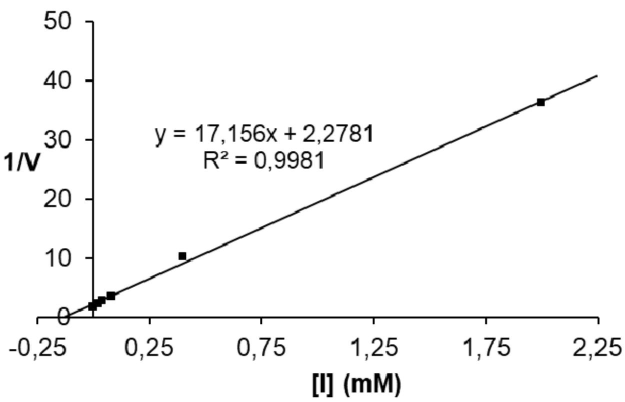

Figure S21. Dixon Plot for K_i determination (33 ± 3 μM) of 23 against *green coffee beans* α-galactosidase.

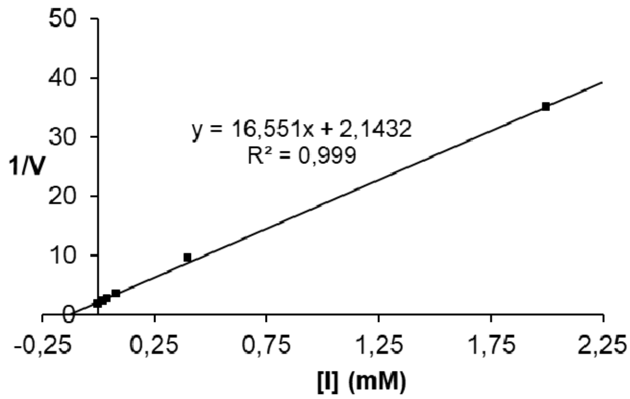

Figure S22. Dixon Plot for K_i determination (36 ± 5 μM) of 24 against *green coffee beans* α-galactosidase.

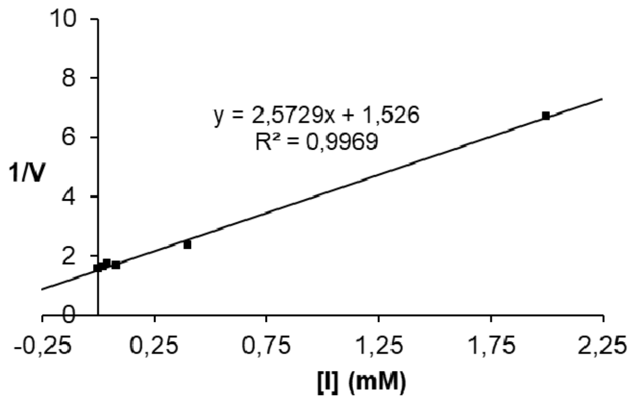

Figure S23. Dixon Plot for K_i determination (313 ± 28 μM) of 25 against *green coffee beans* α-galactosidase.

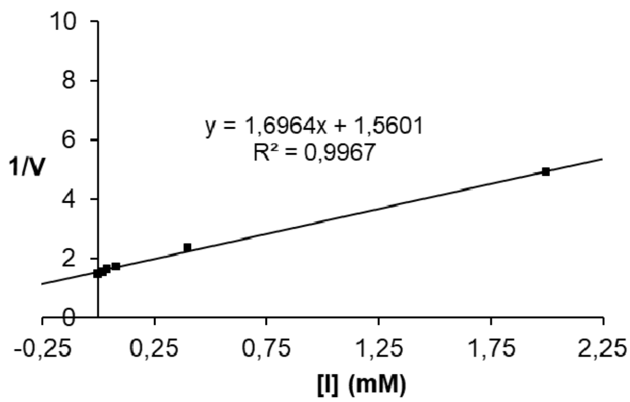

Figure S24. Dixon Plot for K_i determination (223 ± 20 μM) of 33 against *green coffee beans* α-galactosidase.

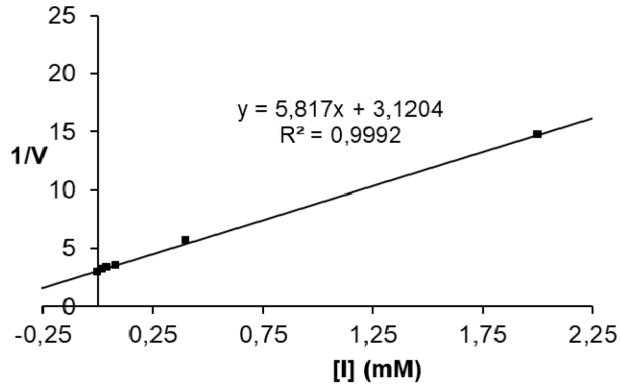

Figure S25. Dixon Plot for K_i determination (153 ± 12 μM) of 24 against *Aspergillus niger* amyloglucosidase.

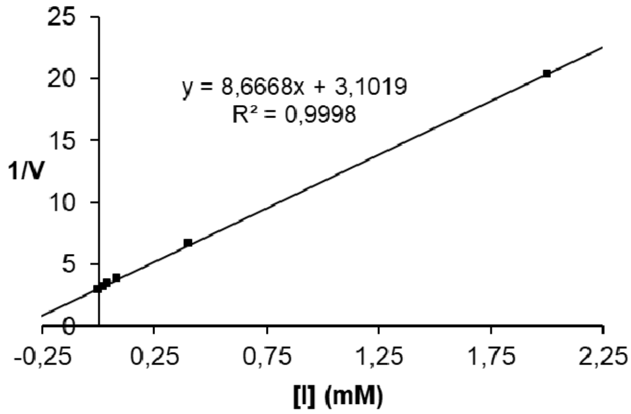

Figure S26. Dixon Plot for K_i determination (116 ± 10 μM) of 26 against *Aspergillus niger* amyloglucosidase.

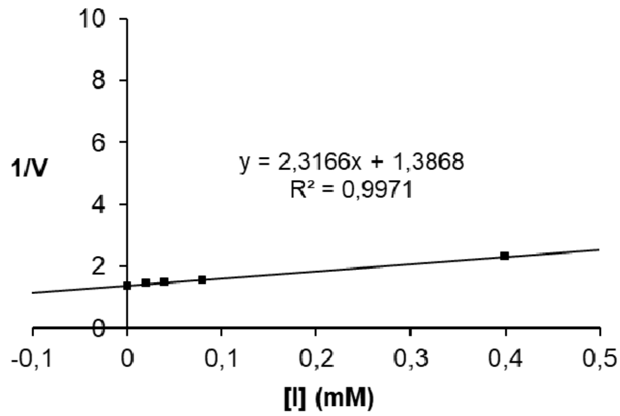

Figure S27. Dixon Plot for K_i determination (463 ± 40 μM) of 27 against *Aspergillus niger* amyloglucosidase.

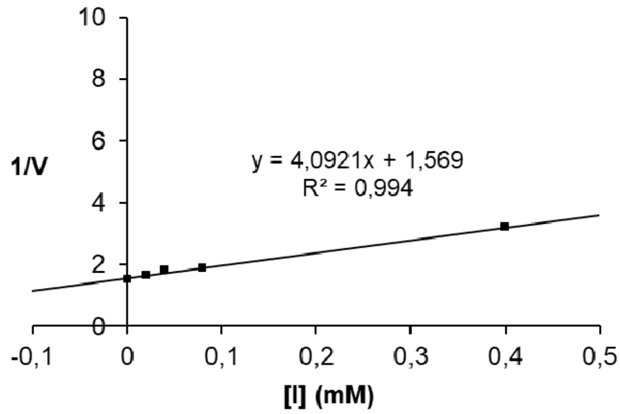

Figure S28. Dixon Plot for K_i determination (169 ± 15 μM) of 28 against *Aspergillus niger* amyloglucosidase.

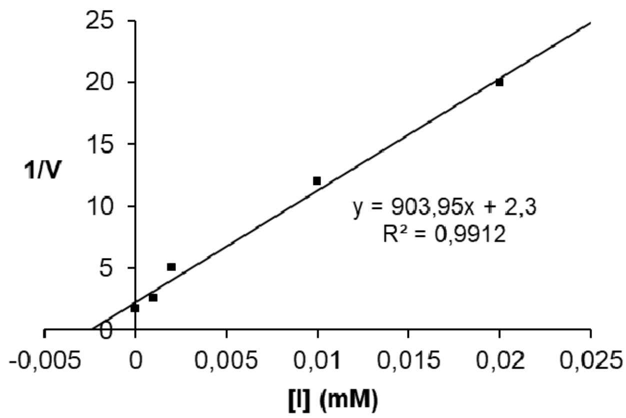

Figure S29. Dixon Plot for K_i determination (1.4 ± 0.1 μM) of 34 against *Aspergillus niger* amyloglucosidase.

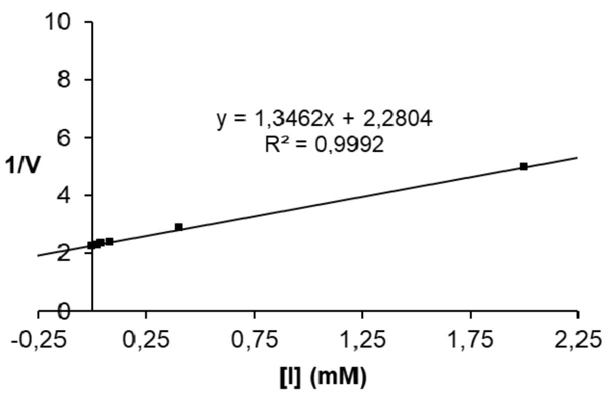

Figure S30. Dixon Plot for K_i determination (550 ± 45 μM) of 35 against *Aspergillus niger* amyloglucosidase.

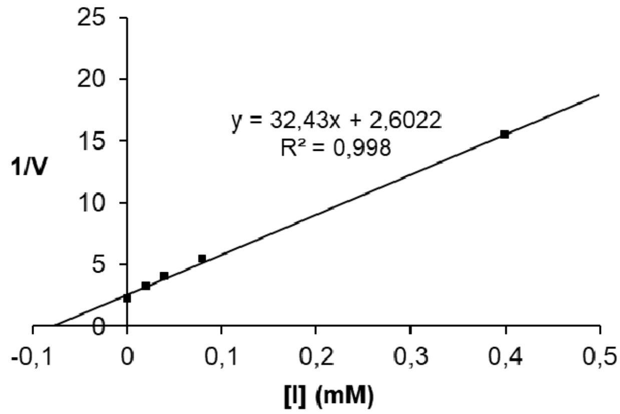

Figure S31. Dixon Plot for K_i determination (22.8 ± 1.9 μM) of 32 against *Aspergillus niger* amyloglucosidase.

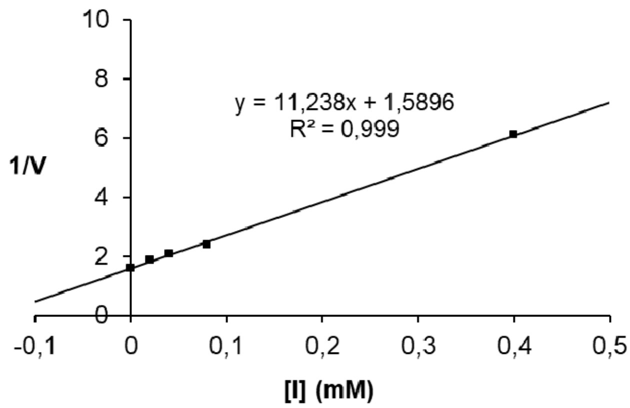

Figure S32. Dixon Plot for K_i determination (115 ± 10 μM) of 25 against *Penicilium decumbes* naringinase.

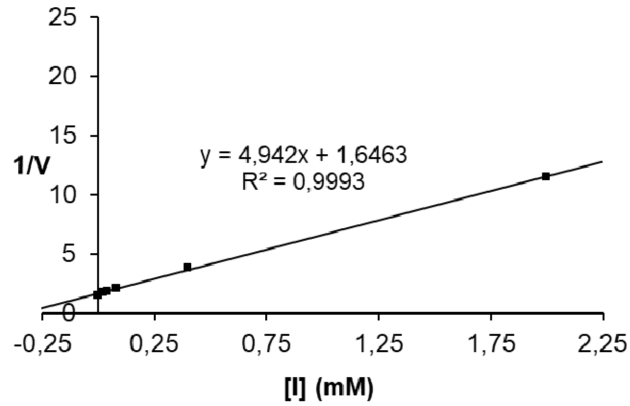

Figure S33. Dixon Plot for K_i determination (76 ± 5 μM) of 26 against *Penicilium decumbes* naringinase.

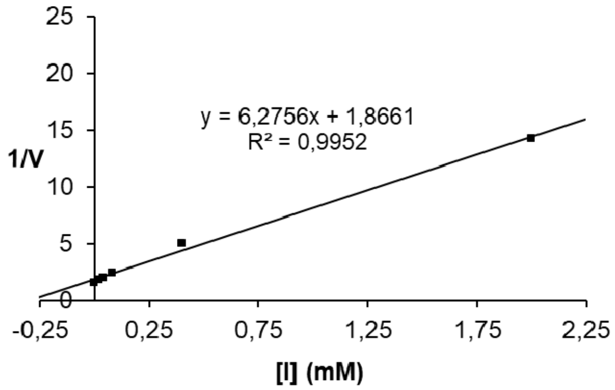

Figure S34. Dixon Plot for K_i determination (131 ± 11 μM) of 27 against *Penicilium decumbes* naringinase.

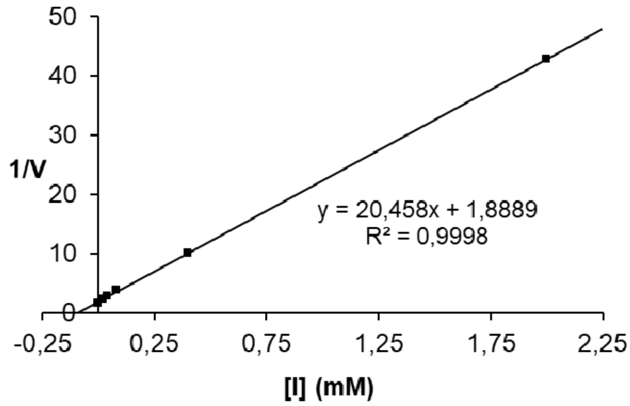

Figure S35. Dixon Plot for K_i determination (45 ± 3 μM) of 28 against *Penicilium decumbes* naringinase.

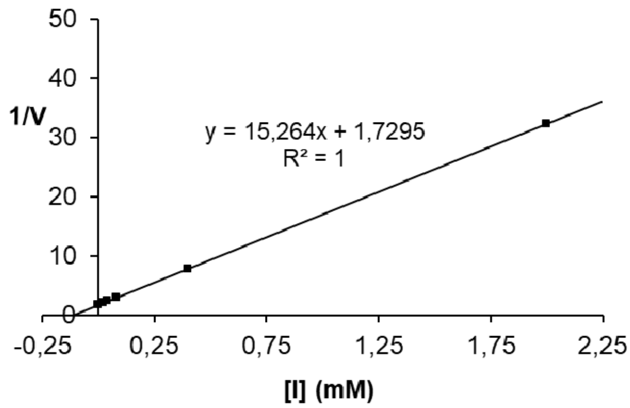

Figure S36. Dixon Plot for K_i determination (50 ± 4 μM) of 29 against *Penicilium decumbes* naringinase.

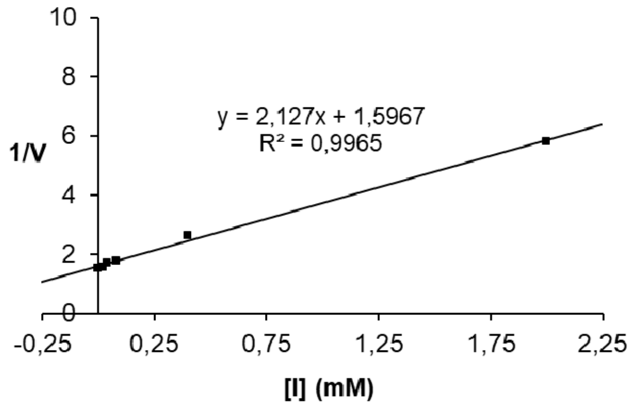

Figure S37. Dixon Plot for K_i determination (224 ± 20 μM) of **30** against *Penicilium decumbes* naringinase.

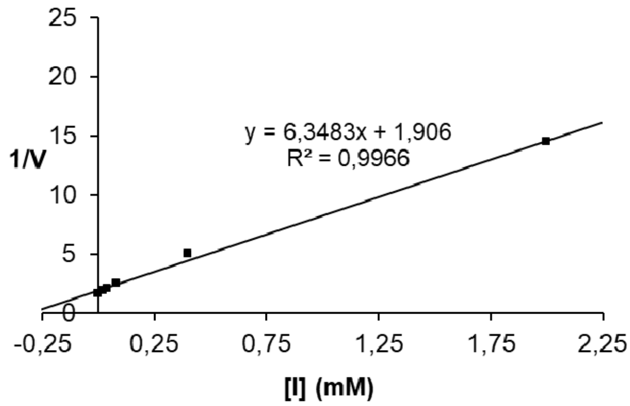

Figure S38. Dixon Plot for K_i determination (67 ± 5 μM) of **34** against *Penicilium decumbes* naringinase.

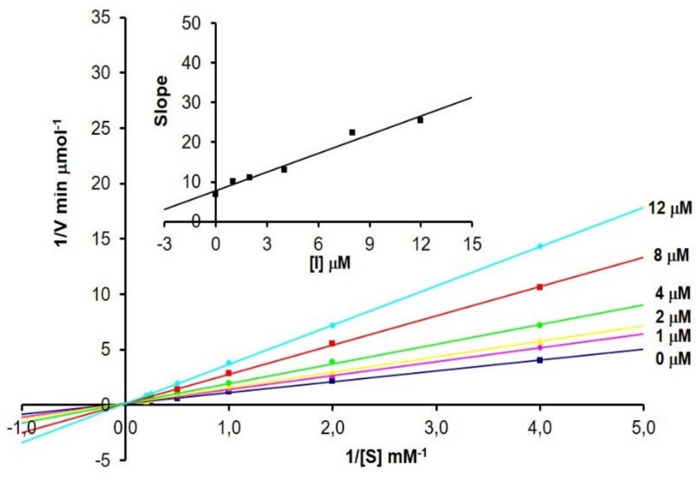

Figure S39. Lineweaver-Burk Plot for K_i determination (4.9 ± 0.5 μM) of **35** against *Penicilium decumbes* naringinase.

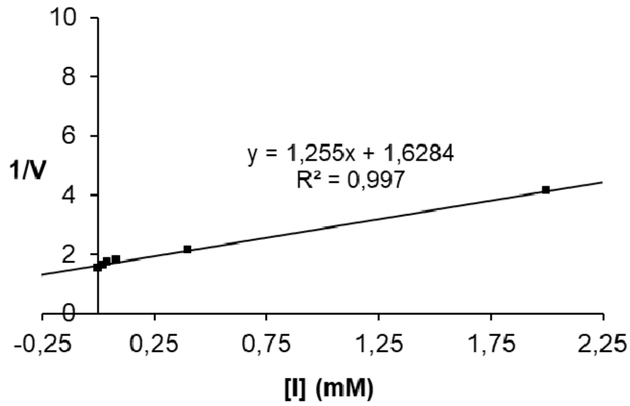

Figure S40. Dixon Plot for K_i determination (272 ± 25 μM) of 32 against *Penicilium decumbes* naringinase.